Experimental investigations on the phase diagram and thermodynamic properties of U-Sn system

by

ASHIT KRISHNA PATTANAIK
(Enrolment No: CHEM02200704004)

Indira Gandhi Centre for Atomic Research, Kalpakkam

A thesis submitted to the
Board of Studies in Chemical Sciences
In partial fulfillment of requirements
For the Degree of

DOCTOR OF PHILOSOPHY

Of

HOMI BHABHA NATIONAL INSTITUTE

August, 2013

Homi Bhabha National Institute

Recommendations of the Viva Voce Committee

As members of the Viva Voce Committee, we certify that we have read the dissertation prepared by Ashit Krishna pattanaik entitled "Experimental investigations on the phase diagram and thermodynamic properties of U-Sn system" and recommend that it may be accepted as fulfilling the thesis requirement for the Degree of Doctor of Philosophy.

Date: 7/2/2014

Chairman – Dr.V. Ganesan

Date: 9/2/14

Convener/Guide – Dr. P.R. Vasudeva Rao

Date:

External Examiner – Prof. Raman S. Srinivasa

Date: 7/2/14

Member – Dr. K. Nagarajan

Date: 07 Feb 2014

Member – Dr. T. Jayakumar

Final approval and acceptance of this dissertation is contingent upon the candidate's submission of the final copies of dissertation to HBNI.

I herby certify that I have read this dissertation prepared under my direction and recommend that it may be accepted as fulfilling the dissertation requirement.

Date: 07/02/2014
Place: Kalpakkam

<GUIDE>

STATEMENT BY AUTHOR

This dissertation has been submitted in partial fulfillment of requirements for an advanc ed degree at Homi Bhabha National Institute (HBNI) and is deposited in the library to be made available to borrowers under rules of the HBNI.

Brief quotations from this dissertation are allowable without special permission, provided that accurate acknowledgement of source is made. Requests for permission for extended quotation from or reproduction of this manuscript in whole or in part may be granted by the Competent Authority of HBNI when in his or her judgment the proposed use of the material is in the interests of scholarship. In all other instances, however, permission must be obtained from the author.

Ashit Krishna Pattanaik

<Ashit Krishna Pattanaik> 07/02/14

DECLARATION

I, hereby declare that the investigation presented in the thesis has been carried out by me. The work is original and has not been submitted earlier as a whole or in part for a degree / diploma at this or any other Institution / University.

Ashit Krishna Pattanaik
<Ashit Krishna Pattanaik> 07/02/14

List of Publications arising from the thesis

Journal

1. Gibbs energies of formation of the intermetallic compounds of U-Sn system, **A.K. Pattanaik**, R. Kandan, K. Nagarajan and P.R.Vasudeva Rao, J. Alloys. Comp., **551** (2013) 249-254.
2. A contribution to U-Sn system, **A. K. Pattanaik**, S. Balakrishnan, K. Ananthasivan, K. Nagarajan and P.R.Vasudeva Rao. (To be communicated).

Conferences:

1. Gibbs free energy formation of USn_3 by galvanic cell measurement, **A. K. Pattanaik**, R. Kandan, K. Ananthasivan, B. Prabhakara Reddy, K. Nagarajan P. R. Vasudeva Rao,Presented at ANM-2011, Mumbai, Feb.9-11, 134-135.
2. Gibbs free energy formation of U_3Sn_7 by galvanic cell measurement, **A. K. Pattanaik**, R. Kandan, K. Ananthasivan, B. Prabhakara Reddy, K. Nagarajan, P. R. Vasudeva Rao, Oral presentation, Chemistry Research Scholar's Meet, Indira Gandhi Centre for Atomic Research, Kalpakkam, India, July 14-15, 2011.
3. Enthalpy of formation of intermetallic compound USn_3, R. Babu, **A.K. Pattanaik,** K. Ananthasivan , K. Nagarajan, conference held at IISC Bangalore December 16-20, 2013, ABS-379-ICA.

Workshop

1. Attended a workshop on "Metallurgy for Non-Metallurgist", Organized by IIM-Chennai Chapter, Chennai, March 3-4 2009.

Ashit-krishna pattanaik
<Ashit Krishna Pattanaik> 07/02/14

DEDICATION

Dedicated

to

My Parents, family and friends.

ACKNOWLEDGEMENT

Firstly, I express my sincere gratitude to my research supervisor Dr. P.R. Vasudeva Rao, Director Chemistry Group and IGCAR, for his wholehearted support, encouragement and bearing with me during difficult times of my Ph.D. His willingness to spend time with me, despite his busy schedule has made my research life smooth and enjoyable.

I thank Dr. K. Nagarajan, Associate Director, Chemistry Group, who is also one of my doctoral committee members for his help and support. I am indebted to him for guiding me in the last couple of years and bearing with me during difficult times of my Ph.D. I also thank other members of my doctoral committee, Dr. V. Ganesan, Project Manager ROMG, and Dr. T. Jayakumar, Director MMG, for their consistent help, support and encouragement. I thank Dr. K. Ananthasivan, S. Balakrishnan, Dr. R. Babu, Ambika and Annie for the help rendered during spot experiments and calorimetric measurements. Dr. B. Prabhakara Reddy, Dr. R. Kandan, Suriyakumari and Suddhasattwa Ghosh for the support and help during molten salt emf measurements. I would also like to thank my lab mates Mrs. S. Vandarkuzhali, Nibedita, Dr. Manish, Nedumaran, Gurudas and Krishan for their help and useful discussions.

I thank Dr. Baldev Raj, former Director, IGCAR for his encouragement, friendliness and creating a research spirit in JRF enclave. I also convey my thanks to Dr. M. Sai Baba, Associate Director, RMG, IGCAR for his help, support and for providing good facilities at JRF enclave.

It is my pleasure to keep a special thank to my beloved friend Biranchi Narayan Mohanty (Babula), who was always there for me during my difficult time and inspired me to finish this Ph.D. I also thank Suddhasattwa Ghosh, Balakrishnan, Madhavan and Dr. Jena for giving moral support and enough confidence to complete this thesis. I am fortunate to have friends around me like Prasana, Bishnu, Babula, Kamalakanta, Kalpataru, Biju, Suranjan, Manikandan, Manas,

Tarun, Ujwal, Sunasira, Abhiram, Vishnu, Trinadh, Rahul and Ashok whose presence makes my staying more exciting and enjoyable in Kalpakkam. I would like to thank each and every member of Chemistry Group, who has helped me in some way or the other to finish this thesis work.

In the last and above all, I would like to express my heartiest gratitude and honor to my parents, Mr. Arun Kumar Pattanaik and Mrs. Sabita Pattanaik, my elder sisters, brother in laws and all other family members for always extending their love, affection and emotional support.

Contents

SYNOPSIS

Energy is the basic need for the growth and future development of any country. The fossil based fuels, renewable sources and nuclear power are the major sources to meet the energy demand of any country. As for as India is concerned, the fossil based fuels contribute to 80 %, renewable sources around to 18 % and nuclear to around 3 % of the total installed electric power generation capacity [1]. The fossil based fuels are the major source for the release of the green houses gases which leads to global warming [2]. The fossil fuels are going to be depleted as they are consumed at a very faster rate. Among the renewable sources except the hydro power, the other sources have not been harnessed properly. Looking at this scenario, enhancing the contribution of nuclear energy to the total energy supply of the country is inevitable to meet the energy demand. Further, nuclear energy is capable of generating clean power.

The fuels used in nuclear reactors essentially comprise uranium and / or plutonium either in their metallic form or in the form of their oxides, carbides and nitrides or their solid solutions. The choice of the chemical form is governed by factors such as target burn-up, ease of fabrication, potential for breeding plutonium, thermal conductivity, fuel cycle economics etc. India has vast thorium resources (225000 t) and moderate resources of uranium (84600 t). In order to fully exploit the available nuclear fuel resources for energy production, a three-stage nuclear program has been envisioned [3, 4]. In the first stage of the program, ^{235}U from natural uranium undergoes fission in a thermal reactor and ^{239}Pu is produced from fertile ^{238}U in the reactor. In the second stage, plutonium and depleted uranium from the first stage would be used as fuel materials in fast reactors. In the third stage, the fissile nuclide, ^{233}U produced from ^{232}Th blankets in fast reactors will be used in thermal or fast breeders to produce electricity as well as to further breed ^{233}U from thorium.

As part of the fast reactor program of the second stage, a test reactor, viz., Fast Breeder Test Reactor (FBTR) has been operating for the last twenty seven years and another fast reactor viz., Prototype Fast Breeder Reactor (PFBR) is at an advanced stage of construction at Kalpakkam. FBTR is the only reactor in the world which employs the mixed carbides of uranium and plutonium as the driver fuel. PFBR will use mixed oxides of uranium and plutonium as the fuel. U-Pu-Zr alloys will be used as the fuel for the future FBRs in view of their highest breeding potential.

FBR fuel is greatly influenced by a the thermophyscial as well as mechanical properties and hence the design of the fuel is based on these. Of these properties the two most important thermophysical properties are the thermal conductivity and the melting temperature.. The composition of the fuel, which is uniform at the beginning of irradiation, undergoes large changes during irradiation due to the buildup of fission products. Accumulation of fission products affects the mechanical properties of the fuel. The solidus and liquidus temperatures of the U-Pu-Zr ternary alloy fuels and their sub-systems are of interest in nuclear technology. Sn is one of the many fission products that are produced in a fast reactor. Thus U-Sn system is among the alloy systems of interest in metal fuel technology. Further, the intermetallic phases $AnPg_3$, $Anpg_4$ and $An(Sn)Pg_2$, In which An= Uor Pu and Pg = Platinum group metal Ru, Rh and Pd were identified in the post irradiation examination of failed mixed oxide fuel pins [5] from FBR. Thus the ternary system uranium-tin-palladium is of relevance for the interpretation of the behavior of irradiated uranium-plutonium oxide fuels containing the fission products, tin and the light platinum metals. In order to understand this ternary system, the phase diagram and the thermodynamic data on the relevant sub-binaries including U-Sn are highly useful. Further, the U-Sn system would serve as a model system that could be used to validate the spot- technique,

an experimental technique for the investigations of the phase diagrams of alloys of relevance to fast reactor fuels. In view of the above reasons, studies on U-Sn system were taken up.

The phase diagram of the U-Sn system was studied by Palenzona et al. [6] using differential thermal analysis, metallographic X-ray diffraction and electron microscopy have identified five phases viz, USn_3, U_3Sn_7, USn_2, USn and U_5Sn_4 of which the first four are peritectically melting and the last one melts congruently. The peritectic melting temperatures of the first four intermetallics are very closely placed and Palenzona et al. have also reported contamination of the melt with the container material in the composition range 35 to 75 at % Sn.

Ananthasivan et al. [7] used a novel spot technique to resolve the discrepancies in the values reported by Palenzona et al. In this technique, the sample is heated in a Knudsen cell by using a non-contact technique (either RF induction or electron bombardment). Upon melting of the sample, a liquid miniscus is formed which reflects the image of the orifice as a black spot that can be viewed through a suitable magnifying device. The temperature of the Knudsen cell is measured by focusing a pyrometer on to a black body hole drilled at the bottom of the cell. When the transformation being observed corresponds to a two phase reaction involving a liquid and a solid, broken spots begin to appear. These grow in size and coalesce to form a single large spot, when liquefaction gets completed. Thus with the same experimental technique, the solidus and liquidus temperatures could be simultaneously measured with reasonable accuracy. Since this technique does not depend on the thermal effects for the determination of transition temperatures, even steep liquidus boundaries involving low heats of transformations could be delineated with the help of this technique. The investigations carried out by Ananthasivan et al. [7] by using the spot technique could only partly resolve the uncertainties reported in the earlier measurements. So in order to resolve the discrepancies completely, the present investigation of

the peritectic transformation temperatures of the first four intermetallics and congruent melting temperature of U_5Sn_4 was taken up by using the spot technique by employing improvised equipment and a relatively inert container material.

The Gibbs energy formation data have been reported reported only for USn_3. For the other intermetallic compound U_3Sn_7, USn_2 and USn no data have been reported. There exist a large difference among the values reported by various investigators for the Gibbs energy formation of USn3.The Gibbs energies of formation of these intermetallics are needed to assess their stabilities out various temperature. Hence the Gibbs energies formation of these intermetallic compounds, USn_3, U_3Sn_7, USn_2 and USn were determined in the temperature range 682-905 K by using molten salt galvanic cell emf method and the enthalpy of formation of the intermetallic compound, USn_3 at 298.15 K was determined by using aluminum solution calorimetric method.

The thesis is divided into six chapters. A brief description of the contents of the chapter is given below.

CHAPTER 1: Introduction

This chapter gives a brief description of nuclear energy as the essential option to meet the energy demands of the country. It discusses about the various types of nuclear fuel and nuclear reactors. The importance of the U-Sn system is also discussed. The earlier investigations of phase diagram and thermodynamic properties of the U-Sn system reported in the literature are also discussed here.

CHAPTER 2: Thermodynamic studies

This chapter deals with the various experimental methods which are generally employed to determine the thermodynamic properties of alloys. In the first section, the techniques

employed for the determination of phase transformation temperature including the spot technique are discussed. The second section deals with the experimental methods for determining the thermodynamic activities of the constituents of an alloy including the vapor pressure measurements and galvanic cell measurements with more elaborate discussion on the molten salt galvanic cell emf measurements. The third section gives a brief description of calorimetric techniques with special emphasis on the high temperature solution calorimetry. This chapter also gives a brief description on Miedema's empirical model for estimation of the enthalpies of formation of the intermetallics which has been used to estimate the enthalpy of formation of USn_3 and about the calculations carried out with FactSage 6.2 to compute the Gibbs energies of formation of the oxides of U, Sn, Th, Y and Mo. These calculations were used to predict the chemical compatibility of the alloys with the material of construction of the crucible.

CHAPTER: 3 Experimental

This chapter is divided into two parts. In the first part, the experimental procedure used for measurements by using the spot technique is discussed. In the second, molten salt galvanic cell emf (electro motive force) method and calorimetric measurements are discussed.

Preparation of the intermetallic compounds by using an arc melting furnace and its characterization are described in the first part. This section describes the salient features of the improvised experimental system of spot technique used in this study. Incorporation of an imaging system facilitated the production of the first ever video image of this experimental system [8]. Calibration of the temperature measurements was carried out with the help of high purity metals with different melting points that included gold, copper and nickel. The rate of heating was controlled by adjusting the power supplied to the primary of the RF induction generator in steps.

Preparation of the eutectic salt mixture of LiCl-KCl, its purification and the loading of UCl_3 in the eutectic salt melt are described in the latter part of the chapter. The procedure used for quantitatively estimating the amount of uranium in the salt using Davis-Gray method [9] is also described. Preparation of the electrodes and assembling the emf cell inside an argon atmosphere glove box are discussed in detail. The Gibbs energy of formation of the intermetallic compounds has been determined by using high-temperature molten salt galvanic cells [10]. The Galvanic cells constructed for this purpose are of two types which are shown below;

$$X(s)\ //\ XCl_n \text{ in LiCl-KCl (eutectic)}\ //\ <XY_p> + \{Y\} \quad \text{-------- } I$$

$$X(s)\ //\ XCl_n \text{ in LiCl-KCl (eutectic)}\ //\ <XY_p> + \{XY_q\} \text{ --------} II$$

In the cell I, pure metal X is used as the reference electrode and the working electrode is a biphasic mixture of the intermetallic compound, XY_p and liquid phase rich in *Y* saturated with *X*. In the second cell the working electrode used comprised two intermetallic compounds, XY_p and XY_q.

The overall cell reaction in the case of cell I can be written as;

$$X(s) + pY(soln.) \longrightarrow XY_p\ (s)$$

The emf of the cell I, E is measured as a function of temperature, the partial molar Gibbs energy of *X* and the Gibbs energy of formation of XY_p are related by the following equations:

$$\overline{G_U} - G_U^o = -zFE_I$$

and

$$\Delta_f G^0_{\langle XY_P \rangle} = -zFE_I + 3RTlna_Y$$

As a first approximation, the saturated solution was assumed to be ideal and the term $3RTlna_Y$ in the above equation was replaced with $3RTlnX_Y$ where X_Y is the atomic fraction of *Y* in the saturated solution. In view of the fact that the saturated solution is rather dilute in X, the above

assumption is reasonable. So the Gibbs energy formation of the intermetallic compound XY_p can be calculated from the measured emf.

The cell reaction for the cell II is;

$$X(s) + q\,XY_p \longrightarrow p\,XY_q$$

The Gibbs energy formation of the alloy XY_q can be calculated by using the following equations,

$$-zFE_{II} = p\Delta G_f^o(XY_q) - q\Delta G_f^0\,(XY_p)$$

$$\Delta_f G^0_{\langle XY_q\rangle} = -\frac{z}{p}FE_{II}/p + \frac{q}{p}\Delta G_f^0(XY_p)$$

where, E_{II} is the emf of the Cell II.

The Gibbs energies of formation of the intermertallic compounds were calculated from the emf data using the above equations. The experimental procedure used for the emf measurement is also described in this section. A high temperature differential calorimeter (model HT-1500 of M/s. SETARAM, France) used for the calorimetric measurements is described here and the principle of operation of the calorimeter is discussed. High temperature dissolution calorimetry was used to determine the enthalpy of formation of an alloy $A_xB_{(1-x)}$ at 298.15 K [11] by measuring the thermal effect of dissolution of the alloy $A_xB_{(1-x)}$ and its constituent elements, A and B in the same metallic bath at the same temperature. The thermal effects of dissolution, (Q^E)of the solute metal A in the liquid metal solvent S are measured as a function of the concentration of A, by dropping the samples from the ambient into the solvent at the experimental temperature, T in the calorimeter. Since, in general, the thermal effects of dissolution are independent of the concentration of the solutes in the solvent in the dilute solutions, the thermal effect of dissolution of metal A at infinite dilution($Q_A^{E,\infty}$) is obtained taking the mean of the thermal effects of dissolution. The thermal effects of dissolution of B at infinite dissolution($Q_B^{E,\infty}$)

and that of the intermetallic compound, $A_xB_{(1-x)}$ at infinite dissolution ($Q^{E,\infty}_{A_xB_{(1-x)}}$) are obtained by similar measurements in the liquid solvent S and at the same temperature. The enthalpy of formation of the intermetallic compound $A_xB_{(1-x)}$ is calculated from the following equation;

$$\Delta_f H^0_{298.15} < A_xB_{(1-x)} > = xQ^{E,\infty}_A + (1-x)\, Q^{E,\infty}_B - Q^{E,\infty}_{A_xB_{(1-x)}}$$

The procedure used to calculate the enthalpy of formation is described in this section.

CHAPTER 4: Determination of peritectic transformation temperatures of the system U-Sn

In the present study, the peritectic transformation temperatures of the following intermetallic compounds were re-determined by using the spot technique.

(1) Peritectic formation of USn_3

$$Liquid + \langle U_3Sn_7 \rangle \xrightarrow{Cooling} \langle USn_3 \rangle$$

(2) Peritectic formation of U_3Sn_7

$$Liquid + \langle USn_2 \rangle \xrightarrow{Cooling} \langle U_3Sn_7$$

(3) Peritectic formation of USn_2

$$Liquid + \langle USn \rangle \xrightarrow{Cooling} \langle USn_2 \rangle$$

(4) Peritectic formation of USn

$$Liquid + \langle U_5Sn_4 \rangle \xrightarrow{Cooling} \langle USn \rangle$$

The peritectic formation temperatures of the four intermetallic compounds viz., USn, USn_2, U_3Sn_7 and USn_3 were found to be 1642 ± 7, 1628 ± 1, 1622 ± 4, 1600 ± 4 K respectively. The

values thus obtained are compared with values reported earlier [7]. The present values have comparatively less uncertainties than reported earlier. We were able to define the peritectic isotherms in the U-Sn system more precisely.

Chapter 5: Determination of the Gibbs energy and enthalpy of formation of the intermetallic compounds of U-Sn system

The experimental assembly for the emf measurement is discussed in this chapter. The Gibbs energy formation of USn_3 was calculated from the emf measurement of the following cell;

$$U(s) \,//\, UCl_3 \text{ in LiCl-KCl (eutectic)} \,//\, \langle USn_3 \rangle + \{Sn\}$$

in the temperature range 682-905 K.

The Gibbs energy formation of U_3Sn_7 was calculated from the emf measurement of the following cell;

$$U(s) \,//\, UCl_3 \text{ in LiCl-KCl (eutectic)} \,//\, \langle U_3Sn_7 \rangle + \langle USn_3 \rangle$$

in temperature range 693-843 K.

The Gibbs energy formation of USn_2 was calculated from the emf measurement of the following cell;

$$U(s) \,//\, UCl_3 \text{ in LiCl-KCl (eutectic)} \,//\, \langle USn_2 \rangle + \langle U_3Sn_7 \rangle$$

in the temperature range 692-892 K.

The Gibbs energy formation of USn_2 was calculated from the emf measurement of the following cell

U(s) // UCl_3 in LiCl-KCl (eutectic) // <USn> + <USn_2>

in the temperature range 692-892 K.

The Gibbs energies of formation $(\Delta_f G^0)$ of USn_3, U_3Sn_7, USn_2 and USn with respect to α-U and liquid Sn, in the respective temperature ranges determined using galvanic cell emf measurements are given by (*-172.80 + 0.061 T), (-527.8 + 0.200 T), (-174.9 + 0.073 T) and (-176.9 + 0.064 T) kJ mol*$^{-1}$, respectively. For USn_3 the values obtained agree well with the literature value [12]. For the rest of the intermetallic compounds, the Gibbs energy formation data are reported for the first time.

A high temperature dissolution calorimeter was used to calculate the enthalpy of formation USn_3 at 298.15 K. Liquid aluminium was used as the solvent. After determining the thermal effects of dissolution at infinite dilution of U, Sn and USn_3 the enthalpy of formation of USn_3 was calculated using the following equation,

$$\Delta_f H^0_{298.15} < U_{1/4}Sn_{3/4} > = 1/4 Q_U^{E,\infty} + 3/4\, Q_{Sn}^{E,\infty} - Q_{USn_3}^{E,\infty}$$

The value thus obtained was compared with those reported in the literature.

The enthalpy of formation of USn_3 determined by using the aluminium solution calorimetry at 298.15 was found out to be -129.5 kJ mol^{-1}. The value agrees well with the value reported by Colinet et al. [13].

Chapter 6: Summary and scope for further work

This chapter summarizes the major findings of this study.

(1) The peritectic transformation temperatures of the four intermetallics viz.USn_3, U_3Sn_7, USn_2 and USn in the U-Sn system are reported by using spot technique which was developed in house to investigate the high temperature regions of the phase diagram.

(2) Chemically inert and high density ceramic crucibles were used to minimize the contamination and creeping of the molten liquid tin. From these studies yttria seems to be a better container material to hold this molten U-Sn alloy, but still further studies are required to arrive at the final judgement.

(3) There exist closely spaced peritectic isotherms in phase diagram of the U-Sn system and this study was able to delineate them.

(4) The Gibbs free energy formation of USn_3 calculated from the molten salt galvanic cell emf measurement agrees well with value reported by Johnson et al. [12].

(5) The Gibbs energy formation of the U_3Sn_7, USn_2 and USn intermetallics are reported for the first time.

(6) The enthalpy of formation of USn_3 at 298.15 was determined in this study which agrees well with value of Colinet et al. [13].

(7) The (U, Pu) Sn (Ru, Rh, Pd) compound that has been identified in the fuel matrix needs to be studied. Since Pu could be expected to be soluble in U-Sn intermetallic compound, the study of (U,Pu) Sn alloy are also of important to be studied.

Scope for further work

The solidus–liquidus temperatures of the binary system, Pu-Sn and those of the ternary system U-Pu-Sn can be measured using the spot technique.

The Gibbs energies of formation of the intermetallic compounds of the above systems can be measured using the molten salt galvanic cell emf measurements and their enthalpies formation using high temperature calorimetry.

References:

[1] Ministry of Power Government of India.< /http://www.powermin.nic.in/ JSP_SERVLETS/internal.sjsp> [accessed on 15.10.12].

[2] Mazen M., Abu-Khader, Prog. Nucl. Energy 51 (2009) 225-235.

[3] C. Ganguly, Development of plutonium-based advanced LMFBR fuels and thoria-based PHWR fuels in India, IAEA-TECDOC-352, pp 107-127 (1985) P.Vincenzini, Editor, High Tech Ceramics, Elsevier Science Publishers B.V., Amsterdam, 1987, p. 288.

[4] J.P.Schapira, R.K. Singhal, Nucl. Technol. 128 (1999) 25.

[5] H. Kleykamp, S.G. Kang, J. Nucl. Mater. 230 (1996) 280.

[6] A. Palenzona, P. Manfrinetti, J. Alloys Compd. 221 (1995) 157.

[7] K. Ananthasivan, Ph.D. thesis, University of Madras, Chennai, India 2003.

[8] K.C. Harikumar, S. Balakrishnan, K. Ananthasivan, S. Anthonysamy, V. Ganesan, P.R. Vasudeva Rao, Proc. XL CALPHAD 2011, Rio de Janerio, Brazil (2011) 191.R.J.

[9] W. Davies, W. Gray, Talanta. 11 (1964) 1203-1211.

[10] P. Chiotti, J. A. Kateley, J. Nucl. Mater. 32(1969) 135.

[11] B. Prabhakara Reddy, Ph.D thesis, University of Madras, Chennai, India 2000.

[12] I. Johnson, H. M. Federer, Thermodynamic Study of the Compounds of Uranium with Silicon, Germanium, Tin and Lead in the Proceedings of the International Symposium of Thermodynamics of Nuclear Materials, International Atomic Energy Agency, Vienna, 1962, p. 319-328.

[13] C. Colinet, A. Bessound , A.Pasturel, J. Less-Common Met., 143 (1988) 265-278.

LIST OF FIGURES

LIST OF TABLES

Chapter 1: Introduction

1.1 Nuclear energy and Nuclear reactors

Energy is the basic need of any country. For the second most populated and developing country like India energy plays a very important role for its sustainable growth. At present India's economy is growing at a steady rate of 4 to 5% for the past few years [1]. A high growth rate is also predicted for the future which implies a further high growth rate in the consumption of electrical energy. At present fossil fuels – coal, lignite, oil and natural gas are the major contributors to electricity generation, accounting for nearly 80% of the electricity produced annually [2]. Renewable sources – solar thermal power, hydroelectric Power, wind energy, and biomass power – contribute another 18 % (14 % hydroelectric) to the total electricity produced and nuclear energy contributes only 2 %. The fossil fuel resources are major source of the green house gases responsible for the global warming. So there is international pressure to reduce its usage. Although India has reasonable resources of renewable energy, they are not sufficient to meet its future electricity requirements. Eventually, about few years later, the contribution from fossil fuels will also become negligible given the rate at which these are depleting due to their high consumption. So among the other energy resources available to meet the future energy demands, nuclear energy is going to play a vital role, as it has the capability to generate sufficient and clean electricity to meet India's growing energy demands. Among the nuclear fuel resources available, uranium resources in India are limited, however, we have vast resources of thorium. In order to fully exploit the available nuclear fuel resources for energy production, a three-stage nuclear program has been envisioned [3]. This three stage program is based on a closed fuel cycle involving spent fuel reprocessing to recover unused uranium and plutonium to

be used as a fuel in the reactor. At present there are 19 nuclear power reactors in operation with an installed capacity of 4560 MW(e) [4]. The three stages of nuclear program are given below;

1. Natural uranium fuelled Pressurized Heavy Water Reactors (PHWRs).
2. Fast Breeder Reactors (FBRs) utilizing plutonium based fuel.
3. Advanced nuclear reactors for utilization of thorium.

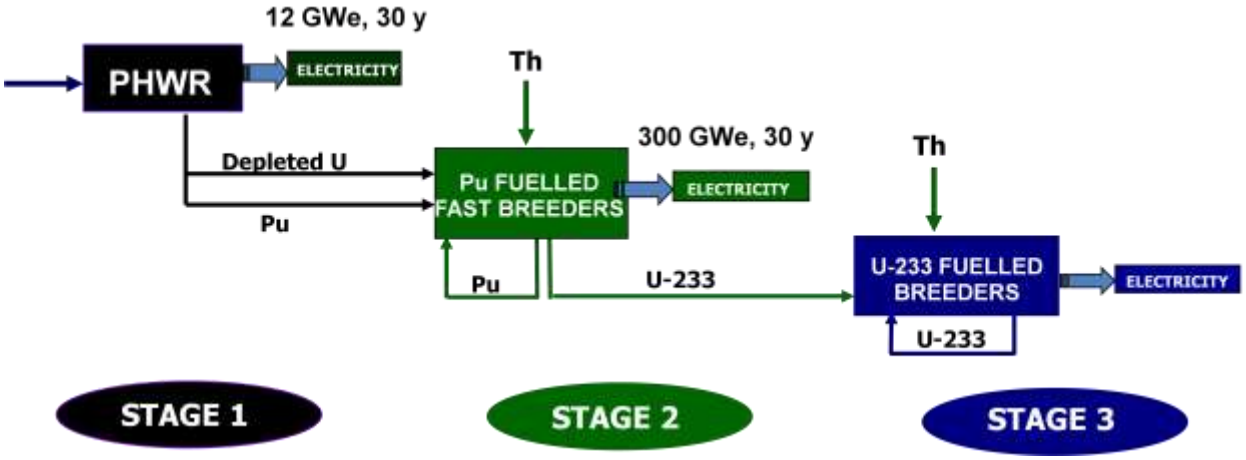

Fig. 1.1 Indian's three stage nuclear program [5].

In the first stage of the program, ^{235}U from natural uranium undergoes fission in a thermal reactor, and produces ^{239}Pu from fertile ^{238}U. At present most of the operating reactors in India is pressurized heavy water reactors (PHWRs) based on the use of natural uranium (0.72% ^{235}U) in the form of oxide. The discharged fuel from these first stage reactors contains plutonium and unutilized ^{235}U.

The second stage of this program comprises a chain of fast breeder reactors (FBRs). Plutonium and depleted uranium from the first stage would be used in these reactors as fuel. FBRs are capable of generating more fuel than they consume and thus are technically capable of growing the nuclear capacity to a very high level. As the first step of the second stage, a 40

MW(th) Fast Breeder Test Reactor (FBTR) was set up and it attained criticality in 1985 at Kalpakkam [6]. It is the only reactor in the world which uses the uranium-plutonium mixed carbide as the driver fuel. A 500 MW(e) Prototype Fast Breeder Reactor (PFBR) that will utilize uranium-plutonium mixed oxide as fuel is at an advanced stage of construction [7].

The third stage would comprise of ^{233}U based thermal reactors to produce power and also efficiently convert ^{232}Th to ^{233}U, ensuring the utilization of the vast reserves of thorium in the country. An Advanced Heavy Water Reactor (AHWR) is being developed at Bhabha Atomic Research Centre (BARC) to expedite transition to thorium-based systems [8].

1.2 Nuclear Fuels

The principal sources of nuclear energy in a reactor are the fissile nuclides ^{235}U, ^{239}Pu and ^{233}U which can undergo fission by neutrons of all energies, Out of these ^{235}U alone is naturally occurring. Natural uranium contains only 0.72% of ^{235}U and the rest being ^{238}U. The other two fissile nuclides are produced from the fertile nuclides namely, ^{238}U and ^{232}Th, by the absorption of a neutron and subsequent β emission. A reactor fuel necessarily has to contain a fissile nuclide in order to sustain the chain reaction. So, the fuel used in a nuclear reactor is plutonium and / or uranium either in the form of metal, oxide, carbide, nitride and their solid solutions or alloy. Some of the important characteristics of the fuels are that they should have high thermal conductivity, should be chemically and mechanically compatible with the clad and coolant, should have high solidus temperature and should not undergo any phase transition during heating, should be resistant to radiation damage, and should have high fissile atom density. The choice of the fuel is based on the type of the reactor in which it is used. Thermal reactors are generally fuelled by the oxides of naturally occurring uranium or sometimes 2-3 % enriched ^{235}U. If enriched uranium is not available, then mixed oxide of uranium and plutonium is used.

For fast reactors, the generally accepted fuel is UO_2-PuO_2 with a higher concentration of PuO_2 than the thermal reactor fuel and it is the fuel exploited commercially worldwide. Other ceramic fuels such as UC-PuC, UN-PuN, (UC)N-(PuC)N and metallic U-Pu-Zr alloys are also the candidate fuels for fast reactors.

1.3 Nuclear fuel reprocessing

Power in a nuclear reactor is produced by the fission of the fissile nuclides ^{235}U, ^{239}Pu and ^{233}U. This fission process yields, apart from about two neutrons per fission, which is necessary to sustain the chain reaction, a wide range of fission products. Heavy elements like Pu, Np, and Am etc. are also produced in the reactor. Some of the fission products like ^{135}Xe and ^{145}Sm are good neutron absorbers and are considered as neutron poisons and if they are not separated from the fuel at the proper time, they may reduce the reactivity of the fuel. The plutonium that is produced is a fissile material and can be recycled in suitable reactors, after separation from the fission products, thus considerably improving the economics of the nuclear fuel cycle. Moreover, prolonged irradiation of the fuel in the reactor causes significant damage to the cladding material due to exposure to intense radiation. Taking into account all these aspects, it is necessary to reprocess the nuclear fuel after a specified level of burn-up or in other words, after specific time of irradiation in the reactor.

The basic steps in the reprocessing of irradiated fuels consist of decladding, decontamination of uranium and plutonium from fission products and finally purification. In some flow sheets, uranium and plutonium are separated. The separated uranium and plutonium will be sent for fabrication of fresh fuel. In some flow sheets, uranium and plutonium are not separated from each other. The methods used for reprocessing are categorized into two groups, namely, aqueous reprocessing and non-aqueous reprocessing methods.

1.3.1 Aqueous reprocessing

The PUREX solvent extraction process serves as the backbone of aqueous reprocessing [9-11]. This process is being used worldwide for the reprocessing of commercial nuclear reactor fuels on an industrial scale since several years. This process yields high-purity plutonium and uranium, free of fission products and minor actinides (Np, Am, Cm). In this process, separation of uranium and plutonium from fission products is achieved by dissolving the irradiated fuel in nitric acid and equilibrating it with a 30 % solution of tri-n-butyl phosphate (TBP) in an organic solvent such as dodecane. Uranium and plutonium are selectively extracted into the organic phase leaving fission product elements in the aqueous phase.

1.3.2 Non-aqueous reprocessing methods

Aqueous processes cannot be used for reprocessing short cooled and high burn up fuels, since the organic solvents used in these processes will undergo radiolytic degradation at high levels of radiation. Further, if the processes are used for the reprocessing of metallic fuels, the flow sheet would involve the reduction of oxide end products back to metals by suitable methods as final step. This would render the process expensive. On the other hand, a non-aqueous process, wherein uranium and plutonium are maintained in their metallic states is more attractive, as it avoids these additional step employed in aqueous reprocessing. Non-aqueous reprocessing methods can be used for reprocessing of short cooled and high burn-up fuels because they employ molten salts and alloys as solvents which can withstand high levels of radiation. They have many other advantages over their aqueous counterparts. These are: (i) The absence of aqueous reagents reduces problems related to criticality. (ii) Higher amount of uranium and plutonium can be accommodated in a given volume during unit operations and so the process volumes are less. This leads to compact process equipment. (iii) The waste produced

in these processes is in solid form and the waste volumes are low making the waste disposal less problematic.

The non-aqueous methods can be classified into the following groups:

a) Methods based on volatilities – fluoride volatility process [12] and nitrofluor process [13] belong to this group.

b) Pyrometallurgical methods – in these processes, the fuel is maintained in the metallic state throughout the process. The melt refining process [14], which was used for the processing of EBR-II fuels, belongs to this category.

c) Pyrochemical methods

Pyrochemical methods [15] employ oxidation-reduction reactions chemically or electrolytically to effect the separation of the fuel materials from the fission products. Salt transport process [16] and salt cycle process [17] are well known examples of pyrochemical methods of reprocessing. The method earlier proposed for reprocessing the Integral Fast Reactor fuel (U-Pu-Zr) is electrorefining in a molten salt medium, which is also a pyrochemical method.

The irradiated carbide fuel from the FBTR is reprocessed by Purex process [18]. The liquid tin process is one of the alternatives suggested for the reprocessing of the irradiated carbide fuel [19]. In this process the irradiated carbide fuel is dissolved in liquid tin at 1773 K. Separation of fission products is achieved by evaporating the volatile fission products followed by nitriding which is carried out by passing nitrogen gas. The actinide nitrides have higher density, so they sink to the bottom and can be mechanically separated from the melt. The fission products remain either in tin solution or form nitrides which float on the melt and can be separated easily. Based on this pyrometallurgical purification method, the carbide fuel from a nuclear reactor was reprocessed and patented [20]. However, difficulties were encountered in

separation of Pu. The chemical incompatibility between the melt and crucibles, as well as inefficient removal of Mo and Zr limit the applicability of this method. ZrN was coprecipitated with UN and (U,Pu)N as it is completely miscible in these phases and Mo has very low solubility in tin and cannot be precipited by nitriding also. Matzke [19] suggested that further work on the multi-component systems, U-Pu-fission product-Sn is required in order to arrive at the final judgment on the efficacy of the liquid tin process. The system U-Sn is important among the binaries that are relevant to the above process.

1.4 Chemical state of irradiated fast reactor fuel

Fresh fast reactor fuel loaded into the reactor will have uniform composition at the start of irradiation. As a result of nuclear fission, thermal energy and a large number of fission products, spanning all the groups in the periodic table, are generated and hence the fuel composition changes with the burn-up. There are about 30 fission product elements which are generated in the fuel under irradiation conditions. Tin is one of the many fission products formed during irradiation. The cumulative fission yield of Sn in U and Pu fission are 0.34% and 0.53% respectively. Table 1.1 enlists the percentage yield of Sn isotopes formed during the fission of ^{235}U and ^{239}Pu in a fast reactor [21]. Further the intermetallic phases (U, Pu) $(Ru, Rh, Pd)_3$, $(U, Pu)_3$ $(Ru, Rh, Pd)_4$ and (U, Pu) Sn $(Rh, Pd)_2$ were identified in the post irradiation examination of failed mixed oxide fuel pins [22]. The cumulative fission yield of Ru, Rh and Pd in U and Pu fission are 24.56, 19.11, 6.61, 6.36 and 7.62,16.59 respectively. Hence, information on the phase diagrams and thermodynamic studies of the ternary systems U-Noble Metal-Sn are necessary for understanding the chemistry of irradiated uranium-plutonium mixed oxide fuels [22] as well. Knowledge of the relevant multicomponent phase diagrams is useful in understanding the phase equilibria in these systems. Thus experimental investigations on the

relevant sub-binaries including U-Sn are important and is also of interest to the fast reactor technology.

Table-1.1 Fission yield of Sn isotopes [21].

Isotopes of Sn	^{239}Pu (% yield)	^{235}U(% yield)
Sn-117	0.045	0.068
Sn-118	0.075	0.046
Sn-119	0.082	0.047
Sn-120	0.09	0.048
Sn-122	0.109	0.0561
Sn-124	0.133	0.0691
Cumulative fission yield	0.53	0.34

1.5 Need for experimental determination of melting point (Solidus) of fuel materials

The melting temperature is a physical property of the fuel that is of importance from safety consideration because the melting of the fuel is highly undesirable. If the fuel is a pure metal, the term melting point is relevant. When the fuel is a multicomponent material, then the lowest temperature at which liquid appears first when the fuel is heated, is used for safety assessments, in the place of melting point. It could be the solidus temperature or the temperature pertaining to a phase equilibria in which liquid is formed. A reasonably accurate knowledge of this temperature is necessary for the following reason.

The most important parameter in the thermal design of the core of a nuclear reactor is the distribution of temperature in the core. Factors such as the specific power, power density and heat flux, all related to a given fuel lattice or cell dimensions, are to be so chosen that together

with the heat removal system they would not result in temperatures that exceed fuel element material limitations leading to its failure [23]. Hence the melting temperature of the fuel often serves as a reference limit for the designer.

The conductivity integral of the fuel given in equation (1) is very useful for the designer [23].

$$4\pi \int_{T_S}^{T_{CL}} \kappa(T)dT = \chi \qquad (1)$$

where, T_{CL} and T_S refer to the center line temperature and the surface temperature of the fuel rod respectively. *k* is the thermal conductivity of the fuel material and χ is the linear heat rating of the fuel pin. Linear heat rating is the amount of power that can be drawn from the unit length of the fuel pin and is expressed as W/cm. The above equation is derived assuming that the fuel pin is a uniform heat source and that the heat transfer occurs only in the radial direction. In principle an approximate value of the temperature at any point along the radius of the fuel cylinder can be computed using an expression similar to equation (1), if the heat output is known and vice versa. Thus from the knowledge of the thermal conductivity and the melting point or the solidus temperature of the fuel, the maximum linear heat rating that can be achieved with a given fuel can be arrived at. Thus the melting temperature along with the thermal conductivity of the fuel pin must be accurately known for designing the fuel pin. The intermetallic phases $(U, Pu) \cdot (Ru, Rh, Pd)_3$, $(U, Pu)_3 .(Ru, Rh, Pd)_4$ and $(U, Pu)Sn(Rh, Pd)_2$ have been identified to be present in the post irradiation examination of failed mixed oxide fuel pins [22]. Melting of these inclusions present in the irradiated fuel could lead to deleterious chemical interactions between the fuel and clad. Hence information on the phase diagrams of the ternary systems U-Noble Metal-Sn are of relevance to understand the behavior mixed oxide fuels during irradiation [22].

Knowledge of the relevant multicomponent phase diagrams is useful in understanding the phase equilibria in these systems. Thus experimental investigations on the relevant sub-binaries including U-Sn are useful.

1.6 Literature survey on the U-Sn System

1.6.1 Phase diagram studies

Rough et al. [25] reported the phase diagram of the system U-Sn over the whole composition range. They reported the existence of three intermetallics <USn_3>, <U_3Sn_5> and <U_5Sn_4>. This diagram is based on the results of metallographic and X-ray diffraction studies. They reported that except for <USn_3> the exact composition was not accurately determined for the other two compounds because of the pyrophoricity of these compounds and the resultant difficulty in handling. Sari et al. [26] investigated the system U-Pu-Sn and found evidence for the existence of the following phases: MSn_3, M_3Sn_7, MSn_2, M_4Sn_5, MSn, M_5Sn_4 and M_5Sn_3 ($M=U_xPu_{1-x}$). Sheldon et al. [27] studied the phase diagram over the whole composition range and reported the existence of the three phases; the first two were the same as reported by Rough et al. [25]. They reported a new phase <U_3Sn_2> instead of <U_5Sn_4> reported earlier [25]. They also reported that the diagram be regarded as tentative especially for the uranium rich (>25 at %) compositions range and alloys at intermediate compositions are brittle and pyrophoric. Palenzona et al. [28] reinvestigated the phase diagram in the composition range, 0-90 at. % U. The examination of the system by using differential thermal analysis, metallography, X-ray diffraction and electron microscopy revealed the presence of five intermetallics, viz, <USn_3>, <U_3Sn_7>, <USn_2>, <USn> and <U_5Sn_4>. The first four are peritectic melting alloys while the last intermetallic melts congruently. The phase diagram of the U-Sn system based on Palenzona et al. [28] work is given in Fig. 1.2. Crystallographic data and phase transformation in the U-Sn

system are given in Table 1.2. Based on Palenzona's work, Ananthasivan [29] reinvestigated the sytem to remove the ambiguity in the melting temperatures of the intermetallics by using the spot technique. He also studied the system in the composition range 1-4 at % uranium (Sn rich region) by using a new variant of the spot technique called the illuminated spot technique [30].

1.6.2 Thermodynamics and other physical properties measurement studies on the U-Sn system

A lot of investigations have been done in the most tin rich compound <USn_3> owing to its easy handling than the rest. Faber et al. [31] have carried out neutron diffraction studies, Bihan et al. [32] have carried out high pressure studies, Colinet et al. [33] have measured the enthalpy of formation, Maaren et al. [34] have reported the specific heat, while the Gibbs free energy formation ($\Delta_f G^0$) of <USn_3> was reported by Johnson et al. [35] by using molten salt emf method. Pourghazi et al. [36] have done first principle calculations on the intermetallic <USn_3>. Szajek et al. [37] have studied the electronic and magnetic properties of the compound USn_2. Alcock et al. [38] have estimated the values of $\Delta_f G^0$ of <USn_3>, <U_3Sn_5> and <U_3Sn_2> by using vapor pressure measurements. Based on Palenzona's [28] work, Boulet et al. [39] has studied the magnetic properties of all the five intermetallics. . Boulet et al. [40] have reported the structure of the intermetallic compounds <USn_2> and <U_3Sn_7> by using neutron diffraction. Transport and magnetic properties of <U_3Sn_7> and <U_3Sn_5> were studied by Fukuhara et al. [41].

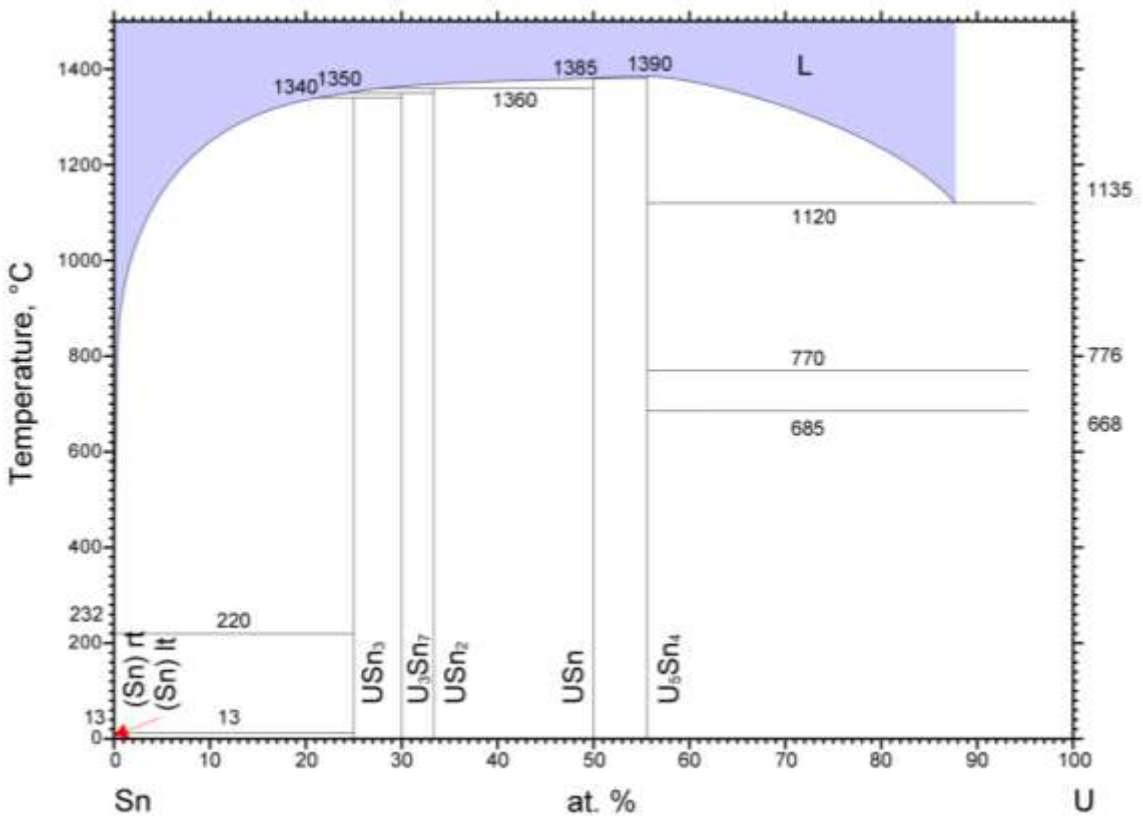

Fig.1.2 Phase diagram of U-Sn investigated in range 0-90 at. % U [28] shading showing the liquid region.

Table 1.2 Crystallographic data and phase transformations in the system, U-Sn [28]

Compound	Pearson Symbol	Space group (No.)	Isotype	a (nm)	b (nm)	c (nm)	References
$<U_5Sn_4>$	hP18	$P6_3/mcm(193)$	Ti_5Ga_4	0.9327	-	0.6230	Palenzona et al. [28]
<USn>	oP24	Pbcm(57)	ThIn	1.0488	0.9552	0.6213	Palenzona et al. [28]
$<USn_2>$	oC12	Cmmm(65)	$ZrGa_2$	0.4430	1.5456	0.4460	Palenzona et al. [28]
$<U_3Sn_7>$	oC20	Cmmm(65)	Ce_3Sn_7	0.4497	2.4725	0.4509	Palenzona et al. [28]
$<USn_3>$	cP4	Pm-3m(21)	$AuCu_3$	0.4610	-	-	Palenzona et al [28]
				0.4626	-	-	Sheldon et al. [27]

Phase / Invariant reaction	Temperature [28] / K	Type of the invariant reaction	Reference
$Liquid \xrightarrow{Cooling} \langle U \rangle + \langle U_5Sn_4 \rangle$	1393	Eutectic transformation	Palenzona et al. [28]
$\{U_5Sn_4\} \xrightarrow{Cooling} \langle U_5Sn_4 \rangle$	1663	Congruent melting	Palenzona et al. [28]
$Liquid + \langle U_5Sn_4 \rangle \xrightarrow{Cooling} \langle USn \rangle$	1658	Peritectic formation	Palenzona et al. [28]
$Liquid + \langle USn \rangle \xrightarrow{Cooling} \langle USn_2 \rangle$	1633	Peritectic formation	Palenzona et al. [28]
$Liquid + \langle USn_2 \rangle \xrightarrow{Cooling} \langle U_3Sn_7 \rangle$	1623	Peritectic formation	Palenzona et al. [28]
$Liquid + \langle U_3Sn_7 \rangle \xrightarrow{Cooling} \langle USn_3 \rangle$	1613	Peritectic formation	Palenzona et al. [28]
$Liquid \xrightarrow{Cooling} \langle Sn \rangle + \langle USn_3 \rangle$	493	Eutectic transformation	Palenzona et al. [28]

1.7 Need and Scope of the present work

The design and the performance of a fuel in a fast breeder reactor are primarily based on two important thermophysical properties namely the thermal conductivity and the melting temperature, as mentioned in section 1.5. The composition of the fuel, which is uniform at the beginning of irradiation, undergoes large changes during irradiation due to the build up of fission products. Sn is one of the many fission products that are produced in a fast reactor. Thus U-Sn system is among the alloy systems of interest to fast reactor technology. As stated earlier [22], U phases contains Pu with Sn and noble metal fission products have been reported to be found in the irradiated (U,Pu) mixed oxide fuels, So thermodynamic data of the binary U-Sn system are importanct.

Ternary alloys of U, Pu and Zr are being considered as candidate fuels for the future fast reactors in India. The data on the thermodynamic and thermophysical properties of these advanced fuels are rather scant. Hence at IGCAR an experimental program is currently underway in order to determine the same. As part of this endeavor an experimental system housed in a glove box, based on the “spot technique”, was developed indigenously, in order to determine the solidus and liquidus temperatures of these fuel materials. The experimental procedure and system were both validated by carrying out measurements on pure metals as well as in the system Cu-Ni [42]. In order to examine the suitability of this experimental apparatus and procedure for carrying out experiments on reactive U bearing alloys the system U-Sn was chosen as a model system.

Palenzona et al. [28] has reported the peritectic and congruent melting temperatures of all the five intermetallics. They encountered difficulties in determining the phase boundaries in the range 0 – 15 at % Sn owing to the reactivity of U-Sn alloys. In the measurements made in the

composition range 35-75 at % Sn, in which the temperatures were above 1673 K, the samples were found to be contaminated by the container material viz., molybdenum. Further owing to the inherent difficulties in the determination of the liquidus by using DTA, their data on the liquidus temperatures and closely spaced peritectic isotherms reported by these authors are rather less reliable. Thus, it is amply evident that, in spite of the detailed investigations carried out, uncertainties continue to prevail in the values of the peritectic melting temperature of the intermetallics in this system. Primarily these uncertainties stem from the experimental difficulties owing to the high chemical reactivity of the melt with the container as well as the proximity of the peritectic isotherms. Further, the liquidus boundary in the U-rich region in this system is not well established. In view of the above Ananthasivan [29] reinvestigated the system U-Sn by using the spot-technique and used inert ceramic cups to contain the melt. However, this author was not able to completely resolve the uncertainties. Containment of liquid alloys in the ceramic crucibles, creeping and surface diffusion of the liquid alloys posed difficulties in determining accurate values of these peritectic isotherms. Hence, the pertitectic melting temperatures of the intermetallics in this system U-Sn need to be re-investigated Yttrium oxide cups were used in this study so as to minimize the containment problem with the molten liquid.

Johnson et al. [35] and Alcock et al. [38] have reported the $\Delta_f G^0$ values of <USn_3>, but there is a huge difference between these two values. There is no other thermodynamic data available for the rest four intermetallic reported by Palenzona et al. [28]. In the view of all these there is a need to determine the $\Delta_f G^0$ of <USn_3> and the other four intermetallics.

References:-

1. South Asia Monitor, Center of strategic and International studies, Washington, No.98, September 7, 2006, p. 231.
2. Sukhatme, S.P., "Meeting India's future needs of electricity through renewable energy Sources", Current science 101(5), 2011, p. 624.
3. H.J. Bhabha, in: Conference on Development of Atomic Energy for Peaceful Purposes in India, New Delhi, (1954), p. 7.
4. S. K. Jain, Int. J. of nuclear power. 12 (2010) 24.
5. http://www.igcar.ernet.in/nuclear/reactors.htm, accessed on 19-4-2012.
6. Baldev Raj, Int. J. Nuc. Energy Science and Tech. 12 (2005) 164.
7. H.S. Kamath, "Fabrication of Mixed Oxide Fuels for Indian Nuclear Power Programme", in: Nuclear Fuel Cycle Technologies, (Eds.,) Baldev Raj and P.R. Vasudeva Rao, BRNS, DAE, (2006), p. 122.
8. B. Bhattacharjee, "An overview of R&D in Fuel Cycle Activities of AHWR" in : Nuclear Fuel Cycle Technologies, (Eds.,) Baldev Raj and P.R. Vasudeva Rao, BRNS, DAE, (2006), p. 3.
9. D. E. Ferguson, "Chemical Reprocessing of Nuclear Fuel", 24th International Congress of Pure and Applied Chemists, Vol. 6 (London: Butterworths, 1974), p. 337.
10. W.D. Bond, Light Water Reactor Nuclear Fuel Cycle, ed. R.G. Wymer and B.L. Vondra (Boca Raton, FL: CRC Press, 1981), p. 103.
11. J.L. Swanson, Sci. and Tech. Of Tributyl Phsophate, Vol. 3, ed. W.W. Schulz, L.L.

Burger, and J.D. Navratil (Boca Raton, FL: CRC Press, 1989), p. 55.

12. M. J. Steindler, L.J. Anastasia, L.E. Treverrow and A.A. Chilenskas, J. Nucl. Mat. 15 (1969) 177.
13. G. Strickland and F.L. Horn in: Prog. In Nucl. Energy, Series III, Process Chemistry, Vol. 4, Ed. C. E. Stevenson, E. A. Mason and A. T. Gresky, Pergamon Press, Oxford, 1970, p. 393.
14. C. E. Stevenson, EBR-II Fuel Cycle Story, American Nuclear Society, 1987, p. 45.
15. R. K. Steunenberg, R. D. Pierce and I. Johnson, Proc. Symp. On Reprocessing of Nuclear Fuels, Ames, Iowa, 1969, Ed. P. Chiotti, USAEC, 1969, p. 325.
16. J. B. Knighton, I. Johnson and R. K. Steunenberg in: Proc. Symp. On Reprocessing of Nuclear Fuels, Ames, Iowa, 1969, Ed. P. Chiotti, USAEC, 1969, p. 337.
17. K. M. Harmon and G. Jansen, Jr., in: Prog. In Nucl. Energy Series III, Process Chemistry, Vol. 4 Ed. Stevenson, E. A. Mason and A. T. Gresky, Pergamon press, Oxford, 1970, p. 429.
18. Baldev Raj, J. Nucl. Mater.385 (2009) 142.
19. Hj. Matzke, Science of Advanced LMFBR Fuels, North-Holland, Amsterdam, 1986, p. 637.
20. R.N. Anderson, N.A.D. Parlee, Candian Patent Nr. 931763 (1973). (cited from Ref.17. p-641).
21. E. A. C. Crouch, Atomic data and nuclear data tables: Fission product yields from neutron fission, Academic Press, New York and London, 19 (1977), p. 501.
22. H. Kleykamp, S.G. Kang, J. Nucl. Mater. 230 (1996) 280.
23. Ioan Ursu, Physics and Technology of Nuclear Materials, Pergamon Press, New York,

1985, p. 278.

24. A.E. Watar and A.B. Reynolds, Fast Breeder Reactors, Pergamon Press, New York, 1981 p. 123.
25. F. A. Rough, A. A. Bauer, Uranium-Tin in Constitution of uranium and thorium alloys, BMI report-1300, UC-25 Metallurgy and Ceramics, Battelle Memorial Institute, Ohio, 2 June 1958, p. 71.
26. C. Sari, F. Vernaza, W. Muller, J. Less-Common Met. 92 (1983) 301.
27. R. I. Sheldon, E. M. Foltyn, D. E. Peterson, The Sn-U (Tin-Uranium) system, Bull. Alloy Phase Diagr. 8 (1987) 347.
28. A. Palenzona, P. Manfrinetti, J. Alloys Compd. 221 (1995) 157.
29. K. Ananthasivan, Ph.D. dissertation, University of Madras, Chennai, India 2003.
30. K. Ananthasivan, I. Kaliappan, P. R. Vasudeva Rao, J. Alloys Compd. 352 (2003) 148.
31. J. Faber, G. H. Lander, P. J. Brown, Acta Cryst. 37 (1981) 558.
32. T. L. Bihan, S. Heathman, C. Abraham, High Press. Res. 23 (1996) 28.
33. C. Colinet, A. Bessound, A.Pasturel, J. Less-Common Met. 143 (1988) 265.
34. M. H. Van Maaren, H.T. Van Daal, K.H. J. Buschow, Solid State Commun., 14(1974) 145.
35. I. Johnson, H. M. Federer, Thermodynamic study of the compounds of uranium with Silicon, Germanium, Tin and Lead in the proceeding of the International Symposium of Thermodynamics of Nuclear Materials, International Atomic Energy Agency, Vienna, 1962, p. 319.
36. A. Pourghazi and Z. Nourbakhsh, Int. J. Mod Phys B. 19 (2005) 3049.

37. A. Szajek, Acta Phy. Pol., B 105 (2004) 485.

38. C. B. Alcock, P. Grieveson, J. Inst. Met. 93 (1961) 304.

39. P. Boulet, H. Noel, Solid State Commun. 107 (1998) 135.

40. P. Bulet, G. Andre, F. Bouree, H. Noel, J. Alloys and Compd. 329 (2001) 47.

41. T. Fukuhara, H. Sato, Y. Onuki, J. Phys. Soc. Jpn. 63 (1994) 2343.

42. K. Ananthasivan, S. Balakrishnan, I. Kaliappan, S. Anthonysamy, R. Pankajavalli, P.R. Vasudeva Rao, J. Alloys Compd. 468 (2009) 275.

Chapter 2: Thermodynamic studies

Pelton [1, 2] described a phase diagram as the geometrical representation of the loci of thermodynamic variables, when equilibrium between different phases, under a specified set of conditions, is established. In other words, it is a graphical representation which shows the existence of the various thermodynamic equilibrium states in a system. There are various experimental methods to determine the phase diagram [3-5] of a system. The first section of the present chapter describes some experimental techniques used for the determination of binary phase diagrams.

Section 2.1: Techniques for the determination of solid-liquid phase transformation in a binary system

2.1.1: Methods based on the enthalpy of phase transformation

2.1.1.1 Thermal analysis (The Cooling Curve)

According to the Richards rule [3], for solid-liquid equilibria the latent heat of freezing or fusion is around 2 $T_{m,}$ where T_m is the melting point in Kelvin and the specific heat of metals is about 20 J g atom^{-1}K^{-1}. Thus during solidification, the thermal arrest is very pronounced and can be measured by a plot of temperature versus time. Alloys have a range of temperatures over which the latent heat is liberated, and hence changes in the slope of the cooling and heating curves give the solidus and liquidus temperatures [1, 3]. Eutectic and peritectic transformations of alloys being isothermal, exhibit thermal arrests similar to that obtained for pure metals. Idealized heating and cooling curves are illustrated in Fig. 2.1. along with the corresponding hypothetical phase diagram. It is evident from these figures that when a liquid phase is present the charge cools at a faster rate compared to both a mixture of solid and liquid as well as pure solid. Further perceptible thermal arrests are seen at the phase transformation temperatures.

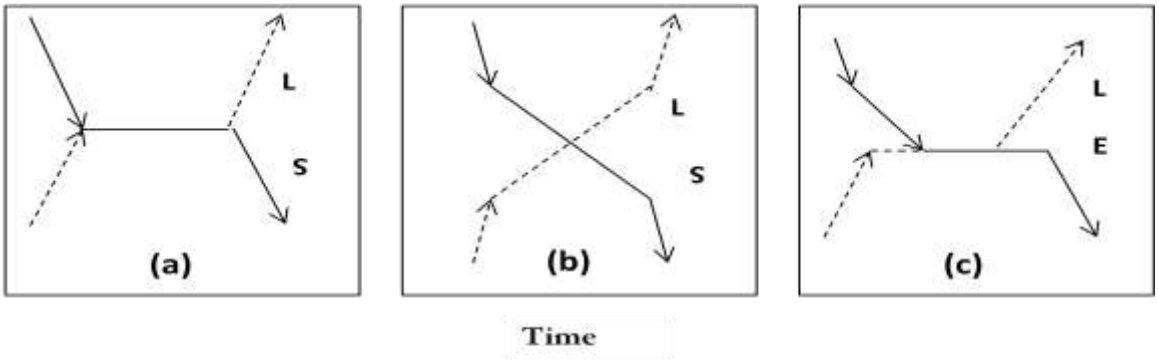

Fig. 2.1 Idealized heating and cooling curves for (a) a pure metal, b) an alloy with a range of freezing, and (c) an alloy with with a range of freezing and eutectic transformation. L,S,E are liquidus, solidus and eutectic temperatures respectively [1].The solid lines shows the cooling curve and the broken lines shows the heating curves.

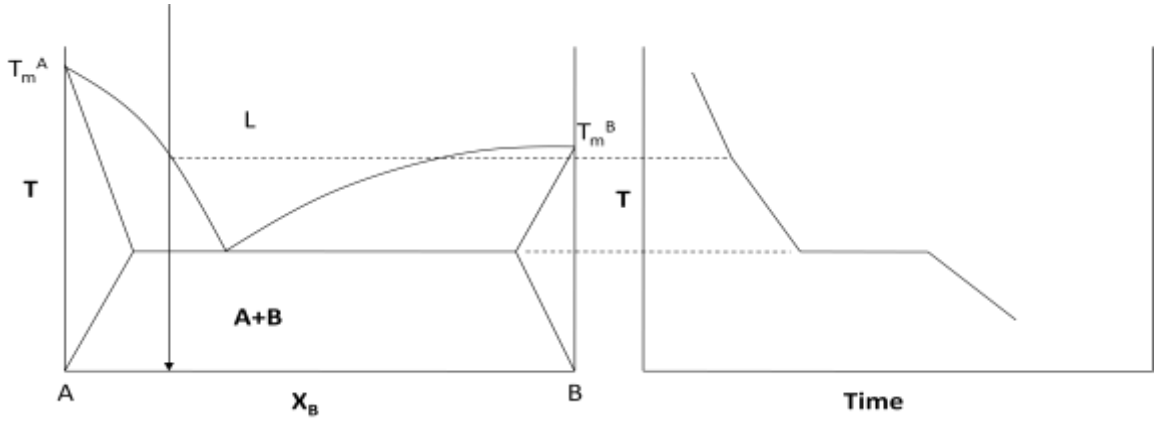

Cooling curves of a typical binary alloy with partial miscibilty

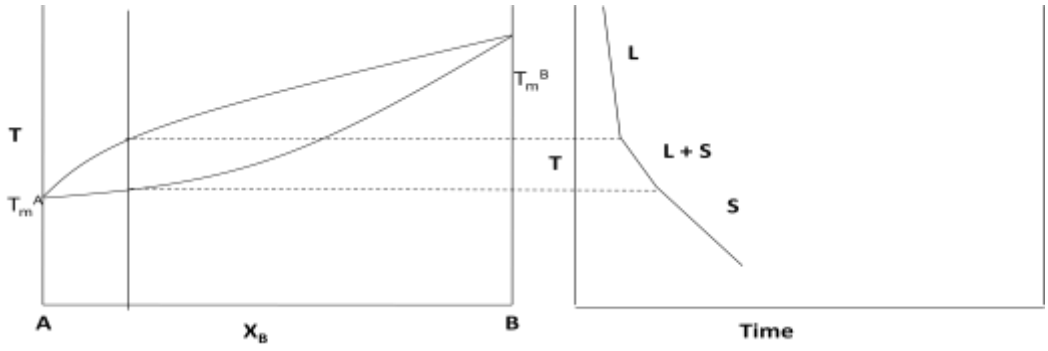

Cooling curves of a typical isomorphous system

The liquidus of alloys cannot be measured accurately, when there is supercooling. However this can be taken care by stirring the liquid or seeding it with the alloy powder. As an alloy freezes, segregation may take place, as result of which solidus temperature cannot be measured accurately. For those systems where segregation takes place annealing would help to eliminate these errors [3]. This technique is very simple, but it requires a large amount of sample and for those systems where segregation is profound, the solidus temperature cannot be measured accurately. True thermodynamic equilibrium is also not obtained. The idealized heating curves are also indicated in these figures. Even though the heating curves are better, in that they do not involve errors associated with the supercooling of the alloy, they are difficult to realize experimentally owing to the difficulties encountered in maintaining uniform temperature throughout the charge. With smaller charge more accurate values could be obtained. However, the sensitivity has to be compromised. These limitations are overcome in differential thermal analysis wherein both the small samples could be heated at pre-determined rates.

2.1.1.2 Differential thermal analysis (DTA)

Differential thermal analysis is defined by the International Confederation for Thermal Analysis and Calorimetry (ICTAC) [6] as "a technique in which the difference between the sample and a reference material is monitored against time or temperature, while the temperature of the sample in a specified atmosphere is programmed." In a typical DTA experiment, a test sample and an inert reference are heated or cooled under identical conditions and the temperature difference between them, if any, is recorded. This differential temperature is then plotted against time, or temperature. The changes in the sample such as a phase transition that lead to the absorption or evolution of heat are detected relative to an inert reference. So, it is helpful in phase transition studies.

Commercial DTA equipment is available in various configurations, which are used to investigate phase transitions up to 2273 K under various atmospheres including vacuum. The requirement of only a small quantity of the sample, wide range of measuring conditions (temperature range and atmospheres) and the enhanced sensitivity arising from the differential principle are the major advantages of this technique. However, the transitions involving small heat effects (eg. liquidus points in binary systems with steep liquidus boundaries) are often difficult to be determined, even with the enhanced sensitivity. Since DTA is a dynamic technique, the attainment of true thermodynamic equilibrium within the specimen during the measurement is not assured. The compatibility between the sample and the container material could also become a problem especially at high temperature.

2.1.1.3 Differential scanning calorimetry (DSC)

In DSC, the difference between heat flow rate (or power) to the sample and the reference sample is monitored against time, while the sample and reference crucible are heated at a predetermined rate. Depending on the method of measurement used, the DSC is classified into two types, viz. heat-flux DSC and power compensation DSC.

In a heat-flux DSC instrument, the temperature difference between the sample and the reference is recorded after suitable calorimetric calibration, as a direct measure of the difference in heat flow rates or the difference in power. In the power compensation instrument, the difference in power supplied to the sample and the reference, to keep their temperatures nearly the same, is measured directly [9].

DTA and DSC are generally employed for the study of the solidus temperature which is obtained from the extrapolated onset temperature. Sophisticated softwares are available with the commercial equipment to give the exact solidus temperature. The basic difference between the

DTA and DSC is that DTA measures the difference in temperatures, while DSC measures the difference in energy. While DTA can be used upto 2273 K, DSC can only be operated upto 1073 K, above which loss of heat by radiation makes the maintenance of identical temperature for both sample and reference difficult. Both DTA and DSC are helpful in determining the solidus temperature, but have difficulty in determining the liquidus temperature.

2.1.2 Method based on X-ray diffraction

X-ray diffraction is primarily used for studying the solid-solid equilibria. The method of measuring phase transformation temperatures involves synthesizing a series of alloys with different compositions, quenching them after annealing at a desired temperature [3, 5, 8], and measuring the lattice parameters of these specimens. In a binary alloy (under isothermal, isobaric conditions), the lattice spacing would continuously vary with composition in a single phase region, while it would remain constant in a two phase region. At the phase boundary, a sharp change in the lattice parameter would be observed. Thus when the lattice parameters of alloys are plotted against composition, the point at which a sharp change in the lattice parameter is observed, would correspond to the phase boundary. By repeating this experiment at different compositions under similar conditions, phase boundaries could be constructed. This method cannot be applied to transitions involving liquids. High temperature XRD is also an alternative for the above method, but in most cases there is reaction between the molten liquid and the container material [5].

2.1.3 The segregation method

When steep liquidus curves are encountered as discussed above, it is often difficult to determine the same by thermal halts, DTA and DSC [5]. For the determination of such liquidus equilibria, the segregation method can be used. In this method, the liquid alloy is heated either in

an inert crucible along with the solute or in a crucible made out of the solute metal itself. Segregation method could be of great value when (i) the solid-liquid mixture contains relatively large quantities of the liquid and (ii) when the solid has a higher density than that of the liquid. Under such conditions, the liquid in equilibrium can be extracted and chemically assayed. A quartz or tantalum tube is generally used for sampling the liquid alloy. If the solid settles at the bottom of the crucible that is holding the mixture, then the liquid can be sampled easily. When the solid floats on the surface, special devices are required for sampling the liquid without contamination [5]. This method is useful only for a simple binary eutectic system in the absence of any intermetallic compound. Careful sampling and accuracy of the chemical analysis are the two important prerequisites for this method. Oxidation and contamination of the alloy have to be prevented by making proper choice of the atmosphere and crucible material.

Schram et al. [9] measured the solubilities of tantalum and tungsten in liquid uranium and Dennison et al. [10, 11] measured the solubility of uranium in liquid rare-earth metals upto 2423 K, employing this method. Solubilities of C, Cr, Mo, V, Nb, Ta, W and Rh in liquid plutonium up to 1273 K were measured by Bowersox and Leary [12, 13] using a calcium fluoride crucible. Kawabata et al. [14] employed this method for measuring the liquidus temperature in the Ru-Sn system. Grain boundary diffusion and creep can often pose problems in these experiments. The accuracy of the measured values of the solubilities could vary from 5 to 15 %. Garg et al. [15] employed a method, which was similar to the segregation method, for the determination of liquidus temperature; they could also determine the composition and solid solubility of the intermetallics. In this method, a known amount of sample is weighed and taken in a single crystal cup made of the solute metal (which has a higher melting point) and placed inside a Knudsen effusion cell. The sample is then heated under vacuum in a suitable furnace to the desired

temperature (above the melting point of the sample) and held at that temperature for about 10 minutes to ensure the saturation of the melt with the cup material. Subsequently the heating is stopped and the sample is allowed to cool. The solidified solvent metal, saturated with the solute, is then selectively dissolved using a suitable reagent (usually HCl or HF) and removed from the cup. The solvent metal reacts vigorously with the reagent and leaves behind the inert solute as a finely divided residue. The single crystal cup is then cleaned, dried and weighed. From the weight loss of the cup and the initial amount of the solvent metal, the saturation solubility corresponding to the liquidus composition at the temperature of measurement is then calculated. This method is only applicable to those systems where the solubility of the solute metal in the solvent is low and the diffusion coefficient of the solvent metal is small, so that the amount of the solvent metal that diffuses into the cup is negligible compared to the weight loss of the cup.

2.1.4 Methods based on the measurement of thermodynamic activity

According to the Gibbs phase rule, the thermodynamic activity of a given component in a multi-component system depends upon the number of components in the system as well as the number of phases that coexist in equilibrium at a given temperature and pressure. Thus for the equilibria involving condensed phases in a binary system at constant pressure, the thermodynamic activity of either of the two components would be univariant in the single phase region, while it would remain constant in a two-phase region. Thus plots of activity vs. composition for a two component system will show sharp variation at the phase boundaries between the single phase regions and two phase regions and the phase boundaries respectively. Thus the compositions pertaining to the phase boundaries can be recognized from the measurements on thermodynamic activity and with the determination of phase boundaries, the phase diagram can be constructed.

The thermodynamic activity can be determined by a variety of techniques like vapor pressure measurement, gas equilibration method, thermogravimetric analysis and emf measurements etc., depending on the nature of the constituent components. The basic principles, the details of construction of the apparatus, experimental procedure, precautions as well as the merits and demerits of these techniques are discussed in detail in refs. [16-19]. Measurement of thermodynamic activity using galvanic cell emf method with molten salt electrolyte or solid electrolyte is well known [20, 21]. The only disadvantage of the emf method is that it is very time consuming and a number of samples with varying compositions have to be studied to arrive at the phase boundaries.

2.1.5 Methods based on the change of emissivity

2.1.5.1 Williams method

This method was reported by Pirani et al. [22]. It exploits the change in emissivity of the metallic surface due to formation of liquid while melting. Williams [23] designed a special apparatus for this measurement. In this method, the specimen (an alloy of known composition) is shaped in the form of a neck down bar, having a blind hole drilled into it at its center and normal to its length. This bar is then heated resistively by holding it between two electrodes. The blind hole (which serves as a black-body hole) is observed using an optical pyrometer. The thickness of the specimen is the least at the bottom of the hole, and the maximum heating takes place at this portion. The solidus temperature is obtained by determining the temperature at which the black-body condition at the bottom of the hole is disrupted and a black spot appears. The approximate liquidus temperature can also be determined using this method [24]. To accomplish this, the surface temperature of the specimen is calibrated against the black-body temperature by a series of measurements made below the solidus temperature. Subsequently the specimen is

heated above its solidus. The temperature at which the continuity of the electric circuit is lost due to the melting of the central portion is taken to be the liquidus temperature, after making appropriate corrections for the emissivity.

Though this method is simple, it fails to provide an accurate estimate of the liquidus temperature, when the alloy sample collapses due to the poor mechanical strength of the solid liquid mixture, even before complete melting takes place. Fabrication of the specimen into a neck down bar, difficulties encountered in accurate temperature control and the presence of large thermal gradients are the major limitations of this method.

2.1.5.2 The spot technique

Ackermann et al. [25] were the first group of authors to report the "spot technique". The idea was based on an observation made during a Knudsen cell measurement. Later on Ackermann and Raugh [26-28], Das et al. [29], Garg [8], Garg et al. [15, 30-33], Bhatt et al. [34] and Ananthasivan et al. [7, 35 and 36] have used this technique for the determination of phase diagrams. The spot technique makes use of the mirror effect of the molten phase of the sample. In this technique, a small amount of sample, usually of the order of 500 mg of known composition, is placed in an inert cup. This cup is centered inside a Knudsen cell and heated under high vacuum. The orifice of the Knudsen cell is viewed through a pyrometer. As long as the sample remains solid, the Knudsen orifice approximates a black body and appears as a uniformly lit bright disc and the temperature measured under such conditions would correspond to its brightness temperature. However, at the solidus temperature, when a liquid phase begins to appear, a thin film of the liquid is formed on the surface of the sample. The orifice of the Knudsen cell exhibits a dual behavior, when a reflecting mirror surface is present. It is an incandescent object with respect to the pyrometer, as the latter receives maximum radiation from

it. However, for the liquid mirror, it is a perfect black object, since the surface receives radiation from all directions within the effusion cell, except from the orifice. Hence the reflected image of the orifice appears as a black spot, when observed through the pyrometer. The temperature, at which this dark spot is sighted first, corresponds to the solidus temperature of the alloy under investigation. On further heating, several dark spots appear. When the melting is complete, all the dark spots coalesce suddenly into a single large spot. This temperature corresponds to the liquidus. In order to observe the spot effect, the cup has to be centrally located in the Knudsen cell and sufficient quantity of the sample should be taken. It is also necessary to use a non-contact mode of heating (electron bombardment or radiofrequency (RF) induction) in order to observe this effect. Using this technique, Ananthasivan et al. studied many systems like Cu-Ni [35], U-Zr [36] and more recently determined the solidus temperature of the mixed carbide fuel (Mark I) of Fast Breeder Test Reactor [37] in operation at IGCAR Kalpakkam. The schematic of the experimental set up used by Ananthasivan [7] is given in Fig. 2.2. This technique is convenient for determining the high temperature solid-liquid equilibria in alloys involving refractory metals and is amenable for glove box adaptation. In addition, this method has the additional advantages of in-situ alloying and small sample size. The main disadvantage is that phase transitions from solid to liquid at temperatures below incandescence cannot be measured.

However, Ananthasivan et al. [38] further showed that the spot technique could be extended to temperatures lower than 1073 K by using an external illumination procedure. This technique is essentially the same as the conventional spot technique, but for the reversal in the direction of illumination.

Section 2.2: Galvanic cell method

2.2.1 The galvanic cell method

The measurement of the emf of a suitable galvanic cell is one of the methods to determine the Gibbs energy formation of alloys. Therefore all the thermodynamic information about the alloys can be obtained from the Gibbs energy and its derivatives. The type of galvanic cell used in alloy studies is given as below [39];

$$A\,(s,l)\;/\;ionic\;electrolyte, A^{Z+}\,/A_X B_{(1-x)}\,, B(s,l) \qquad (2.1)$$

The more electropositive metal, *A*, is used as one electrode. A two phase mixture comprising the alloy AB and the other component metal, B constitutes the other electrode and a solution of that metal, may be in the solid or in the liquid state is used as the electolyte. At each electrode, there exist an equilibrium between A^{z+} ions in the electrolyte and *A*. Hence the open-circuit emf reflects the difference between the activities of species *A* in the two electrodes. For metallic systems most emf measurement will be carried out above 700 K. The necessary condition to be fulfilled for the application of emf measurements to determine thermodynamic properties accurately are as follows.

1. At constant temperature the emf should be constant for a very long period of time.
2. The cell must operate reversibly (i.e., the emf should not show any drift or polarization effects).
3. The charge of the electropositive ion A^{Z+} has to be known exactly and the charge transfer through the electrolyte should be the only reaction at the surface of the electrodes.
4. The electrical conduction through the electrolyte must be purely ionic; the temperature gradient should be negligible.
5. No reaction should occur between the electrodes, the electrolyte and the lead wire.
6. Concentration changes due to vapor pressure of the electrodes and the electrolyte, if any, must be taken into account.

7. B^{z+} ion should be nobler than the A^{Z+} ion in the electrolyte by at least 5 kJ / mol.
8. The furnace in which the measurements are carried out should be non-inductively wound to avoid any electrical interference with the measurements.
9. The emf measurements must be carried out without any passage of electricity through the cell. This can be achieved by using voltmeters with an impedance of greater than 10^{10} ohms.

Under these conditions, the emf *E* of the above cell is related to the partial Gibbs energy change or the thermodynamic activity of *A* by;

$$\Delta\overline{G_A} = -zFE = RT\ lna_A \tag{2.2}$$

where *R* is the gas constant, *T* the absolute temperature and a_A is the thermodynamic activity of *A* in the alloy A_xB_{1-x}. From the emf of the cell measured as function of temperature, the other partial properties of component *A* in $A_XB_{(1-x)}$ can be derived [39]:

$$\Delta\overline{S_A} = zF\left(\partial E/_{\partial T}\right) \tag{2.3}$$

$$\Delta\overline{H_A} = zF\left[T.\left(\partial E/_{\partial T}\right) - E\right] \tag{2.4}$$

Two types of electrolytes are generally used in the thermodynamic measurements, namely the liquid electrolyte and solid electrolyte.

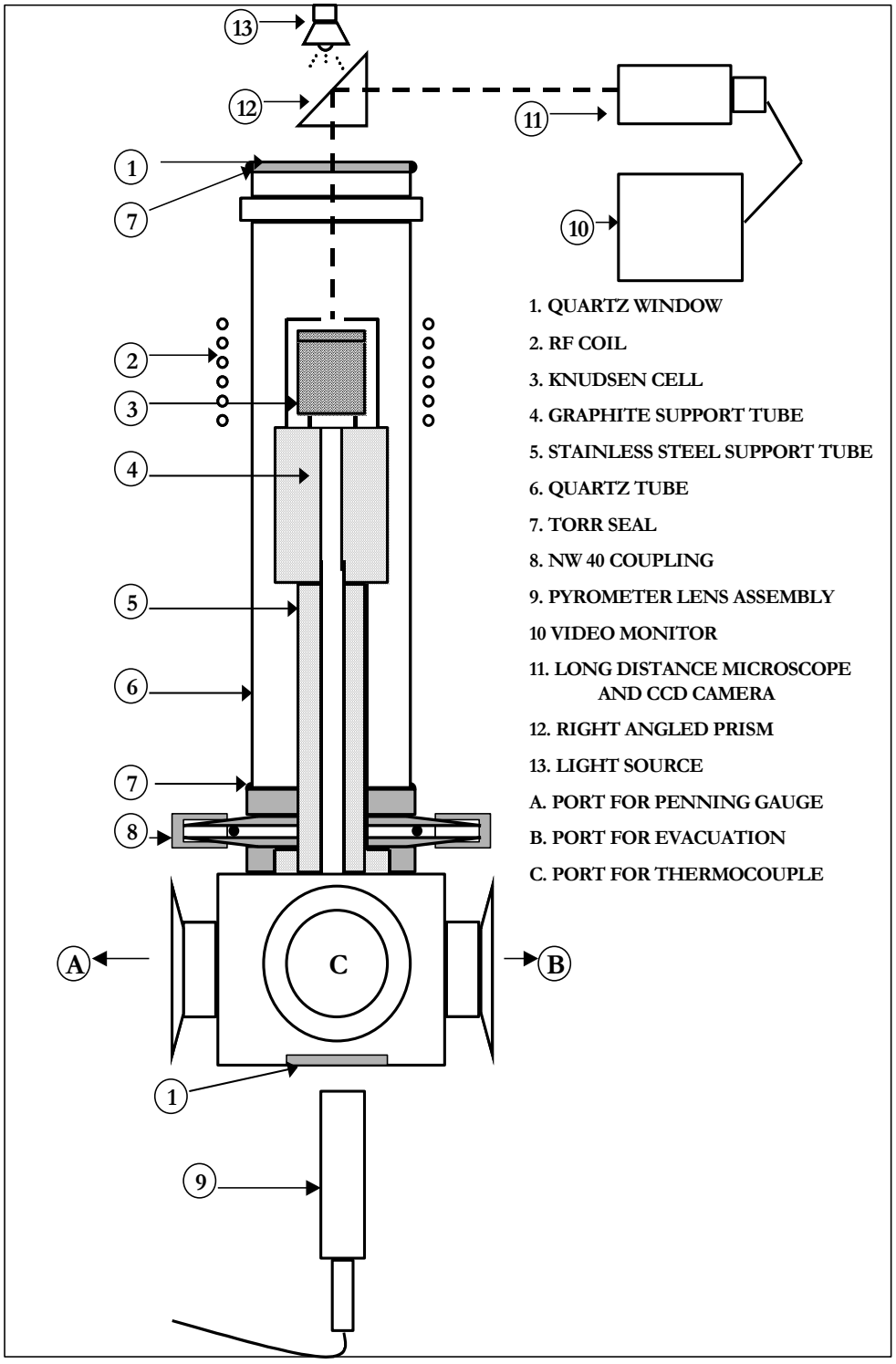

Fig. 2.2 Schematic of the experimental set up used for spot technique [7]

2 .2.1.1 Solid electrolyte galvanic cell

Solid electrolyte galvanic cells are the most convenient ones for high temperature measurements. Solid electrolyte emf cells have been widely used for the measurement of the thermodynamic properties of solid and liquid alloys both in binary and ternary systems. There are more than 30 solid electrolytes used so far for the thermodynamic studies, which may be oxides, sulfides, halides or any other type of solid material. Kiukkola et al. [40] was the first to use stabilized Zirconia (ZrO_2) to determine the oxygen potentials of metal oxides. Cation conducting as well as anion conducting solid electrolytes has been used for alloy studies. But, cation conducting solid electrolytes cannot always be used for alloy systems because they may decompose, when placed in contact with the alloy. Among the anion conducting solid electrolytes, oxide-ion-conducting electrolytes and fluoride-ion-conducting electrolytes, are extensively used for alloy studies.

Emf cells based on oxide ion conducting solid electrolyte can be represented formally as follows:

$$Pt, O_2(\mu'_{O_2}) /\ Solid\ oxide\ electrolyte /\ O_2(\mu''_{O_2}), Pt \tag{2.5}$$

The quantities, μ'_{O_2} and μ''_{O_2} represent the relevant chemical potentials of oxygen at the two electrodes, respectively. Provided local thermodynamic equilibrium is maintained at the interfaces between the various phases, the emf, E, of the cell is given by

$$E = \frac{-1}{4F}\left(\mu'_{O_2} - \mu''_{O_2}\right) + \frac{1}{4F}\int_{\mu''_{O_2}}^{\mu'_{O_2}} t_e\, d\,\mu_{O_2} \tag{2.6}$$

where $\mu'_{O_2} < \mu''_{O_2}$, F is the Faraday constant and t_e is the electronic transference number in the electrolyte. In general, it is not possible to evaluate the integral in this expression with sufficient

accuracy owing to the want of necessary information. This term can be reduced to insignificant magnitude by choosing a proper electrolyte and experimental set up. This is possible, when t_e is less than 0.01 in the oxygen chemical potential range under study.

For the thermodynamic study of alloys, the most stable oxide of the alloy components must be added to establish the oxygen potential in the electrode. Generally the difference in the standard Gibbs energies of formation for the oxides of the component elements in the alloy should be greater than 60 kJ / mol O_2, since the oxide must be equilibrated with the alloy, information on the corresponding phase diagram with oxygen becomes important. Various oxides have been used to stabilize the cubic ZrO_2 phase, but predominantly it is Y_2O_3 (also for low-temperature use in sensors), CaO (medium-temperature range), and MgO (high temperature range), where the latter is especially suitable for use in corrosive atmospheres (for example, in metallurgical slags). An extensive review on ZrO_2 based electrolytes is given by Scaife et al. [41]. Jacob et al. [42] have used ZrO_2- based solid electrolyte for determining the activity of Ga in Co-Ga and Co-Ga-Sb systems.

Fluorides of the alkaline earth metals have also been widely used as solid electrolytes in alloy studies. Mainly calcium fluoride has been used as the solid electrolyte to measure fluoride chemical potentials and thus the activities in alloys. Ure et al. [43] obtained the transport number and diffusion coefficient in CaF_2 doped with NaF and YF_3 and they showed that it is an F^-ion conductor.

Schaller and co-workers studied the application of CaF_2 as electrolyte for the determination of thermodynamic properties in alloy systems, For example, they have studied La-Ni system [44], Ni-Tb system [45] and in La-Pt system [46]. Lewin et al. [47] have studied the

Cu-Mn system. A typical cell for metal system M-Q used in the above studies can be represented as;

$$M/Q, QF_3\ /CaF_2/M-Q, QF_3/M \quad (2.7)$$

Kleykamp et al. [48] have used CaF_2 as electrolyte for the determination of Gibbs energy of formation of chromium chloride by using emf method. Also, Jacob et al. [49] and Fukuyama et al. [50] have used the emf method to determine the Gibbs energy of formation of the ternary oxides. Metal ion conducting electrolytes are also used in thermodynamic investigation. Mainly sodium-β-alumina, a Na^+ ion conductor is used as the electrolyte in the investigation of liquid Na-Sn and Bi-Na alloys by Itoh et al. [51], Tumidajski et al. [52] and others. There are reports of electrolytes conducting metal ions like Ca^{2+} [53], Li^{1+} [54], La^{3+} [55] and Sr^{2+} [56] used in the thermodynamic investigations of alloy systems. The review article by J.N. Pratt [57] has summarized the various thermodynamic investigations on different types of solid electrolytes.

2 .2.1.2 Liquid electrolytes

Liquid electrolytes used in the thermodynamic measurements enable attainment of equilibrium at a given temperature much faster than the solid electrolytes as the diffusion processes in solids are quite slow. A liquid electrolyte can be water based, with the ion responsible for establishing the corresponding potential as a solute. However, such aqueous electrolytes are usually used only for determining the thermodynamic properties of various electrolytes and their mixtures in aqueous solutions. In many such cases, special ion-selective electrodes (ISEs) are employed for the emf measurements. Investigators like Galleguillos et al. [58], Jun et al. [59] and Zhang et al. [60] have used such cells to find the thermodynamics of NaCl + $CaCl_2$, RbCl+Rb_2SO_4+CH_3OH and KCl+K_2SO_4 solutions. Rard et al. [61] reviewed the errors and difficulties in the emf measurements in aqueous solutions. Touch Instant Emf method

employed for emf measurements in metallic systems using aqueous electrolytes was reported by Kutsenok et al. [62] and Rostovtsev et al. [63], but it is considered to be highly controversial among scientific community. The standard liquid electrolytes used for measurements at elevated temperatures are based on molten salts in which an ionic compound is dissolved to generate the ions responsible for establishing the emf. A detailed discussion on determinating of the thermodynamic properties of alloy systems using molten salts is given in the following section.

2 .2.1.2.1 Molten salt electrolytes

Molten salt electrolyte cells are similar to concentration cells with liquid or solid electrodes and aqueous electrolytes. The cell used to measure the emf of an alloy system is similar to the cell used in equation (2.1)

$$A\ (s,l)\ /\ AN\ salt(in\ solution)/AB(alloy), B(s,l) \qquad (2.7)$$

The overall cell reaction in this case is given by;

$$< A > \rightarrow [A] \qquad (2.8)$$

The change in the chemical potential, $\Delta\overline{G_A}$ for the transfer of A from the pure component at unit activity to the alloy, where the activity of this component has a lower value, a_A is given by the equation (2.9) that is similar to equation (2.2).

$$\Delta\overline{G_A} = \overline{G_A} - G_A^0 - zFE = RT\ lna_A \qquad (2.9)$$

An important aspect in emf measurements using molten salt as an electrolyte is the purification of the electrolyte prior to its use, in order to make sure that it does not contain any moisture. The accuracy of thermodynamic functions such as partial excess Gibbs energy, activity and activity coefficient resulting from the emf method is about 2-5 % depending on the particular system, while partial enthalpy and entropy calculated from slopes entail higher error that could

even exceed 50 %. In molten salt electrolytes, the emf of the cell will drift, in the case of metal electrode dissolution in the molten salt. This may be due to electron conducting properties of the electrolyte, or the possibility of cations of more than one valency for a given metal in the melt [20].

The most common liquid electrolyte based on salts is the eutectic mixture of LiCl and KCl which melts at 627 K [64]. Gasior et al. studied in the thermodynamic properties of Cu-Li [65], Al-Cu-Li [66] and Li-Mg [67] systems using this electrolyte. Vassiliev et al. [68, 69] measured the partial Gibbs energies in the systems In-Sn, Sb-Sn and In-Sb-Sn in the liquid state. The activity of zinc in liquid Pb-Sn-Zn [70] and liquid Cu-Zn alloys [71] was determined by the same method. Examples of other salt mixtures used in such emf measurements are LiCl-RbCl for the Lu-Pb system by Borzone et al. [72] and ternary KCl-LiCl-$BaCl_2$ mixture for the Pb-Pd system by Vassiliev et al. [73]. Fujiwara et al. [74] used molten lithium silicate electrolyte to determine the thermodynamic properties of molybdenum silicides.

Section 2.3: Calorimetry and Software

2.3.1: Calorimetry and broad classification

A calorimeter is an instrument that measures the thermal energy changes associated with the change in the state of a material. The change in the state of material can be a change of phase, temperature, pressure, volume, chemical composition or any other property of the material, which is associated with the change in thermal energy. It is difficult to separate the thermal energy associated with the change of state from the other forms of energy and hence its measurement is complex. A calorimeter consists of a reaction vessel, known as the calorimeter proper in which the thermal processes occur and a surrounding shield or jacket which may be kept at a constant or varying temperature. Generally heat capacities of solid substances, integral

enthalpies of mixing of liquid alloys, enthalpies of formation of solid alloys and the enthalpies of transformation and fusion of pure substances are measured by calorimetry. Of course, no single apparatus of any one type can be employed to measure all these quantities. Several types of calorimeters are used for the measurements in experimental thermodynamics. Experimentalists have proposed many classifications.

2.3.1.1 Classification of calorimeters

The temperature of the calorimeter vessel $T_{C,}$ the temperature of the surrounding shield T_S, and the calorific power W, i.e., the heat produced in unit time, are the three important parameters that are usually measured in a calorimetric experiment. Zielenkiewicz [75-77] has classified the calorimeters based on the temperature of the calorimetric vessel and the surrounding shield. The types of calorimeters are as follows:

a) Adiabatic calorimeter – temperature of the calorimetric vessel and the surrounding shield remain identical throughout the experiment ($T_C = T_S$ varying)
b) Isoperibol calorimeter – the calorimetric vessel undergoes a change in temperature, while surrounding shield is maintained at constant temperature (T_S = constant, T_C = varying).
c) Phase change calorimeter or true isothermal calorimeter – the heat exchange inside the experimental cell is balanced by phase change in a two-phase mixture surrounding the cell ($T_C = T_S$ = constant).
d) Power compensated isothermal calorimeter – same as above, but here the heat exchange inside the experimental cell is compensated by an electrical power ($T_C = T_S$ = constant).
e) Heat flow calorimeter or conduction calorimeter – same as isoperibol calorimeter, but here the heat flux between the reaction cell and a large isothermal heat sink is measured (T_S = constant, T_C varying).

Of these, the isoperibol and adiabatic calorimeters can be operated in the static or dynamic mode and hence they can be further classified based on the mode of operation.

Castanet et al. [78] have broadly classified the calorimetric techniques that are used extensively in experimental thermochemistry into two groups,

1. Calorimetry of non-reacting systems
2. Calorimetry of reacting systems

Calorimetry of non-reacting systems is aimed at the determination of heat capacities and enthalpy increments and enthalpies of phase transformations. Only physical changes and no chemical change take place in these measurements. On the other hand, reaction calorimetric methods are used for the determination of the partial or integral enthalpies of mixing of liquid alloys and the enthalpies of formation of the intermetallic compounds at the ambient temperature as well as at high temperatures. Here the system undergoes changes in chemical composition and the accompanying enthalpies of reaction are measured.

Enthalpies of formation of alloys and solid solutions can be derived by two methods. One is the indirect method or two-stage method wherein the enthalpies of formation are derived from the measured enthalpies of other reactions such as solution, combustion etc., carried out separately on the components and the compound. The enthalpy of formation is then obtained as the difference between the two values by applying the Hess's law of heat summation. The other is direct reaction calorimetry or single stage method in which the reaction of the formation of the compound occurs during the calorimetric experiment. Methods based on mode of operation, based on principle of measurement and construction are other ways of classifying the calorimeters [79].

2.3.1.2 High temperature solution calorimetry

Solution calorimetry is one of the methods used to measure the enthalpies of formation of intermetallic compounds in the solid state at room temperature. The application of solution calorimetry to alloy thermochemistry is based on the dissolution, in separate runs, of the intermetallic compound (prepapred and characterized) and its components in a suitable bath. Acid solution calorimetry at ambient temperature using HCl as the solvent is well known [80]. In high temperature solution calorimetry the enthalpy of formation of an alloy $A_xB_{(1-x)}$ at 298.15 K is determined by measuring the thermal effects of dissolution of the alloy $A_xB_{(1-x)}$ and its constituent elements , *A* and *B* in the same metallic bath at the same temperature. The thermal effects of dissolution, (Q^E)of the solute metal, *A* in the liquid metal solvent, S are measured as a function of the concentration of *A*, by dropping the samples from the ambient temperature into the solvent at the experimental temperature, T in the calorimeter. In general, the thermal effects of dissolution are independent of the concentration of the solute in the solvent in the dilute solutions, Hence the thermal effect of dissolution of metal A at infinite dilution ($Q_A^{E,\infty}$), for example is obtained taking the mean of the thermal effects of dissolution. The thermal effects of dissolution of B at infinite dissolution ($Q_B^{E,\infty}$) and that of the intermetallic compound, $A_xB_{(1-x)}$ at infinite dissolution ($Q_{A_xB_{(1-x)}}^{E,\infty}$) are obtained by similar measurements in the liquid solvent S and at the same temperature. The enthalpy of formation of the intermetallic compound $A_xB_{(1-x)}$ is then calculated from the following equation;

$$\Delta_f H_{298.15}^0 < A_xB_{(1-x)} > = xQ_A^{E,\infty} + (1-x)\, Q_B^{E,\infty} - Q_{A_xB_{(1-x)}}^{E,\infty} \qquad (2.10)$$

The most important factor is the choice of solvent. The solvent must dissolve solutes in a reasonable time and it must not have high vapor pressure so as not to cause losses by evaporation and it must give moderate heats of dissolution of solutes to minimize errors. The enthalpies of

dissolution of metal or alloy solutes are large when aqueous inorganic solvents, such as hydrochloric acid or hydrofluoric acids are used as solvent baths, compared to the enthalpies of formation and so, the accuracy is often very poor. Liquid metal solvents are preferred, since the enthalpies of solution will be of the same magnitude as the enthalpies of formation of the alloys. Liquid tin has been used as a favored solvent for many systems, because it can dissolve many metals and alloys at moderate temperatures. Kleppa et al. [81] extensively used tin as solvent for binary and ternary alloys to determine the enthalpies of formation. Many other liquid metal solvent baths such as aluminium [82, 83], gallium [84], copper [85], lead [86], and germanium [87] have also been used for the determination of enthalpies of formation of alloys. Molten alloys also have been used as a solvent instead of pure metal. Kleppa and Hong [88- 90] used $Mn_{0.6}Ni_{0.4}$ as solvent to determine the enthalpies of formation of carbides. Cemic and Kleppa [91-93] used molten $Ni_{0.6}S_{0.4}$ as the solvent for the measurement of enthalpies of formation of sulfides.

2.3.2 Software

There are many software which has been developed since 1970 for calculation of phase diagram and thermodynamic properties like Thermocal, pandat, malt2 and FactSage. Thermocal also produces DICTRA used for simulation of diffusion controlled phase transformation [94]. Pandat is generally used for multicomponent phase diagram calculation [95]. Malt2 is used to generate thermodynamic database like Gibbs energy minimization, mass action law and associated enthalpy consideration and construction of chemical potentials from the viewpoint of material chemistry [96]. The present study uses FactSage and Miedema's model which is described in this section.

2.3.2.1 Miedema's empirical model

Miedema and his co-workers [97-99] have proposed a semi-empirical model known as the "macroscopic atom model" for predicting the enthalpies of formation of binary alloys of arbitrary combinations of metals with accuracy comparable with that of the experimentally measured quantities. It is based on the assumption that atoms as they are embedded in a pure metal can be chosen as the reference system and that many of the considerations that apply to a situation, where macroscopic blocks of two dissimilar metals are brought into contact, remain valid for suitably defined 'atoms in the metallic state'. When this assumption is valid, there is little difference between the interfacial energy between the blocks of two metals and the enthalpy of formation of solid alloy (for liquid alloys also called heat of mixing) formed by the two metals. Energy considerations are made in terms of contact interactions that take place at the interface between dissimilar atoms. In this model, there are two parameters that play an important role in the energy effects of alloy formation. One is an electron density parameter, $n_{ws,}$ and the other is an electronegativity parameter, ϕ^*. This model takes care of all these parameters to compute the enthalpies of formation [100]. It is based on the regular solution model.

2.3.2.2 FactSage

FactSage is the fusion of two well-known software packages in the field of computational thermochemistry: FACT-Win (formerly F*A*C*T) and ChemSage (formerly SOLGASMIX). F*A*C*T - Facility for the Analysis of Chemical Thermodynamics - started in 1976 as a joint research project between two universities, McGill University (W.T. Thompson) and the École Polytechnique de Montréal (C.W. Bale and A.D. Pelton). The initial programs [101] were written in FORTRAN on punched cards and performed chemical thermodynamic calculations involving pure substances and ideal gases. In 1979 F*A*C*T On-Line was offered as an interactive program through the McGill University MUSIC system (accessed via Datapac and Telenet

telephone links) where it was mainly used as a teaching tool [102, 103]. Solution programs and databases were added together with the POTCOMP and TERNFIG algorithms for optimizing, calculating and plotting binary and ternary phase diagrams [104], [105]. In the 1990's the system evolved into the PC-based program FACT-DOS [106] that offered unlimited access to the software and databases. Eriksson et al. [107] developed Chemsage an Integrated Thermodynamic databank System, initially running under DOS. Finally in April 2001 F*A*C*T and ChemSage were merged into one unified package called FactSage 5.0 [108]. Subsequently it was upgraded and Factstage 6.2 was launched in November 2010 and this version has been installed in our laboratory.

The FactSage main menu offers access to the modules of the package. These are grouped into four categories:

1. Info – This includes detailed slide shows (Microsoft Power Point® presentations) of most of the program modules and general information with Frequently Asked Questions on FactSage and its databases.

2. Databases – These program modules enable the user to view, manipulate and edit the pure substances and solution databases that may be private (read/write) or public (read only).

3. Calculate – These modules are the central programs of FactSage. They permit the calculation of phase diagrams and thermochemical equilibria in various forms with direct access to the databases.

4. Manipulate – This group offers various graphical and tabular program modules for post-processing the results and manipulating the calculated phase diagrams and other figures.

The most important module is the calculate module. One can interact with the software and databases in a variety of ways and calculate thermochemical equilibria in various forms. It has

many submodules like Reaction, Predom, EpH, Equilib and Phase diagram and Figure. In the present study Reaction submodule was used to compute the Gibbs energies of formation of the oxides of U, Sn, Th, Y and Mo.

References

1. A.D. Pelton in: Physical Metallurgy, Part IV Ed. Vol. 1, R.W. Cahn and P. Hassen, 1996, p. 525.
2. A.D. Pelton and W.T. Thompson in: Progress in Solid State Chemistry, Vol. 10, Part 3, p. 119.
3. R.A. Buckley, in: Techniques of Metals Research, Editor: R.A. Rapp, Interscience, New York, Vol. IV, part I, p. 425.
4. J.B. Mac Chasney and P.E. Rosenberg in: Phase diagrams – Materials Science and Technology, Editor: A.M. Alper, Academic Press, New York, Vol. 1, Ch. 3, p. 123.
5. G.V. Raynor, Physical metallurgy, 2nd Ed., Editor: R.W. Cahn, Noth Holland Publishing Company, Amsterdam, 1970, p. 309.
6. G. Hohne, W. Hemminger, H.-J. Flammersheim, Differential Scanning Calorimetry, Springer, Berlin, Springer 1995, p. 43.
7. K. Ananthasivan, Ph.D. thesis, University of Madras, 2002.
8. S.P. Garg, Ph.D.thesis, Bombay University, Bombay, India (1980).
9. C.H. Schram, P. Gordon, A.R. Kaufman, Trans. AIME, 188 (1950) 195.
10. D.H. Dennison, M.J. Tschetter, K.A. Gschneidner, Jr., J. Less Common Metals, 10 (1966) 108.
11. D.H. Dennison, M.J. Tschette, K.A. Gschneidner, Jr., J. Less Common Metals, 11 (1966) 423.
12. D.F. Browersox, J.A. Leary, J. Nucl. Mater. 21 (1967) 219.
13. D.F. Browersox , J.A. Leary, J. Nucl. Mater. 27 (1968) 181.
14. R. Kawabata, M. Myo-Chin, M. Iwase, Met. Trans. B 29 (1998) 577.

15. S.P. Garg, Y.J. Bhatt and R. Venakatasubramani, Mater. Sci. Forum, Vol. 3, Trans Tech Publications Ltd., Switzerland, 1985, p. 419.
16. O. Kubaschwski, E.L. Evans, C.B. Alcock, Metallurgical Thermochemistry, Pergamon Press, N.Y., 1967.
17. R.A. Rapp and D.A. Shores, in: Physico-chemical Measurements in Metals Research, Part 2, Editors: R.A. Rapp, Interscience Publishers, John Wiley, N.Y., 1970, p. 23.
18. P. Gordon, Principles of Phase Diagrams in Materials Systems, Mc Graw-Hill, N.Y. 1968, p. 89.
19. Y.K. Rao, in Phase Diagrams, Vol. I, Editor: A.M. Alper, Academic Press, N.Y. 1970, p. 56.
20. Z. Moser, in : Calculation of Phase Diagrams and Thermochemistry of Alloy Phases, Editors: Y.A. Chang and J.F. Smith, Conf. Proc. Met. Soc., AIME, Warrendale, PA 1979, p. 242.
21. H. Kleykamp, Ber. Bunsenges. Phys. Chem. 87 (1983) 777.
22. M. Pirani, H. Alterthurn, Electrochem. 29 (1923) 5 (cited from Ref. 8 p. 4.).
23. J.T. Williams, Trans. AIME 203 (1955) 345. (cited from Ref. 8 p. 4).
24. D.S. Evans, A. Prince, Metal Science 12 (1978) 600.
25. R.J. Ackermann, E.G. Rauh, J. Phys. Chem. 73 (1969) 769.
26. R.J. Ackermann, E.G. Rauh, High Temp. Sci. 4 (1972) 272.
27. R.J. Ackermann, E.G. Rauh, High Temp. Sci. 4 (1972) 496.
28. R.J. Ackermann, S.P. Garg, E.G. Rauh, J. Am. Ceram. Soc. 60 (1977) 341.
29. D. Das, M.S. Chandrasekaraiah, High Temp. Sci. 161 (1986) 21.
30. S.P. Garg, R.J. Ackermann, J. Nucl. Mater. 64 (1977) 265.

31. S.P. Garg, R.J. Ackermann, Trans. IIM 32(1979) 62.

32. S.P. Garg, R.J. Ackermann, Scripta Met. 13 (1979) 611.

33. S.P. Garg, R.J. Ackermann, J. Nucl. Mater. 88 (1980) 309.

34. Y.J. Bhatt, R. Venkatramani, Y.S. Sayi, S.P. Garg, Metals Materials and Processes 2 (1) (1990), p. 49.

35. K. Ananthasivan, S. Balakrishnan, I. Kaliappan, S. Anthonyswamy, R. Pankajavalli, P. R. Vasudeva Rao, J. Alloys Compd. 2681 (2009) 275.

36. K. C. Harikumar, S. Balakrishnan, K.Ananthasivan, S. Anthonyswamy, V. Ganesan, P. R. Vasudeva Rao, Proc. XL CALPHAD 2011, Rio de Janerio, Brazil (2011) 191.

37. Ananthasivan et al., IGC News letter 96 (2013), Published by Indira Gandhi Centre for Atomic Research, p. 8.

38. K. Ananthasivan, I. Kaliappan, P. R. Vasudeva Rao, J. Alloys Compd. 352 (2003) 148.

39. Herbert Ipser, Adolf Mikula, Iwao Katayama, Calphad 34 (2010) 271.

40. K. Kiukkola, C. Wagner, J. Electrochem. Soc., 104 (1957) 379.

41. P.H. Scaife, D.A.J. Swinkels, S.R. Richards, High Temp. Sci. 8 (1976) 31.

42. Sh. Priya, K.T. Jacob, J. Phase Equilib. 21 (2000) 342.

43. R.W. Ure Jr., J. Chem. Phys. 26 (1957) 1363.

44. J. Dischinger, H.-J. Schaller, J. Alloys Compd. 312 (2000) 201.

45. Q. Rong, H.-J. Schaller, J. Alloys Compd. 365 (2004) 188.

46. S. Reimann, H.-J. Schaller, J. Alloys Compd. 419 (2006) 133.

47. K. Lewin, D. Sichen, S. Seetharaman, Scand. J. Metall. 22 (1993) 310.

48. H. Kleykamp, J. Alloys Compd. 321 (2001) 138.

49. St. Forsberg, P. Wikström, E. Rosén, Metall. Mater. Trans. B 33 (2002) 385.

50. H. Fukuyama, K. Shimizu, K. Nagata, High Temp. Mater. Processes 23 (2004) 335.

51. M. Itoh, Z. Kozuka, J. Mater. Sci. 26 (1991) 5221. P.J. Tumidajski, Can. J. Chem. 72 (1994) 369 (cited from Ref. 39 p. 278).

52. P.J. Tumidajski, Can. J. Chem. 72 (1994) 369.

53. G. Róg, A. Kozlowska-Róg, M. Bucko, K. Haberko, Solid State Ion. 176 (2005) 991.

54. G. Róg, W. Kucza, A. Kozlowska-Róg, J. Chem. Thermodyn. 36 (2004) 473.

55. G. Róg, A. Kozlowska-Róg, J. Chem. Thermodyn. 34 (2002) 1311.

56. M.A. Swetnam, R.V. Kumar, D.J. Fray, Metall. Mater. Trans. B 37 (2006) 381.

57. J.N. Pratt, Metall. Trans., 21A (1990) p. 1223.

58. H.R. Galleguillos, F. Hernández-Luis, L. Fernández-Mérida, M.A. Esteso, Chem. Res., Synop. (1999) p. 462 (cited in Ref.39 p. 278).

59. Zh. Jun, G.Sh. Yang, X.Sh. Ping, Y. Yan, Fluid Phase Equilib. 226 (2004) 307.

60. J. Zhang, Sh.-Y. Gao, Sh.-P. Xia, J. Chem. Eng. Data 49 (2004) 444.

61. J.A. Rard, S.L. Clegg, J. Chem. Thermodyn. 27 (1995) 69.

62. I.B. Kutsenok, V.A. Geiderikh, I.A. Valuev, Vestnik Moskov. Univ. Ser. II, Khim 21 (1980) 554. (cited in Ref. 39 p. 278).

63. R.N. Rostovtsev, J. Physique IV France 112 (2003) 341.

64. J. Lumsden, Thermodynamics of Molten Salt Mixtures, Academic Press, London, New York, 1966.

65. W. Gasior, B. Onderka, Z. Moser, A. Debski, T. Gancarz, CALPHAD 33 (2009) 215.

66. Z.Moser,W. Gasior, B. Onderka, F. Sommer, Z. Kim, J. Phase Equilib. 23 (2002) 127.

67. W. Gasior, Z. Moser,W. Zakulski, G. Schwitzgebel, Metall. Mater. Trans. A 27 (1996) 2419.

68. V. Vassiliev, Y. Feutelais, M. Sghaier, B. Legendre, Thermochim. Acta 315 (1998) 129.

69. V. Vassiliev, Y. Feutelais, M. Sghaier, B. Legendre, J. Alloys Compd. 314 (2000) 198.

70. N. David, V. Vassiliev, J. Hertz, J.-M. Fiorani, M. Vilasi, Z. Met.kd. 95 (2004) 123.

71. N. David, J.-M. Fiorani, M. Vilasi, J. Hertz, J. Phase Equilib. 24 (2003) 240.

72. G. Borzone, N. Parodi, R. Ferro, M. Gambino, V. Vassiliev, J.P. Bros, J. Alloys Compd. 220 (1995) 111.

73. V. Vassiliev, G.F. Voronin, G. Borzone, M. Mathon, M. Gambino, J.P. Bros, J. Alloys Compd. 269 (1998) 123.

74. H. Fujiwara, Y. Ueda, J. Alloys Compd. 441 (2007) 168.

75. W. Zielenkiewicz and E. Margas, Nauch. Appara. Sci. Instrum., 1 (1986) 55.

76. J. Rouquerol and W. Zielekiewicz, Thermochim. Acta, 109 (1986) 121.

77. W. Zielenkiewicz, J.Thermal Anal., 33 (1988) 7.

78. R. Castanet, NATO-ASI, Kiel, August (1987) 16-27.

79. R. Babu, Ph.D. thesis, University of Mumbai, 2002.

80. J.P. Coughlin, in: Experimental Thermochemistry, Vol. 2, Editor: H.A. Skinner, Interscience, London, 1962, p. 293.

81. O. J. Kleppa, J.Phys. Chem., 60 (1956) 842.

82. F. Sommer, J. Therm. Anal., 33 (1988) 15.

83. K. Nagarajan, R.Babu and C.K. Mathews, J. Nucl. Mater. 20 (1993) 142.

84. H. Said and R. Castanet, J. Less-Common Met. 68 (1979) 213.

85. P. Merker, J. Less-Common Met. 169 (1991) 23.

86. W. Vogelbein, M. Ellner, and B. Pdredel, Thermochim. Acta. 44 (1981) 141.

87. J. Rogez, R. Castanet, Mater. Chem. Phys. 9 (1983) 597.

88. O. J. Kleppa, K. C. Hong, J. Chem. Thermodyn. 10 (1978) 243.

89. O. J. Kleppa, K. C. Hong, J. Chem. Thermodyn. 10 (1978) 243.

90. K. C. Hong, O. J. Kleppa, J. Chem Thermodyn.10 (1978) 797.

91. L. Cemic, O. J. Kleppa, Geochim. Cosmoschim. Acta. 50 (1986) 1633.

92. L. Cemic, O. J. Kleppa, Phys. Chem. Miner. 14 (1987) 52.

93. L. Cemic and O. J. Kleppa, Phys. Chem. Miner.16 (1988) 172.

94. A.K. Niessen, A.R. Miedema in: Proc. NATO Advanced Study Institute on Thermochemistry of Alloys, Kiel, FRG, 1987, Ed. H. Brodowsky and H.-J. Schaller, Kluwer Academic Publishers, Dordrecht, 1989, p. 29.

94 J.O Andersson, T. Helander, L. Hoglund, P. Shi, B. Sundman, Calphad 26 (2002) 273.

95 S.L. Chen, S. Daniel, F. Zhang, Y.A. Chang, X.Y. Yan, F.Y. Xie, R. Schmid Fetzer, W.A. Oates, Calphad 26 (2002) 175.

96 H. Yokokawa, S. Yamauchi, T. Matsumoto, Thermochim. Acta 245 (1994) 45.

97. F.R. deBoer, R. Boom, W.C.M. Mattens, A.R. Miedema and A.K. Niessen, Cohension in Metals, North-Holland Publishing Co., Amsterdam, 1988.

98. A.K. Niessen, F.R. deBoer, R. Boom, P.F. deChatel, W.C.M. Mattens, A.R. Miedema, Calphad, 7 (1983) 51.

99. B. Prabhakara Reddy, Ph.D.thesis, University of Madras, 2000.

100. A.D. Pelton, C.W. Bale and W.T. Thompson, Application of phase diagram in metallurgy and ceramics, Proc. NBS workshop Gaithersburg, 1977, p. 1077.

101. W.T. Thompson, C.W. Bale, A.D. Pelton, Engineering Education, Nov. 1979, p. 201.

102. W.T. Thompson, A.D. Pelton, C.W. Bale, J. of Metals, 1980, 32, p. 18.

103. P.L. Lin, A.D. Pelton, C.W. Bale, W.T. Thompson, CALPHAD, 1980, 4, p. 47.

104. C.W. Bale, A.D. Pelton, CALPHAD, 1982, 6, p. 255.

105. C.W. Bale, A.D. Pelton and W.T. Thompson, F*A*C*T 2.1 – User's Manual, Ecole Polytechnique de Montreal / Royal Military College, Canada, July 1996.

107. G. Eriksson, K. Hack, Metall. Trans. 1990, 21B, p. 1013.

108. C.W. Bale, P. Chartrand, S.A. Degterov, G. Eriksson, K. Hack, R. Ben Mahfoud, J. Melançon, A.D. Pelton, S. Petersen, CALPHAD, 2002, 26, p. 189.

CHAPTER -3-Experimental

Section 1: Determination of phase transformation temperatures by using the spot technique

3.1.1 Synthesis and preparation of intermetallic compound by arc melting

3.1.1.1 Starting materials

Nuclear grade uranium metal (99.99%) was obtained from BARC, Mumbai in the form of rods (4 mm diameter and about 0.5 cm long). Spectroscopic grade high purity (99.99%) tin metal was procured from M/s. BDH, Poole, U.K. Uranium discs as obtained were cut into smaller pieces by using a diamond cutter procured from M/s. Struers, Copenhagen. These small cut pieces of uranium were first cleaned in concentrated nitric acid thoroughly, then washed with distilled water and stored for few minutes in acetone before melting.

3.1.1.2 Arc melting furnace

In an arc melting furnace, an electric arc is generated by using direct current between two conductors. The tungsten electrode with negative polarity and the hearth with positive polarity. The negative electrode is heated principally by the direct impingement of positive ions coming from the anode and the sample pool receives its greatest amount of heat from the collision of thermionically emitted electrons from the cathode [1]. The molten metal, which forms the anode, is contained in the water –cooled metallic hearth. The melting process results in the vaporization and removal of selected volatile impurities from the liquid metal. In addition, due to the large thermal gradient between the cathode and the molten metal, results in direct solidification which enhances the columnar grain

structure [1]. The basic feature of arc melting furnace is a high temperature electric arc as a heat source, a liquid cooled metallic hearth and an enclosure in which the melting is carried out. In general, three types of arc melting furnaces, namely, vertical arc, tri-arc and horizontal arc furnaces are known. In this study, a tri-arc furnace has been used for the preparation of all the samples.

3.1.1.3 Tri-arc furnace

A tri-arc melting furnace was used for preparing the intermetallic compounds in this study. It is a compact furnace and a schematic of this unit is given in Fig. 3.1. This unit consists of an upper section and a lower water-cooled section, separated by a pyrex glass observation tube. The observation tube also serves as an insulator between the upper and lower electrodes. Power and water are fed to each of these sections by water-cooled power cables. In the upper section, there are three copper rods which carry tungsten electrodes. Each of these rods is mounted onto a swivel ball which allows angular as well as vertical movements. The bottom section contains a tapered opening, which accepts a variety of copper hearths. The melting is done with high purity argon or helium gas at a pressure 1-10 Pa inside the furnace. In a typical experiment, the chamber is first filled with the inert gas and evacuated and then melting is carried out at that pressure. In order to remove the residual oxygen in the arcing chamber, zirconium or uranium was used as an oxygen getter which was melted before melting the actual alloy components. The alloy button thus formed was flipped two or three times for homogenization. Fig. 3.2 and Fig. 3.3 shows the photograph of the arc melting set up, the sample and getter, the buttons obtained after melting. All the alloys of uranium and tin prepared by the above procedure are highly

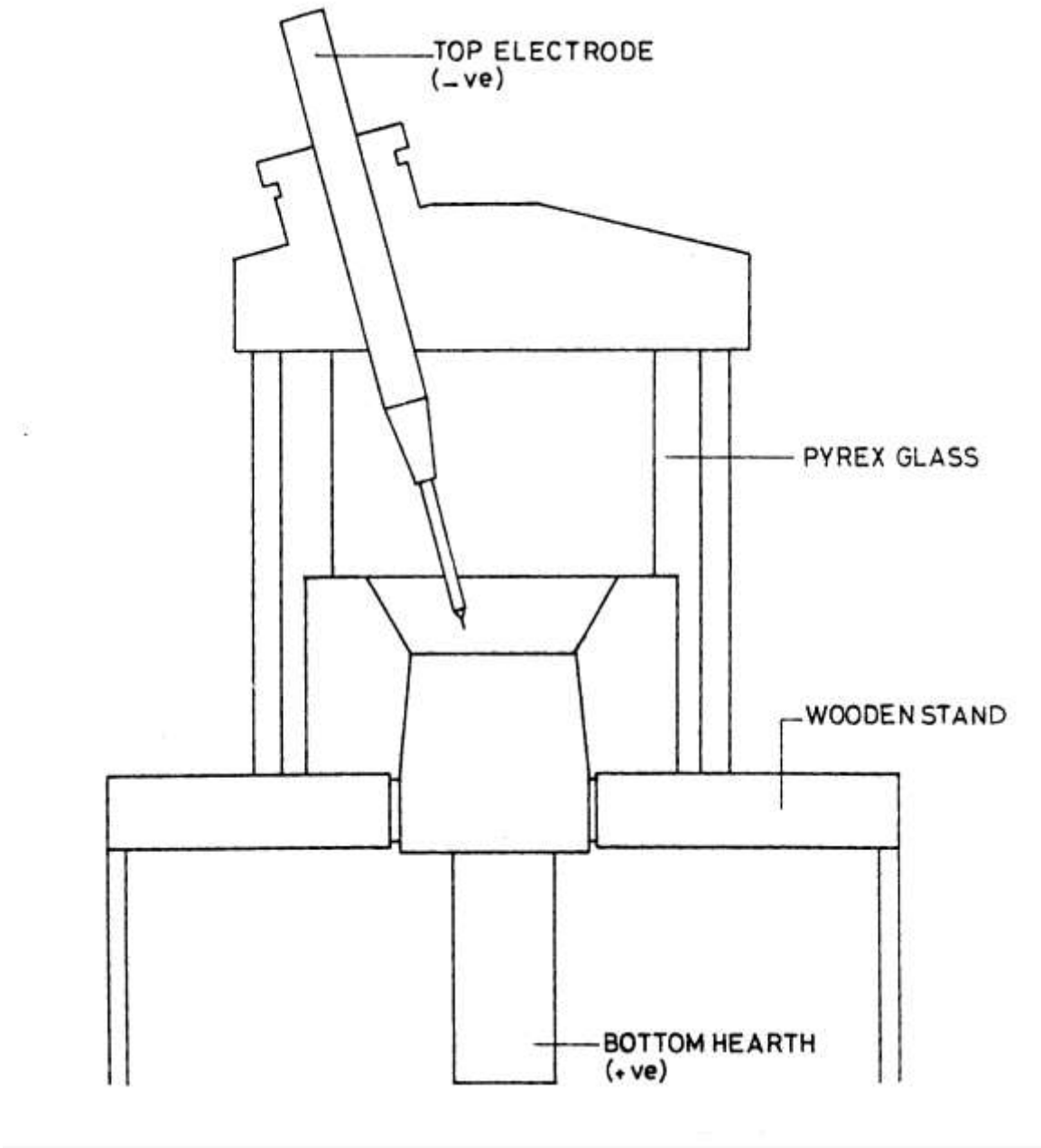

Fig. 3.1 Schematic of the tri-arc furnace

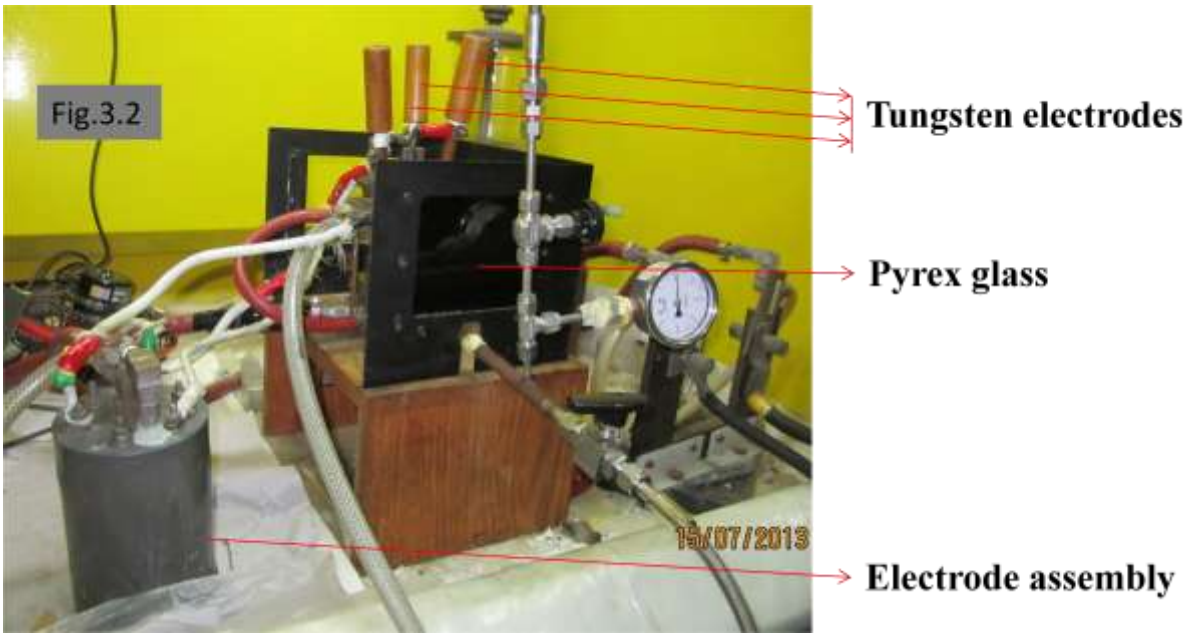

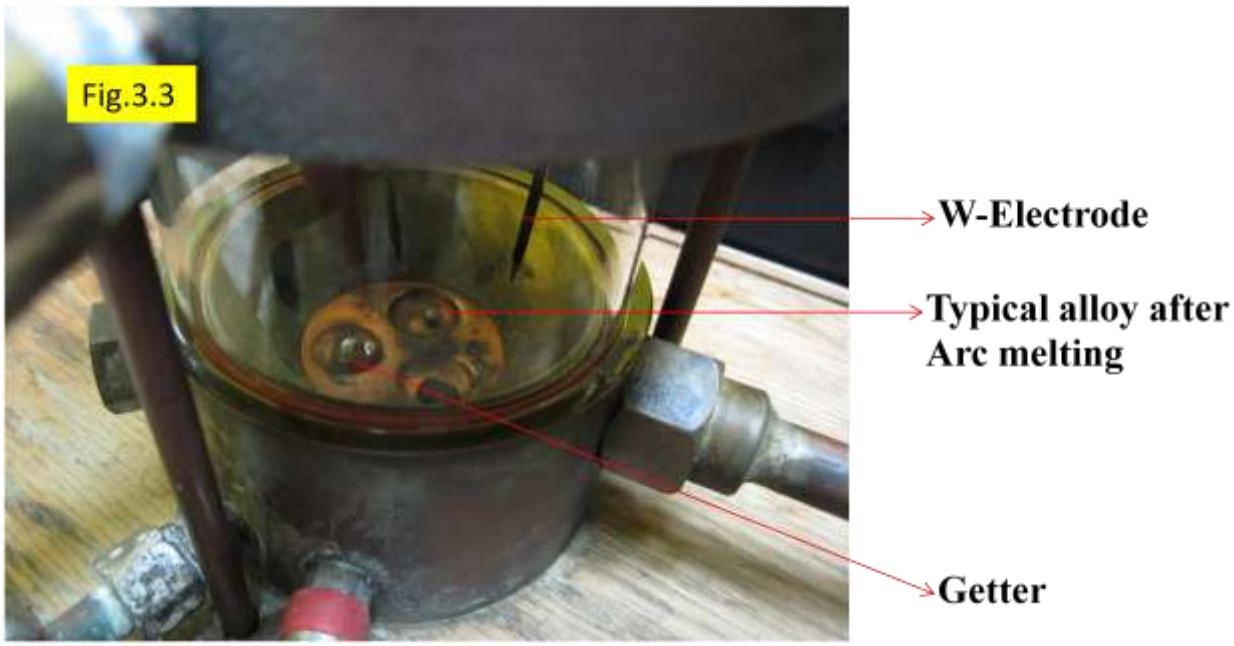

Fig. 3.2 Photographs of the arc melting set up and Fig. 3.3 Sample and getter after melting

pyrophoric and are susceptible to oxidation. So, all these alloys were handled and stored inside an argon atmosphere glove box.

3.1.2 Vacuum sealing, annealing and characterization

The alloy buttons thus prepared were wrapped inside tantalum foils and then encapsulated inside an one end closed quartz tube. The other end of the quartz tube was connected to a vacuum system. The quartz tube was then evacuated to a low pressure of nearly $10^{-2} – 10^{-3}$ Pa and sealed.

The alloys sealed in quartz ampoules were heated at 1173 K for 20 days for annealing the samples. After annealing, the quartz tube was broken inside the argon box. Powders of the samples were obtained by grinding them with the help of a mortar and pestle made out of agate. Powdered samples were then taken inside a glass slide and covered with a polypropylene based thin adhesive tape in order to prevent oxidation / hydrolysis of the sample while handling them outside the glove box. The glass slide was then taken out of the glove box and the alloy samples were characterized by using an X-ray diffractometer (XPERT MPD system) supplied by M/s. Philips, The Netherlands.

3.1.3 Experimental assembly for the spot technique

A schematic of the experimental assembly used in the present study is given in Fig. 3.4. This experimental set up was built in house [2, 3]. Basically the apparatus comprises a sample support assembly, a vacuum chamber that is evacuated by a vacuum system equipped with a diffusion pump (M/s. Balzers GmbH, Switzerland), a pyrometer, an RF generator (11 kW, 400 kHz, M/s. Electronics Devices, Mumbai, India), a Knudsen cell which is held on a support assembly and an image capture system. The sample support

system rests on the bottom flange which has a quartz window affixed to it in order to facilitate the measurement of the temperature of the Knudsen cell by using a pyrometer.

The RF heating coil was positioned concentric with the Knudsen cell. The Knudsen orifice as well as the surface of the specimen held inside the Knudsen cell were viewed remotely by using an image capture system with a magnification of about 100 X. This image capturing system comprised a long distance microscope, a CCD camera and a video monitor. The temperature of the Knudsen cell was measured by focusing an infrared two-color pyrometer with a fiber optic probe, on to the black body hole. Figs. 3.5, 3.6 and 3.7 show the photographs of the experimental assembly, sample mount and K-cell respectively.

3.1.4 Procedure for the spot measurement

In a typical experiment, a metal or an alloy is taken in an inert ceramic cup in a Knudsen cell (K-Cell) and heated by a non-contact means (RF Generator) in vacuum. The K-Cell has two holes, one at the bottom and one on top. From the top, its image is viewed by a long distance microscope and the pyrometer is focused on to the bottom to measure the temperature. As long as the metal remains solid, the image of the orifice will be uniformly bright. But when it melts, the metal or the alloy surface acts as a reflecting mirror which could be concave or convex, depending on the wetting angle. The orifice of the K-Cell plays a dual role. For the pyrometer, it is an incandescent object, as the pyrometer receives the maximum thermal radiation from the orifice. But, for the molten liquid mirror, it is a black object, as it receives the maximum radiation from all the directions expect the orifice. So the image of the orifice appears as a dark spot, when

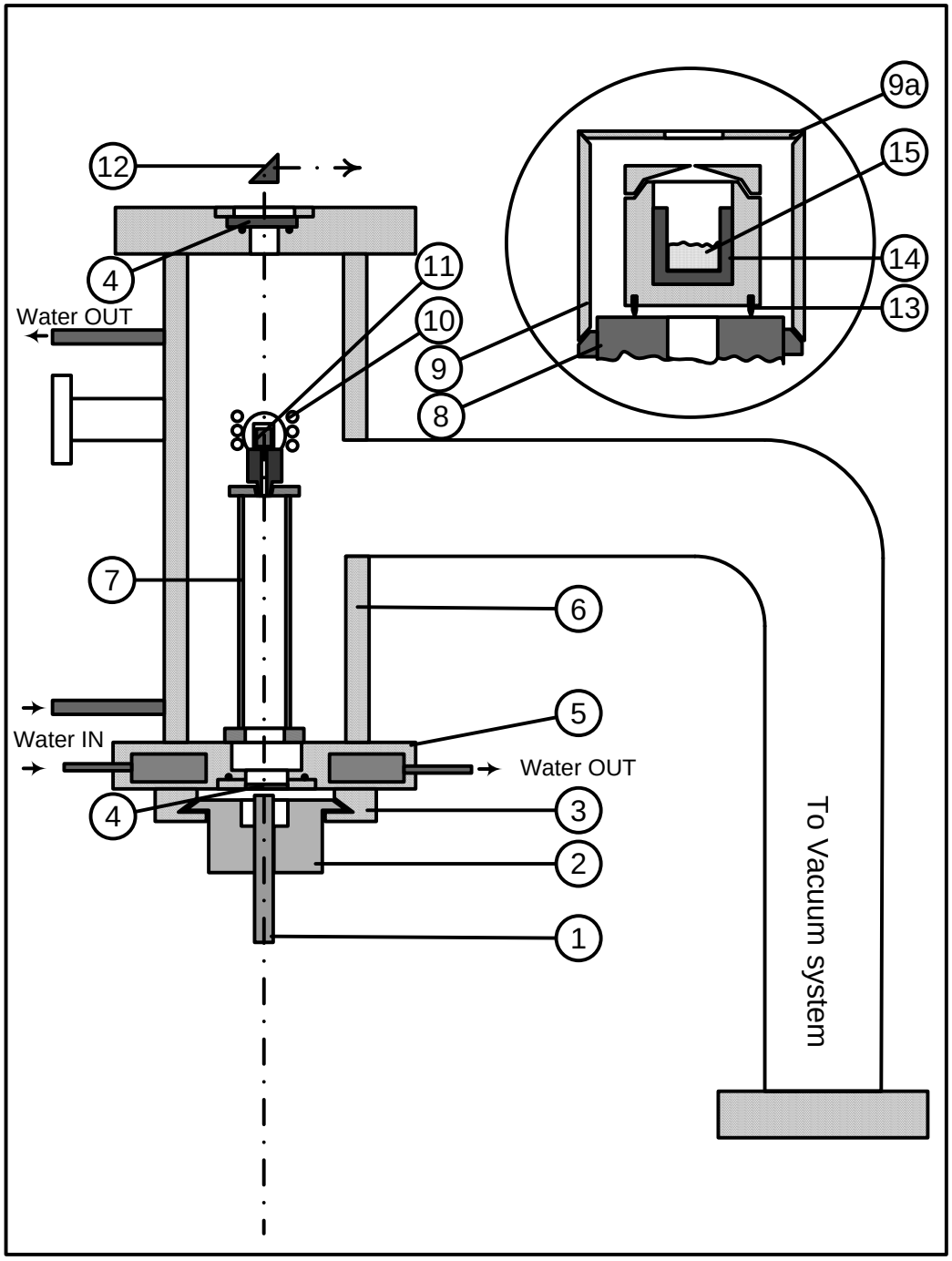

Fig. 3.4 Schematic showing the experimental system used for the spot experiments

1. IR two color pyrometer 2. Fixture for pyrometer 3. Optical rail 4. Quartz optical window 5. Bottom flange 6. Vacuum chamber 7. Sample support assembly 8. Molybdenum table 9. Radiation shield 9a. Top radiation shield 10. RF coil 11. Knudsen cell 12. Quartz prism 13. Tungsten legs 14. Crucible 15. Sample

.

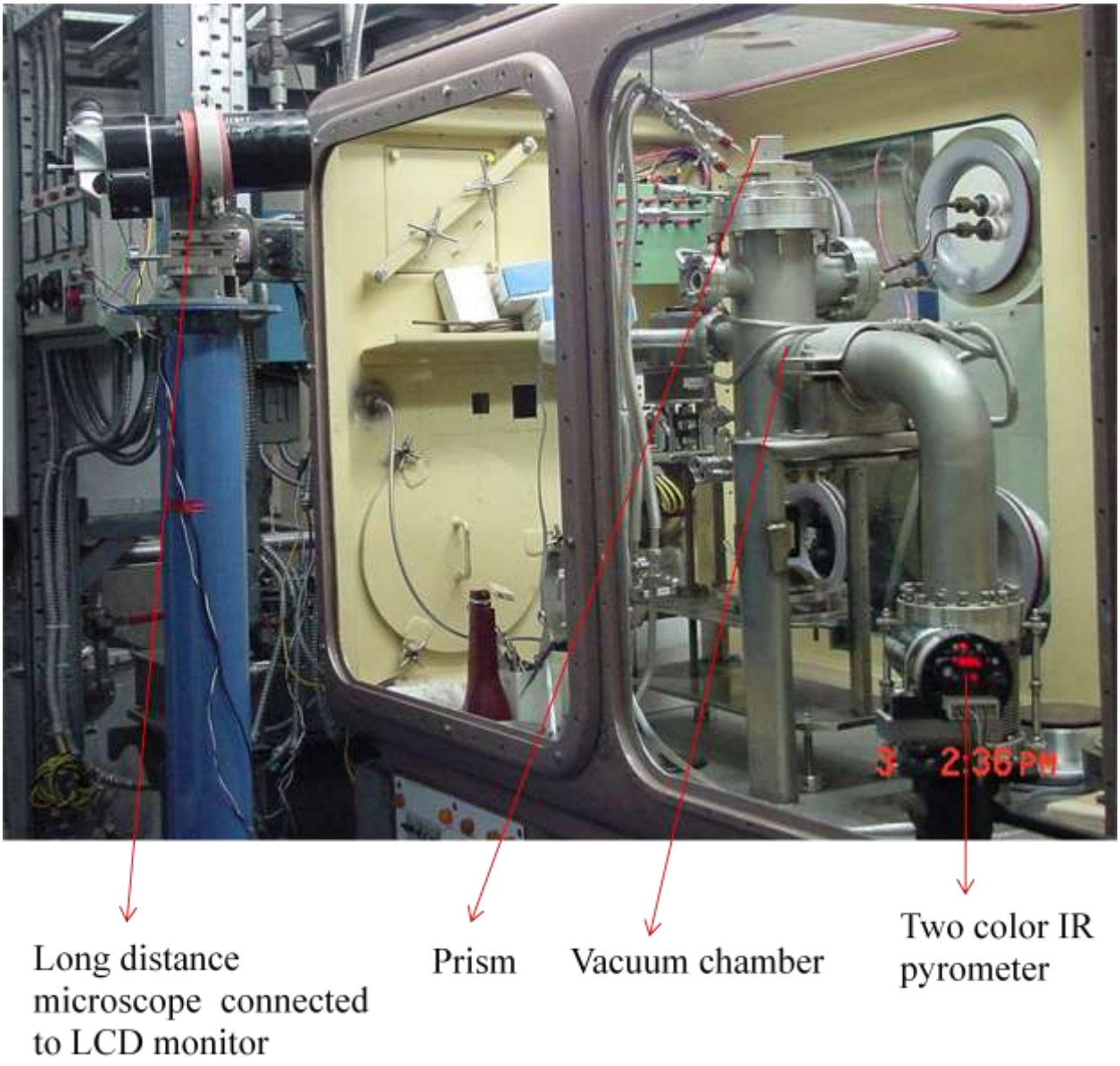

Fig.3.5 Photograph of the experimental set up.

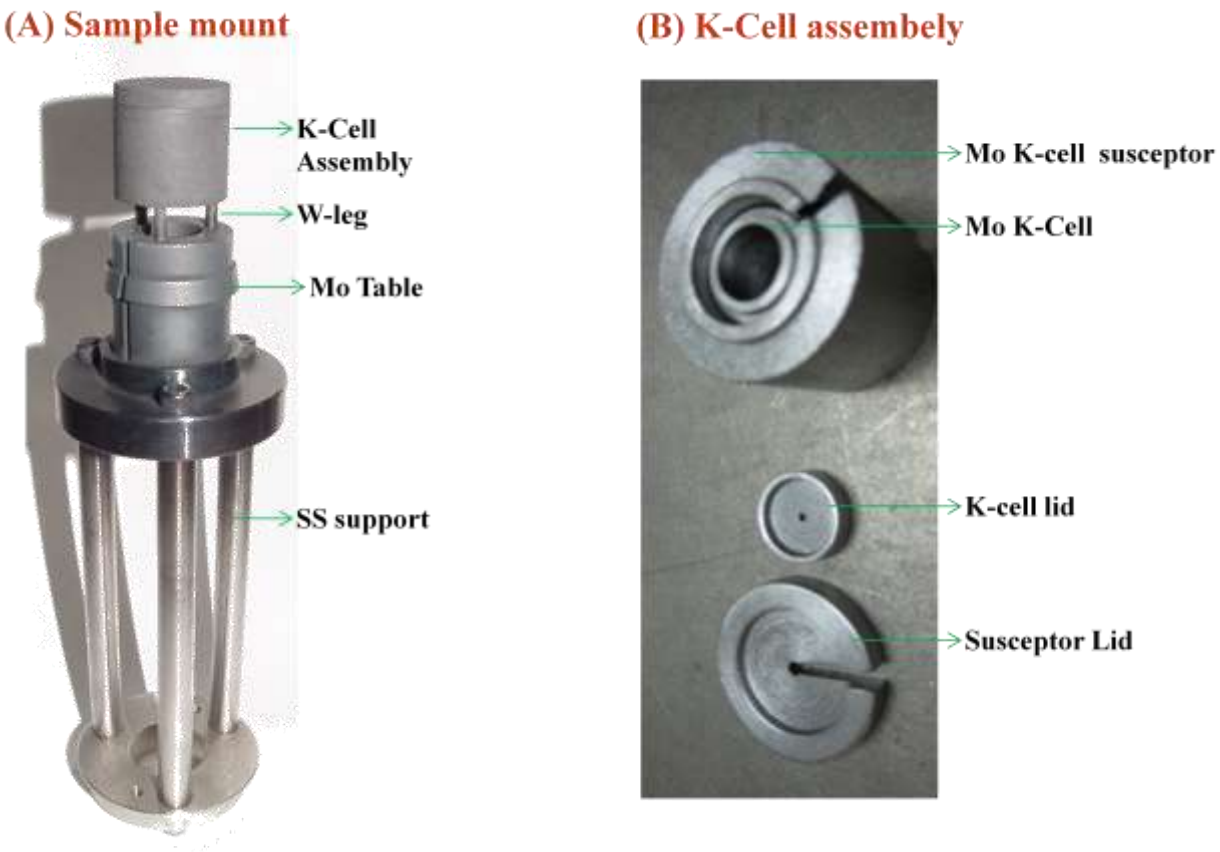

Fig.3.6-(A) – Photograph of the sample mount showing various parts

Fig.3.7-(B) – Photograph of Mo K-cell and susceptor with lids.

viewed through the long distance microscope. During the melting of a metal, a single dark spot appears at its melting temperature. For an alloy the appearance of the first spot similar to the image formed by a broken mirror corresponds to the solidus temperature. These tiny broken spots coalesce to form a single large dark spot at the liquidus temperature. So both the solidus and liquidus temperatures can be determined for various compositions of the alloy. Thus the phase boundary can be traced and the phase diagram can be established. The basic pre-requisite is that the molten liquid should not creep along the walls of the cup in which it is contained, the K-Cell should be placed at the centre of the coil so that both the pyrometer and the long distance microscope can be focused properly and sufficient quantity of the sample should be taken.

Section 2: Molten salt emf method and calorimetric technique

3.2.1 Argon atomsphere glove box

The argon atmosphere glove box [4] used for handling the samples of alloys, salts etc. is of double modular design and is made of 304 stainless steel. It is fitted with two safety glass panels on either side and two on top. Each of the side panels is fitted with four aluminium glove ports. The approximate volume of the box is two cubic meters. It has a port that facilitates transfer of materials. A furnace well made of inconel is attached to the floor of the glove box through a leak tight flange. A split furnace mounted on wheels is fixed at the bottom of the box, surrounding the furnace well. A schematic of the glove box system is shown in Fig. 3.8 and its photograph in Fig. 3.9. The argon gas in the glove box is purified by passing the gas through a purification tower made of stainless steel and filled with a mixture of a copper based deoxo catalyst (M/s. United catalyst India Ltd.,) 4A molecular sieves (supplied by M/s. ACC Ltd., India) for removing oxygen and moisture,

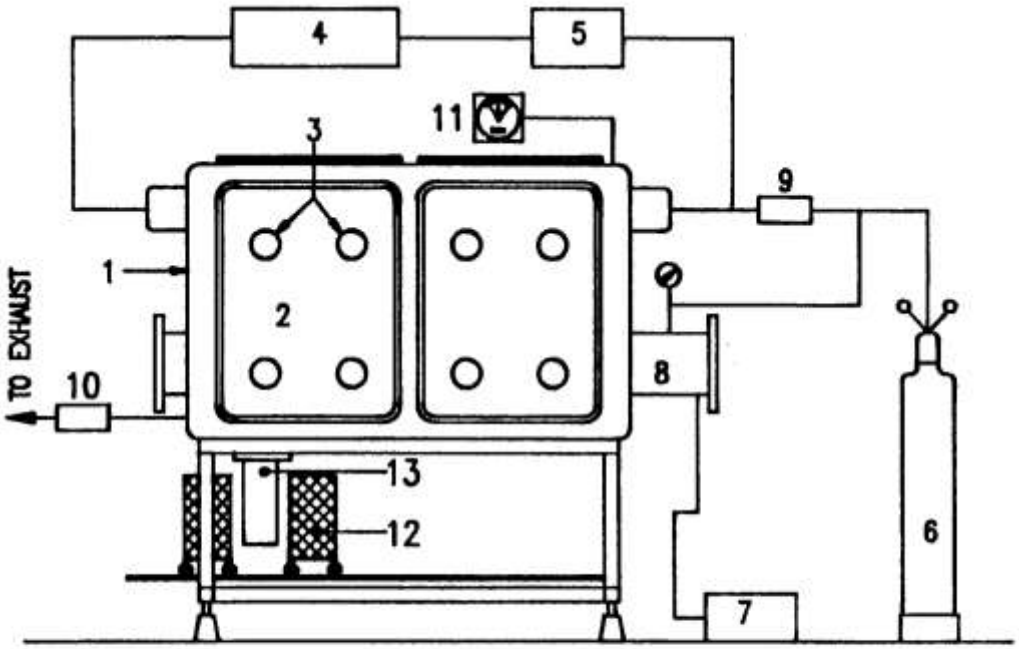

1. GLOVE BOX
2. GLASS PANEL
3. GLOVE PORT
4. PURIFICATION TOWER
5. RECIRCULATION PUMP
6. GAS CYLINDER
7. VACUUM PUMP
8. TRANSFER PORT
9,10. SOLENOID VALVES
11. PHOTOHELIC SWITCH
12. FURNACE ASSEMBLY
13. FURNACE WELL

Fig. 3.8 Schematic diagram of argon atmosphere glove box

Fig. 3.9 Photograph of the glove box.

respectively. The reasons for selecting the copper based deoxo catalyst and molecular sieves are that they can be used at the ambient temperature and also that they can be easily regenerated for further use. The level of impurities moisture and oxygen in the argon gas is maintained below 50 ppm by volume. The pressure inside the box is maintained between 20 and 50 mm of water column above atmosphere by using an automatic pressure regulating system comprising a "Photohelic Switch" and solenoid valves. A hermetically sealed, side channel blower is used for circulating the argon gas. Butyl rubber gauntlets are used in this glove box for minimizing the buildup of impurities (O_2 and H_2O) by diffusion through gloves, since they are more impervious to moisture and oxygen than neoprene gauntlets.

The argon gas inside the box is analyzed for moisture and oxygen by using suitable meters to monitor the levels of these impurities. An electrolytic type moisture monitor (supplied by M/s. Systech Inst., UK) is connected to the box. It measures the current required for the electrolysis of water, moisture chemisorbed on to a sensor comprising P_2O_5 by using the platinum electrodes. An oxygen meter (M/s. Nucon, India) based on the electrolytic principle is used for monitoring the oxygen levels in the box. The argon gas is pumped from glove box through the moisture and oxygen meters by using a small pump housed inside the box. This box was used for handling and storing of metals and alloys with which the emf, spot and calorimetric measurements were carried out. Preparation of samples for X-ray diffraction measurement, preparation of the electrolyte salts containing the chlorides of uranium and assembly of the molten salt galvanic cells were also carried out in the glove box.

3.2.2 Purification of salts

Anhydrous LiCl (> 99%) from M/s. Fluka, Switzerland, analytical grade KCl (99.8%) from M/s. Glaxo Laboratories, India and anhydrous $CdCl_2$ (99%) from M/s. Merck, Germany were used for salt preparation. In all the molten salt galvanic cell measurements used in this study, LiCl-KCl eutectic salt mixture containing UCl_3 was employed as the molten salt electrolyte. It is necessary to purify the LiCl-KCl eutectic salt from moisture and oxygen before using it in the galvanic cells. Initially LiCl and KCl were heated separately in a furnace under a vacuum of 1 Pa at 393 K for 360 h. The dried salts were stored inside an argon atmosphere glove box until further use. Stoichiometric amounts of LiCl (58.5 mol. %) and KCl (41.5 mol. %) were accurately weighed and loaded in an alumina crucible which in turn was placed inside a one end closed quartz tube. This air tight assembly was then taken out of the glove box and kept in a furnace well. The salt mixture was then purified by passing a stream of chlorine gas at 673 K and was subsequently melted, cooled and then remelted under chlorine atmosphere. This was then stored in the box until further use.

3.2.3 Preparation of the electrolytic salt

The purified eutectic salt mixture contained in the apparatus described above was then loaded into a furnace well inside the box and UCl_3 was generated in-situ in this melt by the following procedure. A known amount of $CdCl_2$ was added to the melt and the latter was equilibrated with pure uranium metal in an alumina crucible at 773 K under flowing argon in a glove box. The amount of uranium was so chosen that it was in excess of the stoichiometric amount required by equation (3.1).

$$2U + 3CdCl_2 \leftrightarrow 2UCl_3 + 3Cd \quad (3.1)$$

Thus it was ensured that no $CdCl_2$ remained in the molten electrolyte after the equilibration. The unreacted uranium and the cadmium formed by the reaction (3.1) were left in the crucible, while the salt loaded with UCl_3 was decanted. The amount of uranium in the LiCl–KCl eutectic salt was determined by using potentiometric technique based on the Davis and Gray method [5] which is described in the subsequent section. The amount of Cd in salt was estimated by inductively-coupled plasma atomic emission spectroscopy (ICP-AES) and was found to be below 10 ppm. The electrolyte salt thus prepared was stored in an argon atmosphere glove box until further use.

3.2.4 Davies and Gray method for the estimation of uranium [5]

Samples containing about 3-5 mg/mL of uranium was analyzed by using this method. The electrolyte salt sample was first dissolved in 1:1 nitric acid in order to convert the uranium chloride into uranyl nitrate. Then it was evaporated to dryness and again diluted with nitric acid and this procedure was repeated two to three times in order to ensure complete conversion of uranium chloride to nitrate. The dried residue was then made up with distilled water to the required volume. This salt sample aliquot was then taken in 1M sulphuric acid and few mL of a saturated solution of sulphamic acid was added to this mixture in order to destroy the nitrous acid as the latter may interfere in subsequent steps. An excess quantity of phosphoric acid was then added to convert the entire UO_2^{2+} to $UO_2(H_2PO_4)^+$. Further saturated solution of ferrous ammonium sulfate followed by a mixture containing nitric acid, ammonium molybdate and sulphamic acid were added to this mixture in order to facilitate the conversion of excess ferrous into ferric ions.

The solution was diluted with 1M H_2SO_4 containing vanadyl sulfate to decrease the Phosphoric acid concentration and to catalytically convert U(IV) to U(VI) by Fe(III) releasing quantitative amount of Fe(II). This conversion is very slow. So the detection of end point in a potentiometric titration becomes difficult. Hence vanadyl sulfate was added to catalyze this reaction. Finally Fe(II) was potentiometricaly titrated using 0.05M $K_2Cr_2O_7$ and 0.001M $K_2Cr_2O_7$ by using mercury-mercurous sulphate reference electrode and a platinum indicator electrode.

The amount of uranium was calculated by using equation 3.2.

$$[U] = \frac{\left((Dil.K_2Cr_2O_7 * Dil.Factor) + Conc.K_2Cr_2O_7\right) * 119.5}{Volume\ of\ the\ aliquot} \qquad (3.2)$$

3.2.5 Construction of emf cell

A schematic of the emf cell used in the measurement is shown in Fig. 3.10. The cell essentially comprises a cylindrical vessel made of stainless steel fitted with a knife edged flange having provisions for gas entry and exit, electrode leads and a thermocouple well. The electrolyte was contained in an alumina crucible that was placed inside this stainless steel vessel. The metal / alloys that were used as the electrodes were kept in tantalum cups which were welded to tantalum wires of 1.5 mm diameter. The tantalum wires were drawn through alumina rods having four holes of each 3/8 in. dia for electrical insulation. The alumina rod was inserted through veeco couplings provided on the top flange of the vessel. The tantalum wires served as electrical leads for measuring the potentials. Proper electrical contact between the leads and the electrodes was ensured prior to the assembly of the cell. The empty cell and the electrodes were initially heated in vacuum at 773 K to remove any adsorbed gases and was then stored in an argon atmosphere glove box. Figs. 3.11 and 3.12 show the photographs of the experimental assembly.

3.2.6 Procedure for the emf measurements

The degassed emf cell assembly was taken into an argon atmosphere glove box. The electrolyte contained in an alumina crucible was placed inside the cell. Uranium metal and the alloy specimen were taken in tantalum cups and these cups were crimped. These were then loaded into the cell. This assembly was taken out of the glove box and placed inside a Kanthal wire wound resistance furnace. The temperature of this furnace was controlled within ±1 K by using a proportional integral derivative (PID) controller. The temperature of this galvanic cell was measured by using a calibrated chromel-alumel thermocouple immersed in the electrolyte. High purity argon gas was continuously passed through this cell at a very low flow rate.

The cell was heated to the desired temperature and the emf was monitored. The electromotive force and the temperature were monitored using an Agilent 34970A data acquisition system. After ascertaining the attainment of equilibrium, as indicated by stable reading in the electrometer, the emf was recorded. The variation in the emf value, while ramping the temperature of the cell about a mean value was measured. The reversibility of the cell was verified by establishing a short circuit between the two electrodes with the help of a conducting wire and ascertaining that the emf quickly regained its original value after opening up the circuit.

The Gibbs energy of formation of the intermetallic compound, XY_p was determined by using high-temperature molten salt galvanic cells [6]. The galvanic cells constructed for this purpose are of two types as shown below;

$$<X> // XCl_n \text{ in LiCl-KCl (eutectic)} // < XY_p> + \{Y\} \qquad I$$

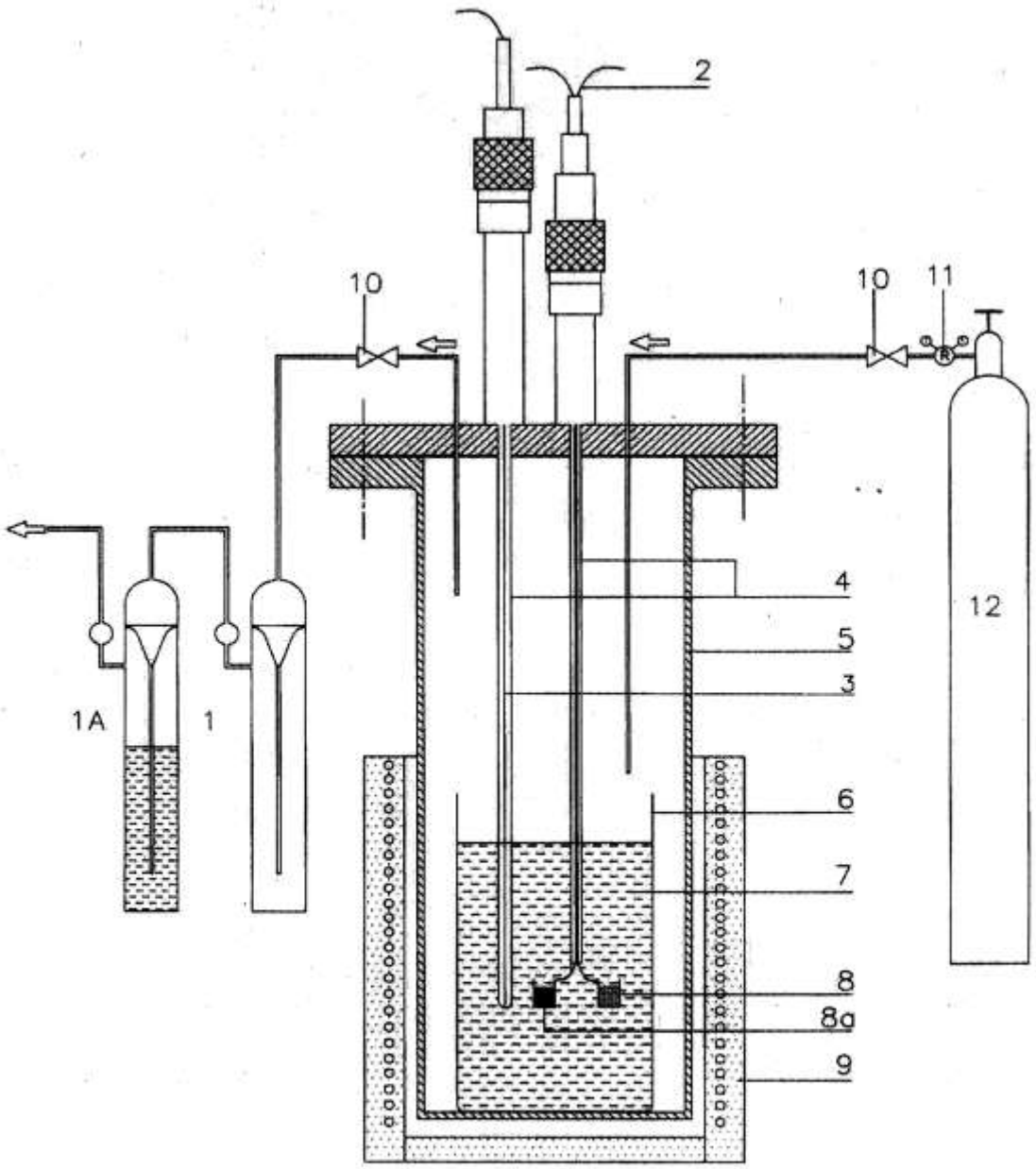

Fig. 3.10 Schematic of the experimental set up for emf measurement

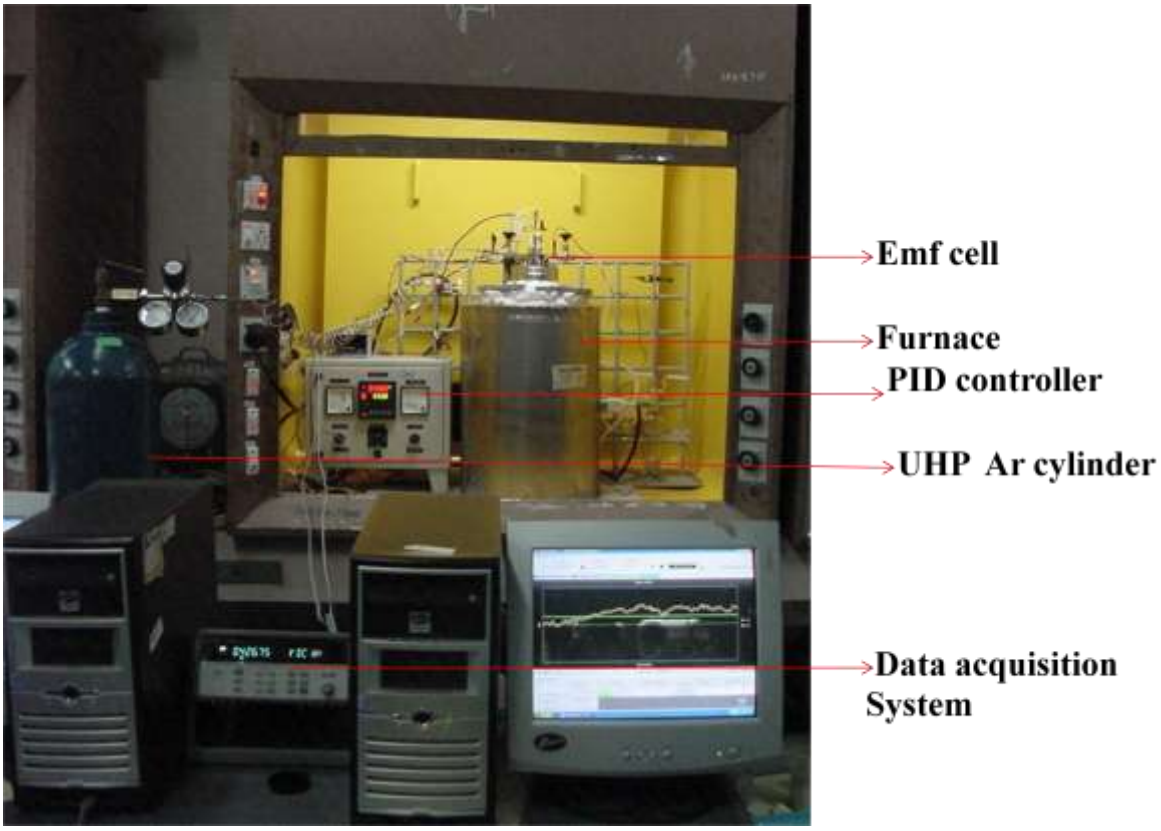

Fig. 3.11 shows the photograph of the experimental assembly

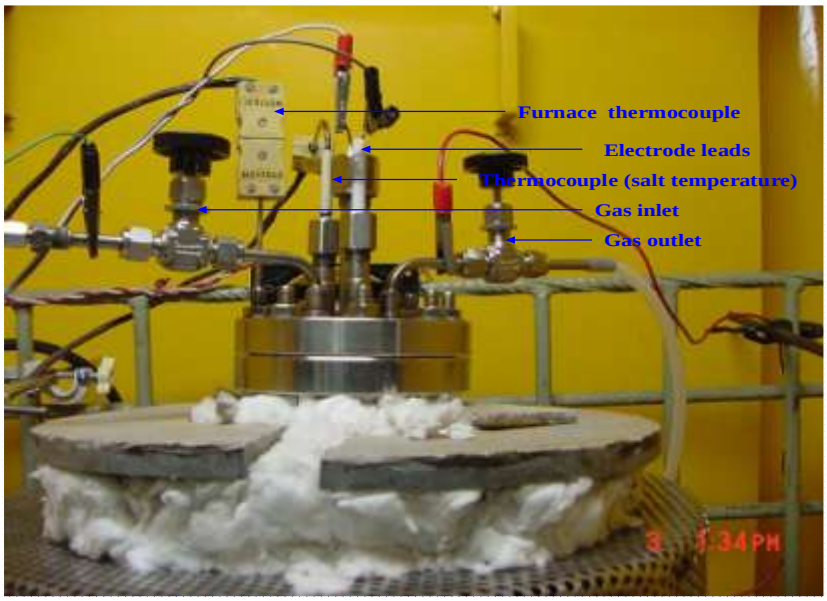

Fig. 3.12 Photograph of emf cell

$$<X> // XCl_n \text{ in LiCl-KCl (eutectic)} // < XY_p> + \{XY_q\} \qquad II$$

In the cell I, one of the pure constituents *X* is used as the reference electrode and the test electrode is a biphasic mixture of the intermetallic compound, XY_p and a liquid phase rich in *Y* saturated with *X*. In the second cell, the test electrode used comprised the intermetallic compounds, XY_p and XY_q.

The overall cell reaction in the case of cell I can be written as;

$$\langle X\rangle + [pY] \rightarrow \langle XY_p\rangle \quad . \qquad (3.3)$$

The emf of the cell I, E, measured as a function of temperature, the partial molar Gibbs energy of *X* and the Gibbs energy of formation of XY_p are related by the following equations:

$$\overline{G_U} - G_U^o = -zFE_I \qquad (3.4)$$

and

$$\Delta_f G^0_{\langle XY_P\rangle} = -zFE_I + 3RTlna_Y \qquad (3.5)$$

As a first approximation, the saturated solution was assumed to be ideal and the term $3RT\ lna_Y$ in the above equation was replaced with $3RTln\ X_Y$ where X_Y is the atomic fraction of *Y* in the saturated solution. In view of the fact that the saturated solution is rather dilute in *X*, the above assumption is reasonable. Thus the Gibbs energy of formation of the intermetallic compound XY_p can be calculated.

The cell reaction for the cell II is;

$$\langle X\rangle + \left[qXY_p\right] \rightarrow \langle pXY_q\rangle \qquad (3.6)$$

The Gibbs energy formation of the alloy, XY_q can be calculated by using the following equation,

$$-zFE_{II} = p\Delta G_f^o(XY_q) - q\Delta G_f^0\ (XY_p) \quad (3.7)$$

$$\Delta_f G^0_{\langle XY_q \rangle} = -\frac{z}{p}FE_{II} + \frac{q}{p}\Delta G_f^0(XY_P) \quad (3.8)$$

where E_{II} is the emf obtained for the Cell II.

The Gibbs energy formation values of the intermertallic compounds were calculated from the emf data by using the above equations.

3.2.7 Procedure for enthalpy measurement using a high temperature solution calorimeter

3.2.7.1 Solution calorimeter

A multi-detector high temperature drop calorimeter (MHTC-96) from M/S. SETARAM, France was used for solution calorimetric measurements [7]. It can be operated up to 1773 K in drop calorimetric mode. The detector of this calorimeter is a thermopile having 28 thermocouples. The sample and the reference crucibles are positioned in the detector. The thermocouples in this calorimeter are at different levels covering the whole surface enabling the measurement of an integrated heat exchange between the crucibles. In the present study, a drop detector, made up of Pt-6%Rh / Pt-30%Rh thermocouple was employed. Figs.3.13 and 3.14 shows the photograph of the calorimetry.

3.2.7.2 Procedure for calorimetric measurement

High temperature dissolution calorimetry was used to determine the enthalpy of formation of an alloy $A_xB_{(1-x)}$ at 298.15K [8] by measuring the thermal effects of

dissolution of the alloy $A_xB_{(1-x)}$ and its constituent elements , A and B in the same metallic bath at the same temperature. The thermal effects of dissolution, (Q^E) of the solute metal *A* in the liquid metal solvent, S were measured as a function of the concentration of *A,* by dropping the samples from the ambient into the solvent at the experimental temperature, *T* in the calorimeter. Since in general, the thermal effects of dissolution are independent of the concentration of the solutes in the solvent, the thermal effect of dissolution of metal A at infinite dilution ($Q_A^{E,\infty}$) was obtained by taking the mean of the thermal effects of dissolution. The thermal effects of dissolution of B at infinite dissolution ($Q_B^{E,\infty}$) and the thermal effect of dissolution of the intermetallic compound, $A_xB_{(1-x)}$ at infinite dissolution ($Q_{A_xB_{(1-x)}}^{E,\infty}$) were obtained by similar measurements in the liquid solvent, S and at the same temperature The enthalpy of formation of the intermetallic compound, $A_xB_{(1-x)}$ was calculated from the following equation;

$$\Delta_f H_{298.15}^0 < A_xB_{(1-x)} > = xQ_A^{E,\infty} + (1-x)\, Q_B^{E,\infty} - Q_{A_xB_{(1-x)}}^{E,\infty} \qquad (3.9)$$

The enthalpy of formation of the compounds at 298.15 was computed by this method.

Fig. 3.13 Multi-detector High Temperature Calorimeter

Fig. 3.14 Photograph of drop detector used in MHTC-96

References:

1. R. F. Bunshah, Techniques of Metals Research, Vol. 1, Part 2, Interscience Publisher, Newyork, 1968, p. 214.

2. K. Ananthasivan, Ph.D.thesis, University of Madras, Chennai, India 2003.

3. K. Ananthasivan, S. Balakrishnan, I. Kaliappan, S. Anthonysamy, R. Pankajavalli, P.R. Vasudeva Rao, J. Alloys Compd. 468 (2009) 275.

4. T. Subramanian, B. Prabhakara Reddy, K. Nagarajan, IGCAR Report, IGC-131 (1992).

5. W. Davies, W. Gray, Talanta. 11 (1964) 1203.

6. P. Chiotti, J. A. Kateley, J. Nucl. Mater. 32(1969) 135.

7. R. Babu, R. Kandan, Hrudananda Jena, K.V. Govindan Kutty, K. Nagarajan, J. Alloys. Compd. 506 (2010) 565.

8. K. Nagarajan, Rita Saha, R.Babu, C. K. Mathews, Thermochim. Acta 90 (1985) 279.

Chapter-4- Determination of peritectic transformation temperatures of the system U-Sn

Rough et al. [1] reported the phase diagram of the system U-Sn over the whole composition range. They reported the existence of three intermetallics <USn_3>, <U_3Sn_5> and <U_5Sn_4>. Sari et al. [2] investigated the system U-Pu-Sn and found evidence for the existence of the following phases: MSn_3, M_3Sn_7, MSn_2, M_4Sn_5, MSn, M_5Sn_4 and M_5Sn_3 ($M=U_xPu_{1-x}$). Sheldon et al. [3] studied the phase diagram over the whole composition range and reported the existence of the three phases; the first two were the same as reported by Rough et al. [1]. They reported a new phase <U_3Sn_2> instead of <U_5Sn_4> as reported earlier [1]. Palenzona et al. [4] reinvestigated the phase diagram in the composition range, 0-90 at. % U. They examined the system by using differential thermal analysis, metallography, X-ray diffraction and electron microscopy. They that there are five intermetallics, viz, <USn_3>, <U_3Sn_7> <USn_2>, <USn> and <U_5Sn_4>. Among these first four intermetallics undergo peritectically melting while U_5Sn_4 melts congruently. Based on Palenzona's work [4], Ananthasivan [5] reinvestigated the sytem to remove the ambiguity in the peritectic melting temperatures of the four intermetallics which are closely placed, but was not able to delineate the same. So the primary objective of this study was to resolve the uncertainties in the experimentally determined values of the peritectic melting temperatures of these four intermetallics. Information on the phase diagrams and thermodynamic studies of the ternary systems U-Noble Metal-Sn are necessary for understanding the chemistry of irradiated uranium plutonium mixed oxide fuels [6]. So in order to understand the above multicomponent system, it is necessary to examine the sub-binaries like U-Sn. The liquid tin process is one of the alternatives suggested for the reprocessing of the irradiated carbide fuel [7]. So studies on the system U-Sn is helpful. Further, the U-Sn system would serve as a model

system that could be used to validate the spot technique, an experimental system built in house for the investigations of the phase diagrams of alloys of relevance to fast reactor fuels. The experimental set up can operate between 1273 to 2273 K. The temperatures associated with the U-Sn system are intermediate within the range of measurement capabilities of the experimental set up. So the system U-Sn was used to validate the experimental setup.

4.1 Experimental assembly

The detailed construction of the experimental set up has already been given in the section 3.1.3. The experimental assembly basically consists of a vacuum chamber, which houses the sample held in a crucible, kept inside a Knudsen cell, a sample support assembly, a vacuum system (M/s. Balzers GmbH, Switzerland, diffusion pumping system Model 100L), a radiofrequency (RF) generator, a pyrometer and an image capturing system. The image capturing system consists of a long distance microscope, a charge coupled device (CCD) camera (M/s. Watec Co. Ltd., Japan, Model No. WAT207A) and a video monitor.

4.2 Measurements using spot technique

The basic principle behind the spot technique has been described in detail in section 3.1.4. In this technique, typically about 500 mg of sample with a known composition is placed in an inert cup. This cup is centered inside a Knudsen cell and heated under high vacuum. The orifice of the Knudsen cell is viewed through a pyrometer. As long as the sample remains solid, the Knudsen orifice approximates a black body and appears as a uniformly lit bright disc. However, at the peritectic temperature of the alloy under investigation when a liquid phase appears, the reflected image of the orifice appears as a black spot when observed through the pyrometer. Both the number and size of these spots increase upon further heating. Finally all these dark spots coalesce into a single large spot at the liquidus. In order to observe the spot

effect, the cup has to be centrally located in the Knudsen cell and sufficient quantity of the sample should be taken. It is also necessary to use a non-contact mode of heating (electron bombardment or radiofrequency (RF) induction) in order to observe this effect. Stoichiometric amounts of uranium and tin were taken and the alloys were prepared using an arc melting furnace as described in section 3.1.2. The desired alloys thus prepared were flipped and melted about six times in order to ensure complete homogenization. Some of these buttons were wrapped in a tantalum foil and encapsulated in quartz ampoules at a pressure of about 1×10^{-3} Pa and then annealed at 1073 K for 15 days for the spot experiments. Before the start of these experiments, the whole experimental assembly, except the lids of the Knudsen cell, was degassed at 1673 K. To validate the experimental procedure gold, nickel and zirconium were melted separately. The calibration is given in Table 4.1. The melting temperatures of all these were recorded and visualized by the formation of spot. The measured values of the melting temperatures of these metals were found to vary within 3 to 5 K. After ascertaining the melting temperatures of these metals within this range, further measurements on the U-Sn system were carried out. To arrive at each peritectic melting temperature of the four intermetallics, about ten to twelve experiments were performed. The data obtained from each experiment were examined and visualized by the camera and those data pertaining to the experiments in which creeping and oxidation were observed, were rejected. The photographs showing various parts getting contaminated due to creeping and oxidation of a typical alloy are shown in Figs. 4.1, 4.2 and 4.3. Reliable data obtained for each intermetallic were taken and the average values are reported here. About 11 spot experiments were performed for <USn_3> but only few could be carried out for other intermetallics because of problems due to creeping and oxidation.

Table 4.1 Melting points of pure metals as measured by the spot technique

Sample	Melting point / K	
	Standard	Experimentally measured
Gold	1337.43	1335 ± 2
Nickel	1728	1730 ± 3
Zirconium	2128	2127 ± 2

4.3 Compatibility of the crucible with alloys

In order to understand the chemical compatibility between the container (Mo) and the alloy (U-Sn), the binary phase diagrams of the systems U-Mo and Mo-Sn [8] were examined. The system U-Mo reveals a maximum terminal solubility of 3 at. % U in Mo at 1557 K, at the peritectic isotherm pertaining to the formation of the solid solution of γ-U. However the liquid solution could dissolve upto 70 at. % U. The phase diagram of the system Mo-Sn shows insignificant terminal solubility of both the components. This system is characterized by three intermetallics. In view of the above, it is evident that Mo will contaminate molten U-Sn alloys. Further presence of an oxide layer on the inner walls of the Mo crucible would oxidize the U-Sn alloy sample. The temperature dependence of Gibbs energy of formation of the metal oxides relevant to the present study was calculated by using the reaction module of FactSage (version 6.2) and is presented in Fig. 4.4. It is evident from Fig. 4.4 that yttria would be the most appropriate choice for the crucible. In addition, it is also evident that any surface oxidation of the crucible (Mo) or the alloy (USn) would lead to the formation of the oxides of U. Even though a detailed analysis of compatibility should consider the stabilities of the intermetallics in the system U-Sn as well, these could not be included for want of information. This analysis could not take into consideration the stabilities of any ternary / quaternary oxides because information on the same is not available. In view of the above it is reasonable to assume that Mo is not the most suitable container, while yttria is best suited to hold the molten U-Sn alloys.

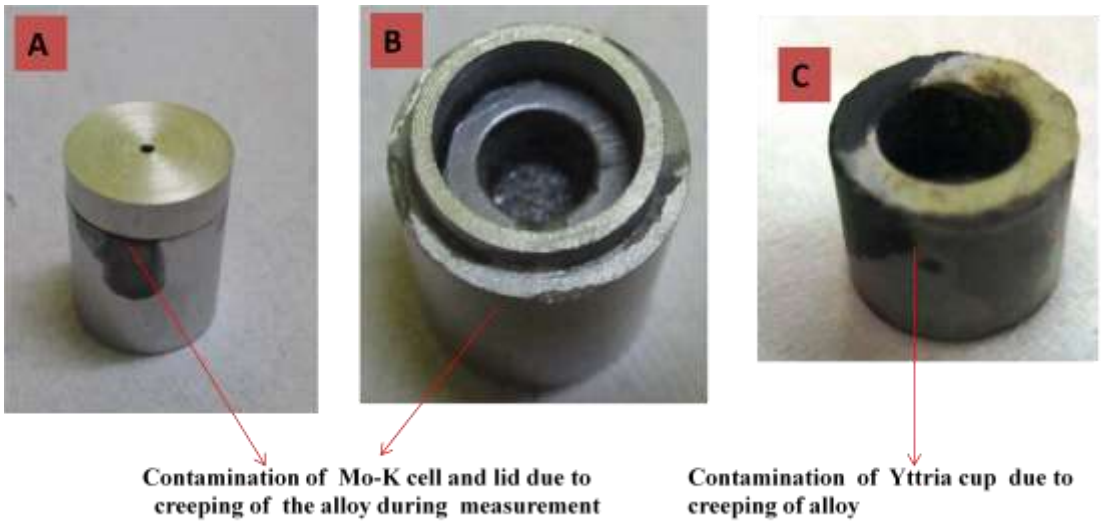

Figs. 4.1, 4.2 and 4.3 shows a typical photograph of various parts getting contaminated due to creeping and oxidation problem of the alloy.

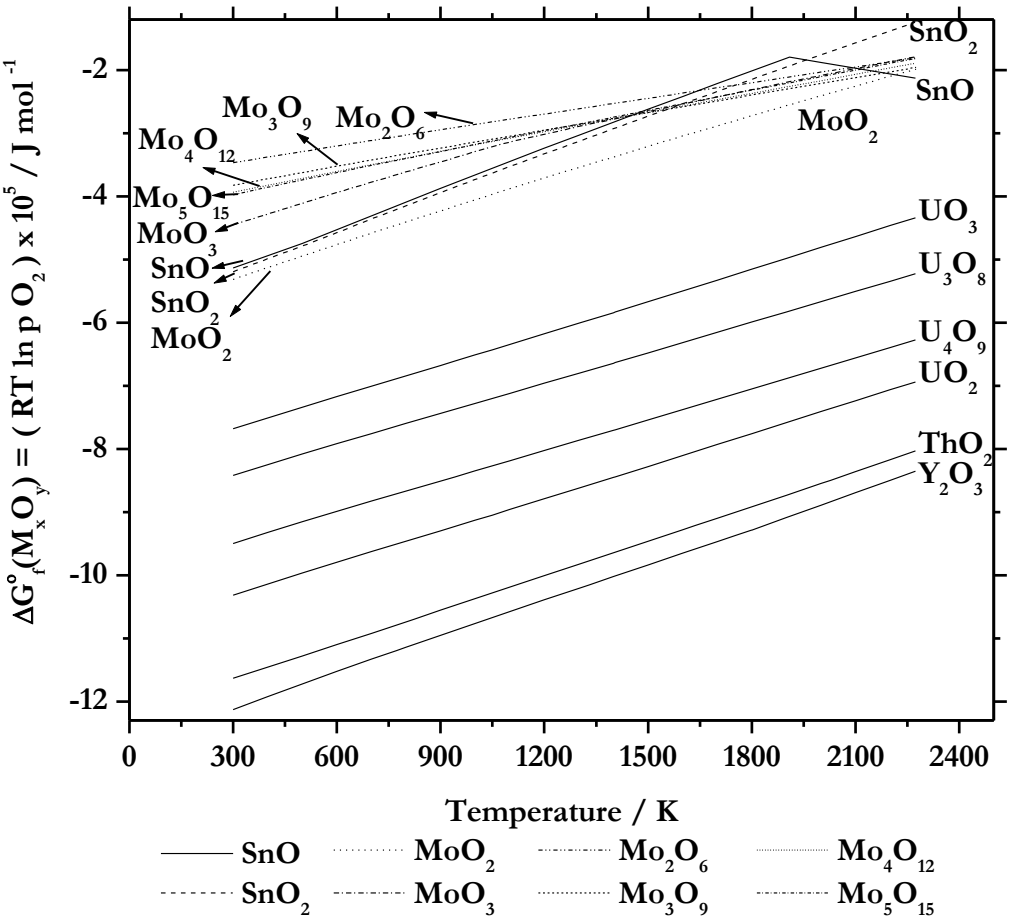

Fig. 4.4 Stabilities of oxides of U, Sn, Mo, Th and Y

4.4 Results and discussion

The crystallographic data and phase transformations in the U-Sn System are presented in Table 4.2. The peritectic melting temperatures of the four intermetallics determined in the present study are given in Table 4.3 and compared with those reported by Palenzona et al. [4].and Ananthasivan [3], while the liquidus measured by Ananthasivan [5] are presented in Table 4.4. All these results are depicted in Fig. 4.5. The invariant phase reactions in the system U-Sn could be represented as follows.

i) Congruent melting of <U_5Sn_4> at 1663 K [4]

$$\{U_5Sn_4\} \xrightarrow{cooling} \langle U_5Sn_4\rangle \quad (4.1)$$

ii) peritectic formation of <USn>

$$Liquid + \langle U_5Sn_4\rangle \xrightarrow{cooling} \langle USn\rangle \quad (4.2)$$

iii) peritectic formation of <USn_2>

$$Liquid + \langle USn\rangle \xrightarrow{cooling} \langle USn_2\rangle \quad (4.3)$$

iv) peritectic formation of <U_3Sn_7>

$$Liquid + \langle USn_2\rangle \xrightarrow{cooling} \langle U_3Sn_7\rangle \quad (4.4)$$

v) peritectic formation of <USn_3>

$$Liquid + \langle U_3Sn_7\rangle \xrightarrow{cooling} \langle USn_3\rangle \quad (4.5)$$

The values reported in ref. [4] have higher uncertainties due to the reaction of the molten alloy with the molybdenum container. Further it is often difficult to delineate this cascade of peritectic isotherms represented by eqns. (4.2) to (4.5) by DTA, for they are closely spaced and could interfere in the determination of each other owing to the diminished magnitude of the heat effects near the isotherm. Recent work carried out by Ananthasivan

Table 4.2 Crystallographic data and phase transformations in the system, U-Sn [4]

Compound	Pearson Symbol	Space group (No.)	Isotype	a (nm)	b (nm)	c (nm)	References
<U_5Sn_4>	hP18	$P6_3/mcm$(193)	Ti_5Ga_4	0.9327	-	0.6230	Palenzona et al. [4]
<USn>	oP24	Pbcm(57)	ThIn	1.0488	0.9552	0.6213	Palenzona et al. [4]
<USn_2>	oC12	Cmmm(65)	$ZrGa_2$	0.4430	1.5456	0.4460	Palenzona et al. [4]
<U_3Sn_7>	oC20	Cmmm(65)	Ce_3Sn_7	0.4497	2.4725	0.4509	Palenzona et al. [4]
<USn_3>	cP4	Pm-3m(21)	$AuCu_3$	0.4610	-	-	Palenzona et al. [4]
				0.4626	-	-	Sheldon et al. [3]

Phase / Invariant reaction	Temperature [4] / K	Type of the invariant reaction	Reference
$Liquid \xrightarrow{Cooling} \langle U \rangle + \langle U_5Sn_4 \rangle$	1393	Eutectic transformation	Palenzona et al. [4]
$\{U_5Sn_4\} \xrightarrow{Cooling} \langle U_5Sn_4 \rangle$	1663	Congruent melting	Palenzona et al. [4]
$Liquid + \langle U_5Sn_4 \rangle \xrightarrow{Cooling} \langle USn \rangle$	1658	Peritectic formation	Palenzona et al. [4]
$Liquid + \langle USn \rangle \xrightarrow{Cooling} \langle USn_2 \rangle$	1633	Peritectic formation	Palenzona et al. [4]
$Liquid + \langle USn_2 \rangle \xrightarrow{Cooling} \langle U_3Sn_7 \rangle$	1623	Peritectic formation	Palenzona et al. [4]
$Liquid + \langle U_3Sn_7 \rangle \xrightarrow{Cooling} \langle USn_3 \rangle$	1613	Peritectic formation	Palenzona et al. [4]
$Liquid \xrightarrow{Cooling} \langle Sn \rangle + \langle USn_3 \rangle$	493	Eutectic transformation	Palenzona et al. [4]

Table 4.3 Comparison of the peritectic temperatures obtained in this study with those reported in literature.

Sample	at % Sn	Palenzona [4]	Ananthasivan [5]		This study	
		T / K	T / K	Mean / K	T / K	Mean / K
<USn_3>	75	1613	1616	1618 ± 3	1600	
			1620		1600	
					1605	
					1594	
					1601	
					1599	1600 ± 4
					1602	
					1592	
					1605	
					1598	
					1600	
<U_3Sn_7>	70	1623		1616 ± 16	1619	1622 ± 4
					1625	
<USn_2>	66.7	1633	1623	1617 ± 8	1628	1628 ± 1
			1620		1629	
			1608			
<USn>	50	1658	1628	1629 ± 1	1641	1642 ± 7
			1629		1649	
			1630		1636	

T: Temperature

Table 4.4 Liquidus temperatures measured by Ananthasivan [5]

Sample	at. % Sn	Liquidus / K	Sample	at. % Sn	Liquidus / K
A	50.4	1648	G	92.8	1368
	50.4	1653		92.8	1368
B	50.3	1651	H	93.9	1338
	50.3	1641		93.9	1345
C	65.9	1648	I	94.7	1339
	65.9	1648		94.7	1335
D	74.3	1626	J	94.9	1331
	74.3	1630		94.9	1334
E	91.9	1394	K	96.2	1303
	91.9	1389	L	96.8	1296
	91.9	1395	M	97.5	1258
	91.9	1390		97.5	1256
F	92.4	1376	N	97.7	1223
	92.4	1379	O	97.8	1293
	92.4	1378			

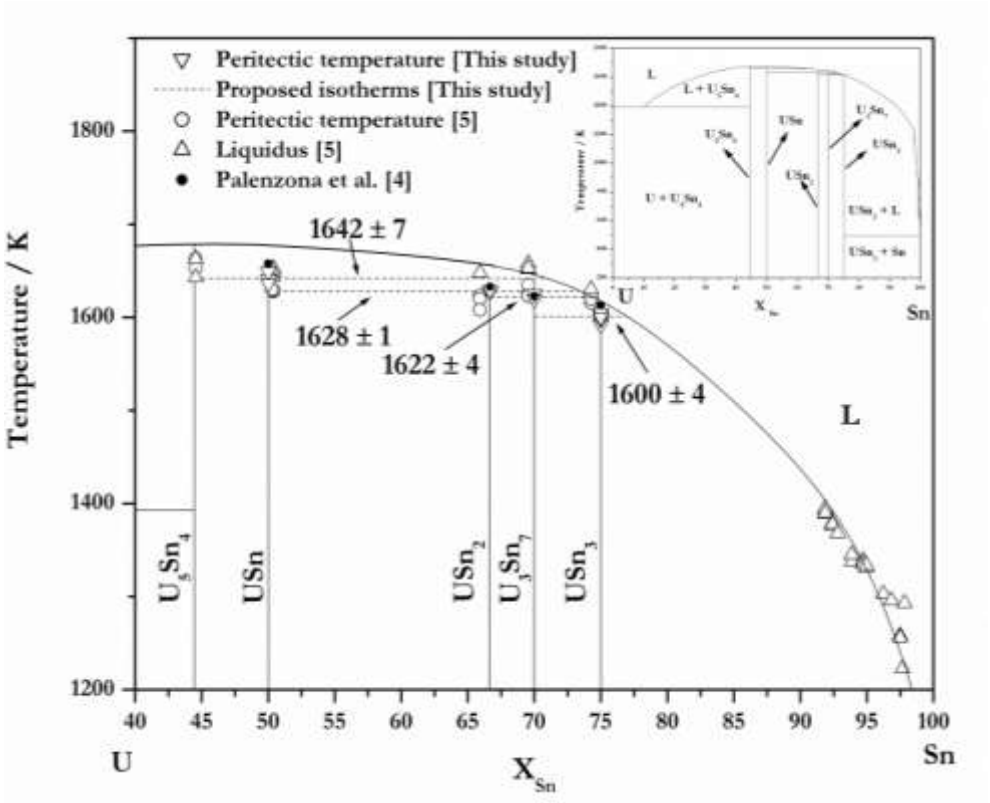

Fig. 4.5 Phase diagram of the system, U-Sn

Inset: Binary Phase Diagram of the system, U-Sn [4]

[5] has shown that these peritectic isotherms are located at 1629 ± 1 K (eqn.4. 2), 1617 ± 8 K (eqn. 4.3), 1616 ± 16 K (eqn. 4.4) and 1618 ± 3 K (eqn. 4. 5) respectively. However, his study failed in unambiguously delineating the peritectic isotherms pertaining to the formation of <USn_2>, <U_3Sn_7> and <USn_3> using thoria crucibles. In these investigations presence of the solid phase at the peritectic isotherm was identified through videography. However, in spite of the care exercised in limiting the reaction of the alloy with the container, surface diffusion and creeping of the liquid within the crucible rendered these measurements inaccurate. In order to eliminate the experimental difficulties encountered in the earlier investigations [2, 3], two changes were made in the experimental condition, first high density yttria crucibles was chosen in place of thoria and the experimental time was reduced so as to limit the chance of reaction between the alloy and the container. It was found that best results could be obtained with sintered yttria cups. However, in alloys containing the phases richer in uranium, creeping and oxidation were more prevalent. The data obtained from such experiments were rejected and the measurements in which the alloy did not undergo significant interaction and weight loss were only considered. Due to significant creeping the congruent melting temperature of the compound <U_5Sn_4> could not be unambiguously determined. The peritectic melting temperatures of the compounds <U_3Sn_7> and <USn_2> were comparable to those reported by Palenzona et al. [4], while the peritectic melting temperature of <USn> reported in this study is more reliable for these samples were devoid of contamination. Further, assay of these alloys for oxygen contamination revealed that the quantity of residual oxygen was rather insignificant (<1000 ppm). Palenzona et al. [4] did not report the probable uncertainty in the temperature, while Ananthasivan [5] reported values that suggested overlap of the isotherms. In view of the

above it could be concluded that the peritectic melting temperatures of the intermetallics <USn_3>, <U_3Sn_7>, <USn_2> and <USn> reported in this study are more reliable and supersede the values reported in the previous measurements.

4.5 Conclusion

The peritectic melting temperatures of the four intermetallics <USn_3>, <U_3Sn_7>, <USn_2> and< USn> in the U-Sn system were measured more reliably by using the spot technique and were found to be 1600 ± 4 K, 1622 ± 4 K, 1628 ± 1 K and 1642 ± 7 K respectively. Chemically inert high density yttria ceramic crucibles were used in order to minimize the contamination of the melt with the container material and creeping of the molten alloy. While we have successfully defined the peritectic isotherms in this system, further investigations are required in order to unambiguously establish the congruent melting point of <U_5Sn_4>, liquidus and the eutectic isotherm at the uranium rich end.

References:

1. F. A. Rough, A. A. Bauer, Uranium-tin in Constitution of uranium and thorium alloys, BMI report-1300, UC-25 Metallurgy and Ceramics, Battelle Memorial Institute, Ohio, 2 June 1958, p. 71.
2. C. Sari, F. Vernaza, W. Muller, J. Less-Common Met. 92 (1983) 301.
3. R. I. Sheldon, E. M. Foltyn, D. E. Peterson, The Sn-U (Tin-uranium) system, Bull. Alloy Phase Diagr. 8 (1987) 347.
4. Palenzona, P. Manfrinetti, J. Alloys Compd. 221 (1995) 157.
5. K. Ananthasivan, Ph.D. thesis, University of Madras, Chennai, India 2003.
6. H. Kleykamp, S.G. Kang, J. Nucl. Mater. 230 (1996) 280.
7. Hj. Matzke, Science of Advanced LMFBR Fuels, North-Holland, Amsterdam, 1986, p. 637.
8. T.B. Massalski, ASM Binary Phase Diagrams, second Ed., ASM International, USA, 1996.

Chapter 5: Determination of the Gibbs energy and enthalpy of formation of the intermetallic compounds of U-Sn system

5.1 Gibbs energy of formation of <USn_3>, <U_3Sn_7>, <USn_2> and <USn> by galvanic cell measurements

5.1.1 Preparation of alloys

The general procedure for determining the Gibbs energy of formation of the intermetallic compounds was described in 3.2. In all the types of emf cells used, biphasic alloys of U-Sn system were used as the test electrodes. The biphasic alloy, <USn_3> + {Sn} was prepared by arc melting, stoichiometric amounts of uranium and tin ($U_{0.23}$ $Sn_{0.77}$) in an arc melting furnace. The alloy button thus formed was wrapped in Ta foil and vacuum sealed in quartz tube. After that the quartz ampoule was annealed at 1173 K for 20 days. After annealing, the quartz tube was taken inside the inert atmosphere glove box and then broken. The sample was removed from the Ta foil, a small amount was broken and powdered using mortar and pestle. The powdered sample was then taken on a slide, in order to prevent direct air contact; it was wrapped with a polypropylene based transparent tape and then taken out from the inert atmosphere glove box for X- ray diffraction analysis. The XRD pattern of the sample confirmed the presence of the biphasic mixture. The XRD pattern of the biphasic mixture of <USn_3> and {Sn} is given in Fig. 5.1. By using a similar procedure, the other biphasic alloys, namely <U_3Sn_7 + USn_3>, <USn_2 + U_3Sn_7> and <USn+USn_2> were prepared and characterized. The XRD peaks of the last three biphasic alloys indicate the presence of traces of uranium oxide (UO_2 and UO_3), which may be due to the surface oxidation of the powder, while preparing it for XRD measurement. However it is expected that the presence of small quantities of uranium oxide would not affect the measurement.

5.1.2 Gibbs energy formation of <USn_3>

The following cell was constructed to measure the Gibbs energy formation of <USn_3>.

<U> // UCl_3 in LiCl-KCl (eutectic) // <USn_3> + {Sn} *Cell I*

where pure uranium was used as the reference electrode and a biphasic mixture of <USn_3> and {Sn} as the test electrode. The constructions of the cell, eutectic salt preparation and the procedure for emf measurement have been already described in the section 3.2. U metal and the two phase alloy of <USn_3> and {Sn} were taken in tantalum cups and the cups were crimped. These were also loaded inside the cell. The assembly was then heated in a furnace. High purity argon gas was continuously passed through the cell at a very low flow rate. The cell was heated to the desired temperature and emf was monitored. The electromotive force and the temperature were monitored using an Agilent 34970A data acquisition system. After ascertaining the attainment of equilibrium, as indicated by a stable reading in the voltmeter, the emf was recorded. The variation in the emf value, while ramping and cooling the temperature of the cell about a mean value was measured. Two heating and cooling cycles were performed to arrive at a particular emf value at that specified temperature. The time taken by the cell to attain initial equilibrium was around 6 h and for the subsequent changes in temperature it took around 2-3 h for attaining stable values of emf. The emf values of cell I are given in Table 5.1. The least squares analysis of the temperature dependence of the emf data for this cell yielded the following expression in the temperature range 682-905 K;

$$E_I / mV = (597.2 \pm 4.3) - (0.213 \pm 0.006)\, T/K \qquad (5.1)$$

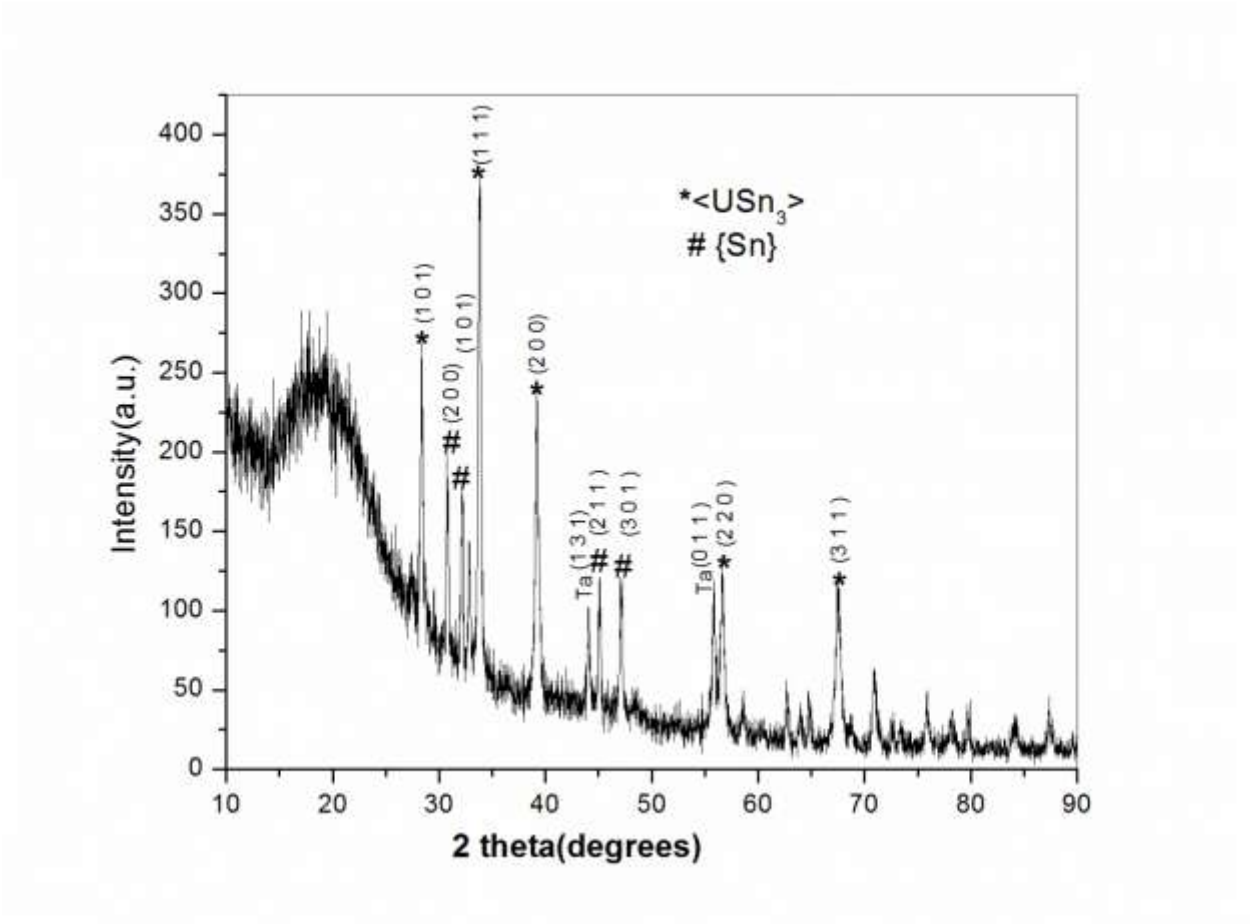

Fig. 5.1 XRD pattern showing the biphasic mixture of <USn_3> and {Sn}

Table 5.1:- Emf values of cell I

<U> // UCl_3 in LiCl-KCl (eutectic) // $\langle USn_3 \rangle$ + {Sn}

Temperature (K)	Emf (mV)*
682 [h]	448.3±0.3
681 [c]	448.3±0.1
707 [h]	446.2±0.2
708 [c]	447.9±0.1
730 [h]	440.9±0.1
731 [c]	443.2±0.1
755 [h]	435.9±4.1
756 [c]	437.3±0.2
780 [h]	431.3±0.2
780 [c]	432.1±0.1
805 [h]	426.3±0.1
806 [c]	427.3±0.1
831 [h]	421.2±0.1
831 [c]	421.2±0.3
853 [h]	415.1±0.1
854 [c]	415.2±0.2
880 [h]	409.2±2.7
880 [c]	406.1±0.3
905 [h]	403.2±0.1
905 [c]	403.1±0.1

h= heating and c= cooling

* Note- The values are the average of three heating and cooling cycles at each temperature.

The errors are the standard deviations in the measured values.

The galvanic cell reaction involves the transfer of uranium from pure solid metal to the alloy electrode where the reaction with the tin occurs to precipitate the solid intermetallic compound as follows;

$$\langle U \rangle \rightarrow [U] \tag{5.2}$$

$$[U] + 3\{Sn\} \rightarrow \langle USn_3 \rangle \tag{5.3}$$

The overall cell reaction is given by;

$$\langle U \rangle + 3\{Sn\} \rightarrow \langle USn_3 \rangle \tag{5.4}$$

The cell emf, E_I and the value of $\Delta_f G^0_{\langle USn_3 \rangle}$ with respect to <α-U> and pure liquid {Sn} are related through the equations (5.5) and (5.6).

$$\overline{G_U} - G^0_U = -zFE_I \tag{5.5}$$

$$\Delta_f G^0_{\langle USn_3 \rangle} = -zFE_I + 3RTlna_{Sn} \tag{5.6}$$

where $\overline{G_U}$ is the partial molar Gibbs energy of U in liquid solution, z (= 3) the number of electrons participating in the electrode reaction, *F*, the Faraday constant and a_{Sn} , the activity of Sn in the saturated solution. As a first approximation the saturated solution was assumed to be ideal and the term $3RTlna_{Sn}$ in eqn. (5.6) was replaced with $3RTln\ X_{Sn}$ where X_{Sn} is the atomic fraction of Sn in the saturated solution. In view of the fact that the saturated solution is rather dilute, the above assumption is reasonable. Thus the temperature dependence of $\Delta_f G^0_{\langle USn_3 \rangle}$ with reference to <α-U> and liquid {Sn} in the temperature range 682-905 K could be expressed as

$$\Delta_f G^0_{\langle USn_3 \rangle} /kJmol^{-1} = -172.8 + 0.061T(\pm 1.200) \tag{5.7}$$

From the above equation, the enthalpy and entropy of formation of <USn_3> at the mean temperature of measurement (794 K) were derived to be -172.8 kJ mol $^{-1}$ and 61 J mol^{-1} K^1, respectively.

The partial molar excess Gibbs energy of uranium in the saturated solution of tin can be computed from the emf data pertaining to the cell I and the variation of the solubility of uranium in liquid tin [1]. The partial molar excess energy calculated is given by

$$\Delta G_U^{-xs}/kJmol^{-1} = -60.2 \pm 0.002T(\pm 1.200) \quad (5.8)$$

Thus the partial molar enthalpy and the partial molar excess entropy of uranium in saturated solution in tin in the mean temperature (794 K) are -60.2 kJ mol^{-1} and 2 J mol^{-1} K^{-1}, respectively.

5.1.3 Gibbs energy formation of <U_3Sn_7>

The biphasic mixture of <USn_3> and <U_3Sn_7> ($U_{0.28}Sn_{0.72}$) was prepared and characterized by the method described earlier. The XRD pattern is given in Fig. 5. 2. The cell constructed for the above intermetallic was;

$$< U > // UCl_3 \text{ in LiCl-KCl (eutectic)} // <U_3Sn_7 + USn_3> \quad \text{Cell II}$$

The overall cell reaction is given below;

$$^7/_2 < USn_3 > + [U] \leftrightarrow {}^3/_2 < U_3Sn_7 > \quad (5.9)$$

We have,

$$-3FE_{II} = {}^3/_2\ \Delta_f G^0_{\langle U_3Sn_7\rangle} - {}^7/_2\ \Delta_f G^0_{\langle USn_3\rangle} \quad (5.10)$$

$$\Delta_f G^0_{\langle U_3Sn_7\rangle} = -2FE_{II} + {}^7/_3\ \Delta_f G^0_{\langle USn_3\rangle} \quad (5.11)$$

The time taken by this cell for initial stabilization was around 25 h and for subsequent change in temperature, it took around 23 h for stabilization of emf values at a particular temperature. The longer duration required for attaining a stable value of emf is due to the sluggish diffusion in the solid state.

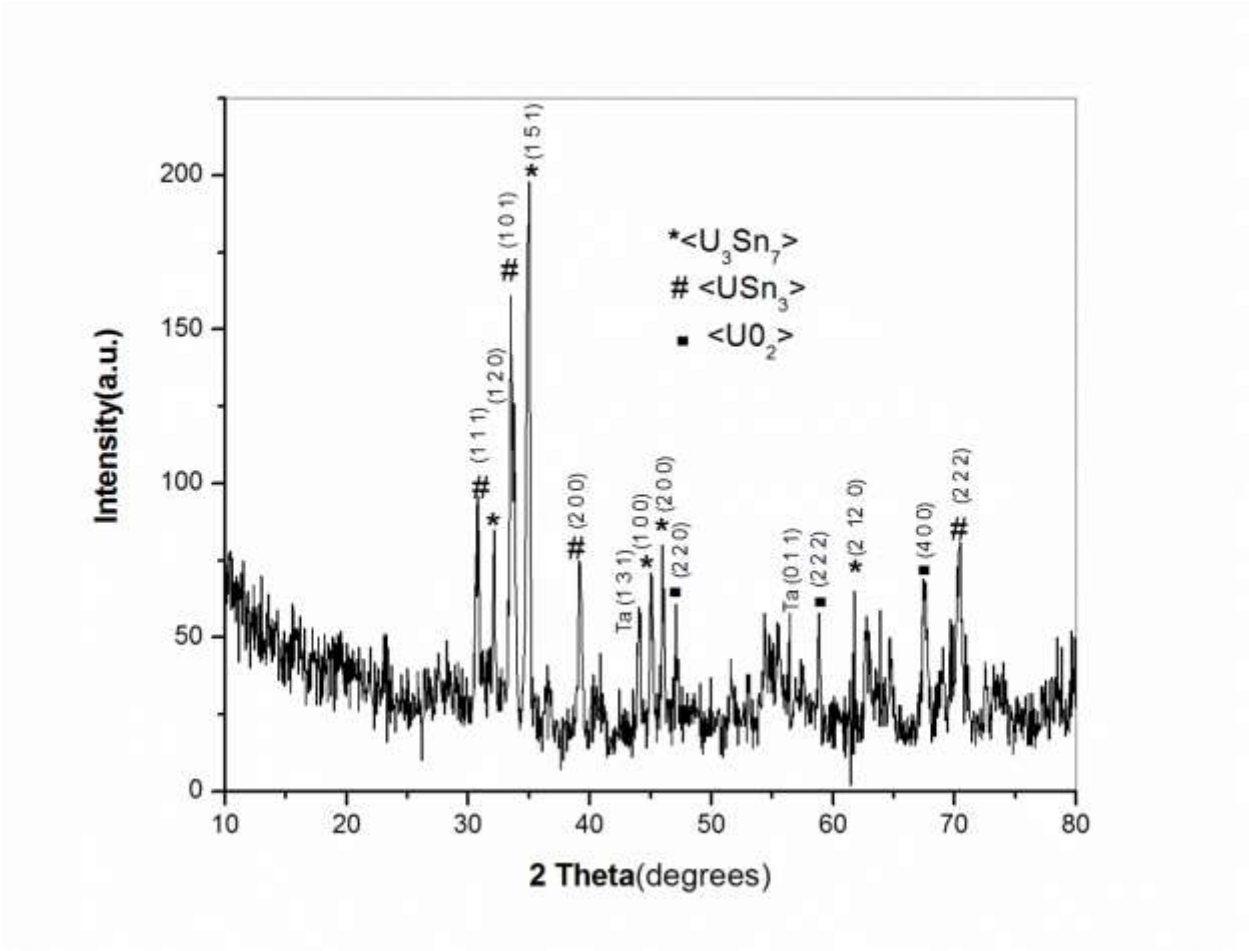

Fig. 5.2 XRD pattern showing the biphasic mixture of <USn_3> and <U_3Sn_7>

Table 5.2:- Emf values of cell II

$$<U>) \,//\, UCl_3 \text{ in LiCl-KCl (eutectic)} \,//\, \langle U_3Sn_7 \rangle + \langle USn_3 \rangle$$

Temperature (K)	Emf (mV)*
693 [h]	442.80±0.1
717 [c]	435.3 ±0.3
718 [h]	434.6±0.2
742 [c]	428.2±0.2
743 [h]	427.3±0.3
767 [c]	421.6±2.3
767 [h]	421.0±8.7
791 [c]	413.3±7.7
792 [h]	412.2±0.2
817 [c]	408.2±0.2
817 [h]	405.2±2.4
842 [c]	398.2±0.2
843 [h]	397.3±0.2

h= heating and c= cooling

* Note- The values are the average of two heating and cooling cycles at each temperature. The errors are the standard deviations in the measured values.

Two experimental runs were carried out. In the first run, no stable emf was obtained during both the heating and cooling cycles, so these values were discarded. In the second run stable emf values within ±1mV were obtained during both the heating and cooling cycles and these values were considered for the measurement.

The emf values of cell II in the temperature range 693-843 K are given in Table-5.2. A least squares regression analysis of the data yielded the following expression.

$$E_{II}\,/mV = (648.2 \pm 0.7) - (0.297 \pm 0.001)\,T/K \qquad (5.12)$$

The standard Gibbs energy of formation of $<U_3Sn_7>$ as a function of temperature was calculated by using the equation 5.11.

The standard Gibbs energy formation of $<USn_3>$ calculated from the measurements obtained by using cell I and the emf values from the fit equation for cell II were used for the calculation. The calculated Gibbs energy of formation of $<U_3Sn_7>$ in the temperature range 693-843 K is given by

$$\Delta_f G^0_{\langle U_3Sn_7\rangle}\,/kJmol^{-1} = -527.8 + 0.200\,T\ (\pm 4.200) \qquad (5.13)$$

Thus the enthalpy and entropy of formation of $<U_3Sn_7>$ at the mean temperature of measurement (768 K) are -527.8 kJ mol^{-1} and 200 J mol^{-1} K^{-1} respectively.

5.1.4 Gibbs energy formation of $<USn_2>$

The biphasic mixture of $<U_3Sn_7>$ and $<USn_2>$ ($U_{0.69}$ $Sn_{0.31}$) was prepared and characterized by the method described earlier. The XRD pattern is given in Fig. 5.3. The cell constructed is given by;

$$< U> \,//\, UCl_3 \text{ in LiCl-KCl (eutectic)} \,//\, <USn_2 + U_3Sn_7> \qquad \text{Cell III}$$

The overall cell reaction is given below;

$$2 < U_3Sn_{7>} + [U] \leftrightarrow\ 7 < USn_2\ > \qquad (5.14)$$

Therefore,

$$-3FE_{III} = 7\,\Delta_f G^0_{\langle USn_2\rangle} + 2\Delta_f G^0_{\langle U_3Sn_7\rangle} \quad (5.15)$$

$$\Delta_f G^0_{\langle USn_2\rangle} = -{}^3/_7\, FE_{III} - {}^2/_7\,\Delta_f G^0_{\langle U_3Sn_7\rangle} \quad (5.16)$$

The time taken by this cell for initial stabilization was around 26 h and in subsequent measurement at different temperature, it took around 24 h for stabilization of emf values at a particular temperature. Two experimental runs were carried out. In the first run, no stable emf values were obtained during heating and cooling cycles, so these values were discarded. In the second run, stable emf values within ±1mV were obtained during both the heating and cooling cycles.

The emf values of the cell III in the temperature range 693-843 K are given in Table 5.3. A least squares regression analysis of the data yielded the following expression

$$E_{III}/m\ V = (581.6 \pm 5.1) - (0.203 \pm 0.006)\ T/K \quad (5.17)$$

The standard Gibbs energy of formation of $\langle USn_2\rangle$ was calculated by using the equation 5.16. The standard Gibbs energy of formation of $\langle USn_2\rangle$ calculated from the measurements on cell II and the emf values from the fit equation for cell III were used for the calculation. The calculated Gibbs energy of formation of $\langle USn_2\rangle$ in the temperature range 692-892 K is given by;

$$\Delta_f G^0_{\langle USn_2\rangle}/kJmol^{-1} = -174.9 + 0.073\,T(\pm 1.200) \quad (5.18)$$

Thus the enthalpy and entropy of formation of $\langle USn_2\rangle$ at the mean temperature of measurement (792 K) are -174.9 kJ mol^{-1} and 73 J mol^{-1} K^{-1} respectively.

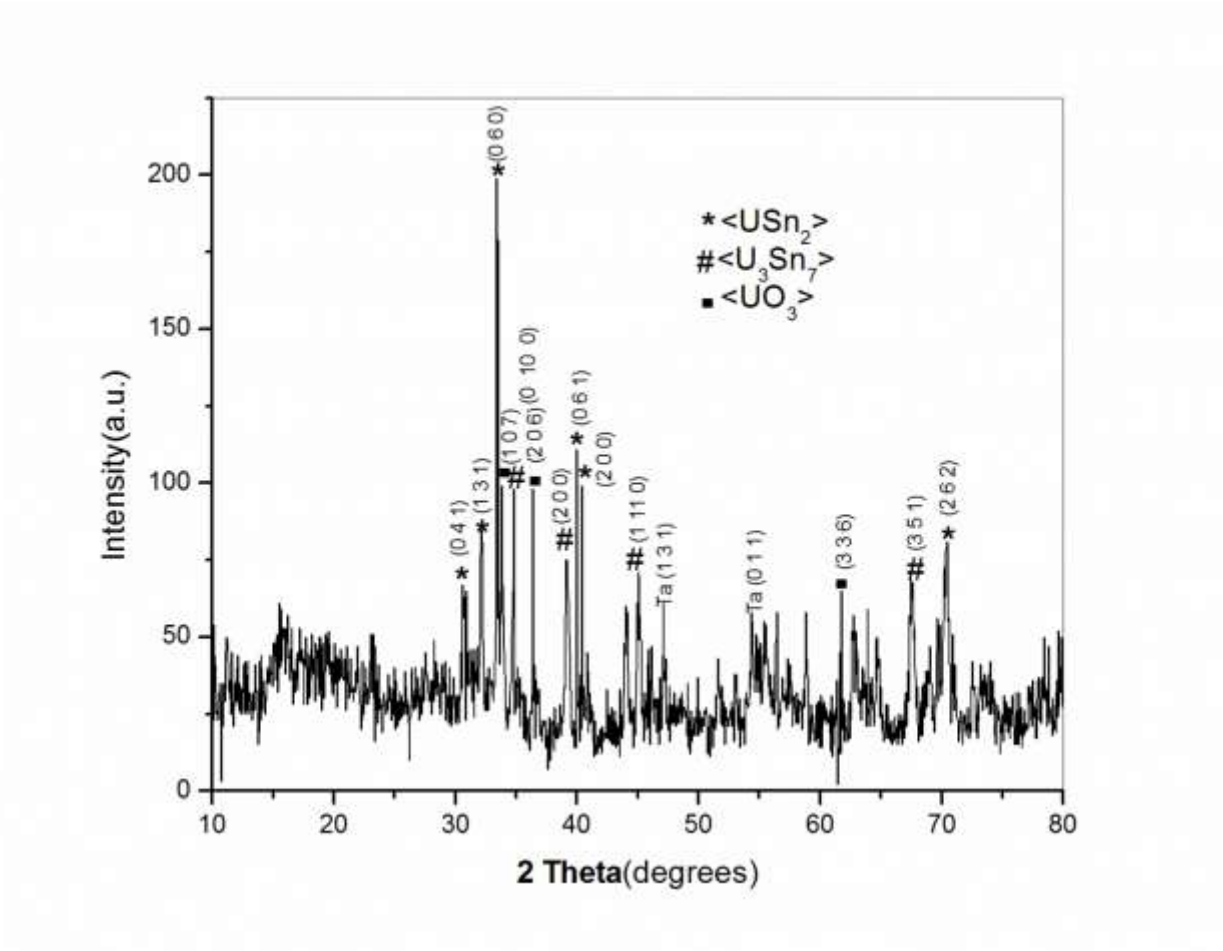

Fig. 5.3 XRD pattern showing the biphasic mixture of $<U_3Sn_7>$ and $<USn_2>$

Table 5.3:- The emf values of cell III

$< U > // UCl_3$ *in LiCl-KCl (eutectic)* $// \langle USn_2 \rangle + \langle U_3Sn_7 \rangle$

Temperature (K)	Emf (mV)*
692 [h]	440.1±1.4
692 [c]	444.3±0.1
716 [h]	436.3±0.2
715 [c]	433.2±0.1
741 [h]	431.3±0.1
740 [c]	431.4±0.6
766 [h]	426.2±8.0
766 [c]	424.4±0.1
792 [h]	421.3±6.8
791 [c]	421.2±0.2
816 [h]	417.1±5.5
816 [c]	415.2±0.2
840 [h]	413.4±4.4
839 [c]	410.9±0.1
865 [h]	404.9±0.1
865 [c]	403.5±0.3
892 [h]	402.7±0.2
892 [c]	401.4±0.1

h= heating and c= cooling

* Note- The values are the average of two heating and cooling cycles at each temperature.
The errors are the standard deviations in the measured values.

5.1.5 Gibbs energy formation of <USn>

The biphasic mixture of <USn_2> and <USn> ($U_{0.53}$ $Sn_{0.47}$) was prepared and characterized by the method described earlier. The XRD pattern is shown in Fig. 5.4. The cell constructed is given by;

< U > // UCl_3 in LiCl-KCl (eutectic) // <USn> + <USn_2> Cell IV

The overall cell reaction as follows,

$$7 < USn_2 > \; + [U] \leftrightarrow \; 2 < USn > \tag{5.19}$$

Therefore

$$\Delta_f G^0_{\langle USn \rangle} = -{}^3/_2 \, F E_{IV} + {}^1/_2 \, \Delta_f G^0_{\langle USn_2 \rangle} \tag{5.20}$$

The time taken by this cell for initial stabilization was around 26 h and in the subsequent measurements at different temperatures it took around 25 h for stabilization of emf values at a particular temperature. Three experimental runs were carried out. In the first two runs, no stable emf was obtained during heating and cooling cycles, so the values were discarded. In the third run, stable emf values within ±1mV were obtained during both the heating and cooling cycles.

The emf values of cell IV in the temperature range 692-892 K are given in Table5.4. . A least squares regression analysis of the data yielded the following expression

$$E_{IV} / mV = (618.1 \pm 3.1) - (0.\ 218 \pm 0.004)\ T/K \tag{5.21}$$

The standard Gibbs energy of formation of <USn_2> was calculated by using the equation 5.20. The standard Gibbs energy of formation of <USn_2> calculated from the measurements on cell III and the emf values from the fit equation for cell IV were used for the calculation.

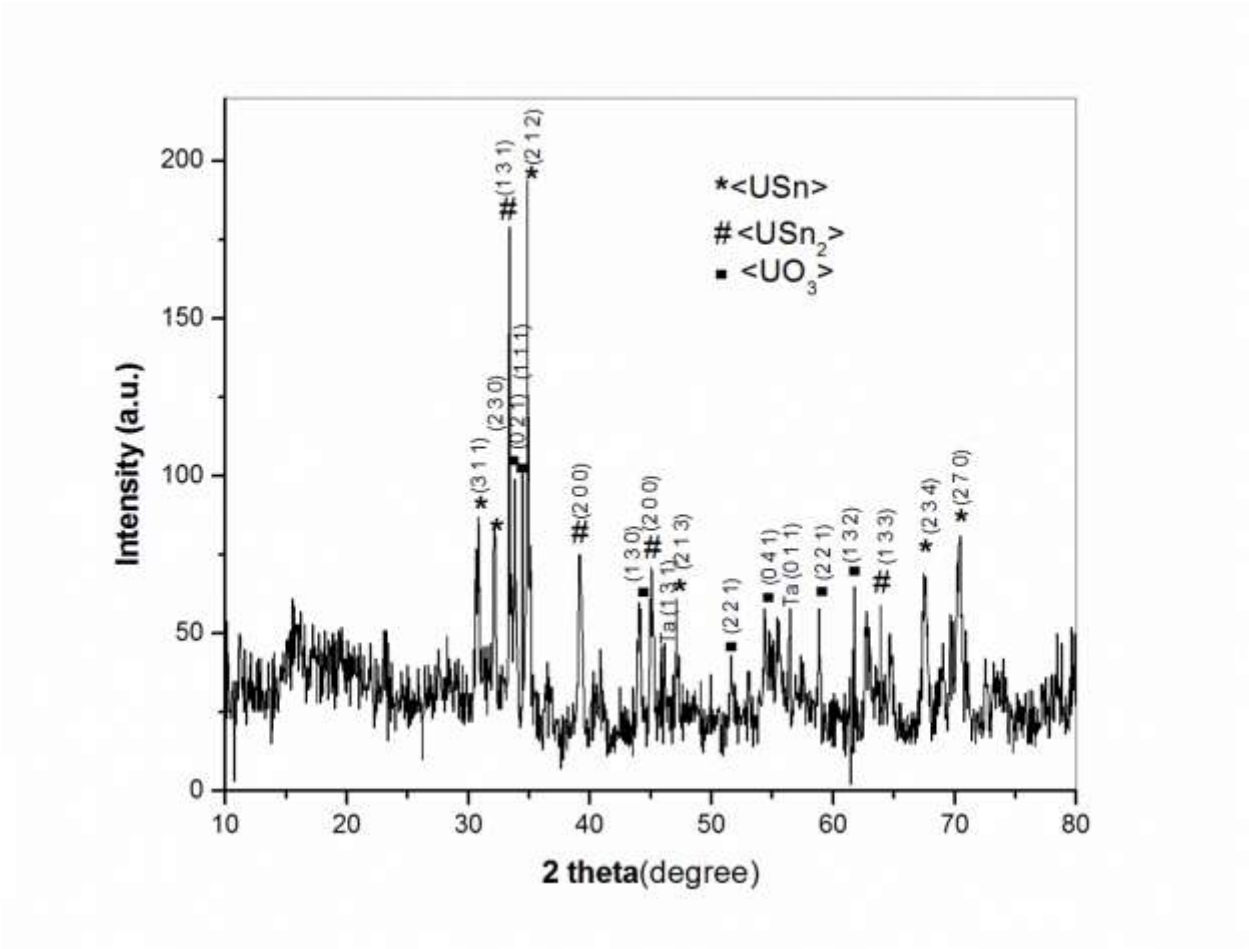

Fig. 5.4 XRD pattern showing the biphasic mixture of <USn_2> and <USn>

Table 5.4: Emf values of cell IV

$< U > // UCl_3$ *in LiCl-KCl (eutectic)* $// \langle USn \rangle + \langle USn_2 \rangle$

Temperature (K)	Emf (mV)*
692 [h]	468.3±0.1
692 [c]	469.3±0.2
716 [h]	462.2±0.2
716 [c]	461.9±0.1
740 [h]	458.2±0.1
741 [c]	456.2±0.1
766 [h]	451.1±0.1
765 [c]	450.2±0.1
792 [h]	446.1
792 [c]	444.3±0.2
816 [h]	440.2±0.1
815 [c]	440.6±0.8
840 [h]	435.2±0.2
839 [c]	434.1±0.1
865 [h]	429.3±4.0
865 [c]	429.3±4.4
892 [h]	425.2±0.1
892 [c]	425.4±0.2

h= heating and c= cooling

* Note- The values are the average of two heating and cooling cycles at each temperature.
The errors are the standard deviations in the measured values.

The calculated Gibbs energy of formation of <USn> in the temperature range 692-892 K is given by;

$$\Delta_f G^0_{\langle USn \rangle} / kJmol^{-1} = -176.9 + 0.064T(\pm 0.800) \quad (5.22)$$

Thus the enthalpy and entropy of formation of <USn> at the mean temperature of measurement (792 K) are -176.9 kJ mol^{-1} and 64 J mol^{-1} K^{-1} respectively.

5.2 Comparison of Gibbs energy of formation of <USn_3>, <U_3Sn_7>, <USn_2> and <USn> with those reported in the literature.

The Gibbs energy of formation of <USn_3> measured by our emf method is compared with those reported in the literature in Table 5.5. The $\Delta_f G^0_{\langle USn_3 \rangle}$ values obtained with respect to α-uranium and liquid tin in this study were found to be in good agreement with those measured by Johnson et al. [2] by using the molten salt emf method. However the values obtained by vapor pressure method by Alcock and Grieveson [3] were more positive than the rest. These are plotted in Fig.5.5. Alcock derived the values of vapor pressure based on the weight loss due to the effusion of vapors of the sample heated in a Knudsen cell [1150-1300 K]. Their values are plausibly in error owing to the inaccuracies arising from the experimental procedure or due to the uncertainties in the auxiliary data employed in arriving at the values of the vapor pressure or both. Fig.5.5(a). shows the actual temperature range were measurement was carried out by Alcock et al. and our values.

There are no experimentally measured values available for the Gibbs energy of formation for <U_3Sn_7>, <USn_2> and <USn>. Based on Miedema's model [4] the enthalpies of formation of <USn_3>, <U_3Sn_7>, <USn_2> and <USn> were computed to be -132, -393.6 -129.8 and -110.6 kJmol^{-1} respectively. The enthalpy values for the compounds <USn_3>, <U_3Sn_7>, <USn_2> and

<USn> calculated from the measured emf values at the mean temperature of measurement are.-172.8, -527.8,-174.9 and -176.9.9 kJ mol^{-1}. The trends in the two sets of value are similar as a function of increasing Sn concentration, but the values calculated from Miedema's model are less exothermic. The reason for low value is that Miedema's model values are based on the assumption of regular solution whereas U-Sn system shows more negative deviation from ideality, as indicated by the formation of many intermetallic compounds. Further, Miedema's model cannot give the enthalpy values as a function of temperature. The enthalpy of formation calculated for $<USn_3>$ at 794 K (-172. 8 kJ mol^{-1}) is in very good agreement with that at 793 K reported by Johnson et al. [6] (-163.9 kJ mol^{-1}). Both these values are in reasonable agreement with the enthalpy of formation at 1145 K obtained by precipitation calorimetry by Colinet et al. [5] (-173.9 kJ mol^{-1}).The Gibbs energy of formation of the $<U_3Sn_7>$, $<USn_2>$ and <USn> intermetallics are being reported for the first time.

The partial molar excess Gibbs energy of uranium in the saturated solution of tin computed from our studies is given by equation (5.22) is

$$\Delta G_U^{-xs}/kJmol^{-1} = -60.2 \pm 0.002T(\pm 1.200) \quad (5.23)$$

The values reported by Johnson et al. [2] in the temperature range 500-800 K are given below

$$\Delta G_U^{-xs}/kJmol^{-1} = -58.94 \pm 0.002T \quad (5.24)$$

It can be seen that the present data are in close agreement with those of Johnson et al. [2].

Table 5.5 Gibbs energy of formation of $\langle USn_3 \rangle$

Compound	$\Delta_f G^0$ ($kJmol^{-1}$)	**Method**	**T (K)**	**Reference**
<USn_3> (w.r.t α-U and liquid {Sn)	-163.93 + 0.04 T + 0.13 x 10^{-4} T^2	emf	636-950	Johnson et al. [2]
	- 96.14 + 0.25 x 10^{-2} T	Vapor pressure	1150-1300	Alcock et al. [3]
	-172.8 + 0.061 T	emf	682-908	This Study
<USn_3 > (w.r.t α-U and liquid Sn	-123.61	emf	805	Johnson et a*l*. [2]
	-94.22	Vapor pressure	805	Alcock et al. [3]
	-123.79	emf	805	This Study

Fig. 5.5 Temperature dependence of Gibbs energy formation of <USn_3 >

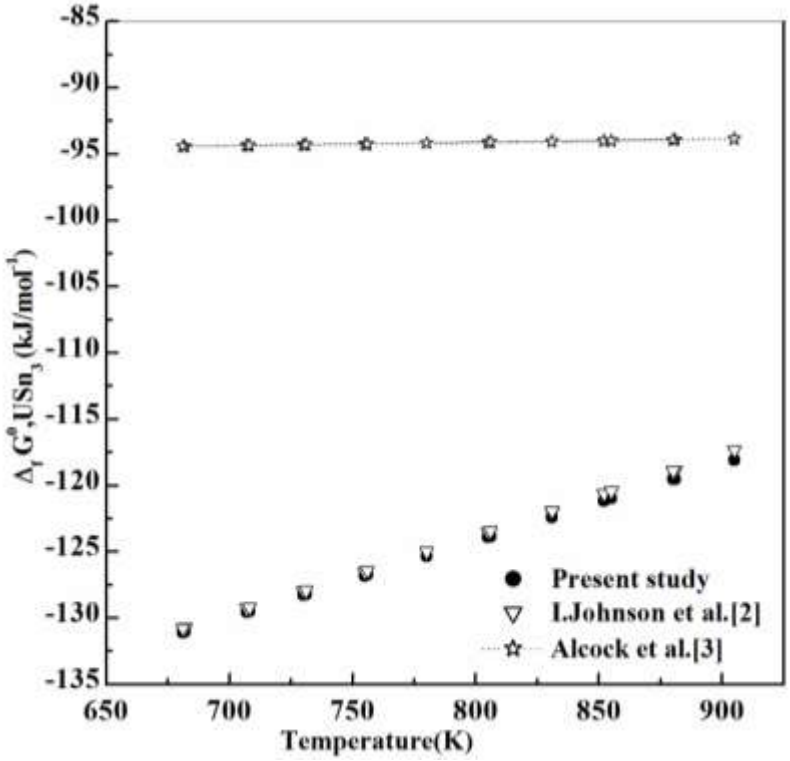

Fig. 5.5 Temperature dependence of Gibbs energy formation of <USn_3 >

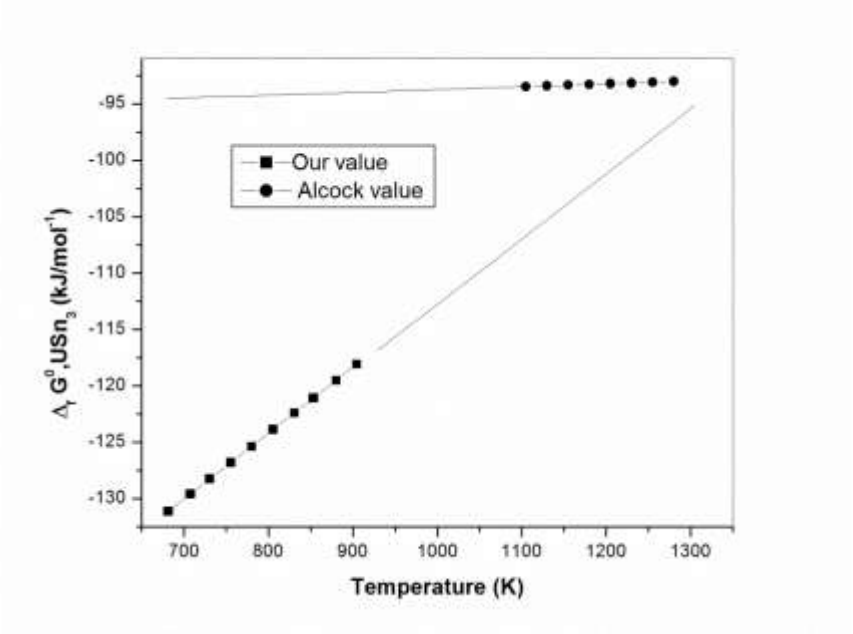

Fig. 5.5(a). Temperature dependence of Gibbs energy formation of <USn_3> in the actual temperature range

5.3 Enthalpy of formation of <USn_3> at 298.15 K by using solution calorimetry.

5.3.1 Solution calorimeter and calorimetric measurement

A multi-detector high temperature drop calorimeter (MHTC-96) from M/S. SETARAM which is described elsewhere [6] was used for solution calorimetric measurements.

Liquid metal solution calorimetric technique using aluminium as the solvent was employed for determining the enthalpies of formation of <USn_3>. The experimental procedure adopted is already described in section 3B.6. The XRD pattern of the intermetallic compound <USn_3> is given in Fig. 5.6. In a typical experiment, approximately 1g of aluminium was taken in an alumina crucible which was loaded into the calorimeter and heated to the temperature of measurement. Then it was calibrated by successively dropping aluminium samples, each weighing around 300 mg, from the ambient temperature to the temperature of measurement. Subsequently, Sn samples, each weighing around 200 mg, were dropped from the ambient temperature into liquid aluminium at the temperature of measurement. The amount of tin added to aluminium was so chosen that it forms a dilute solution ($X_{Sn} < 0.02$) after dropping all the samples. The calorimetric signal recorded corresponds to the thermal effect of dissolution of tin in liquid aluminium (Q_{Sn}^{E}) at the temperature of measurement. A Similar procedure was followed to measure the thermal effect of dissolution of USn_3 ($Q_{USn_3}^{E}$) in liquid aluminium by dropping samples of the compound, each weighing around 18-30 mg, were dropped in liquid aluminium at the experimental temperature in a separate experiment. The values for the thermal effect of dissolution of tin in liquid aluminium (Q_{Sn}^{E})at 980 K measured by adding tin at 298.15 K to aluminium at 980 K are given in Table-5.6.

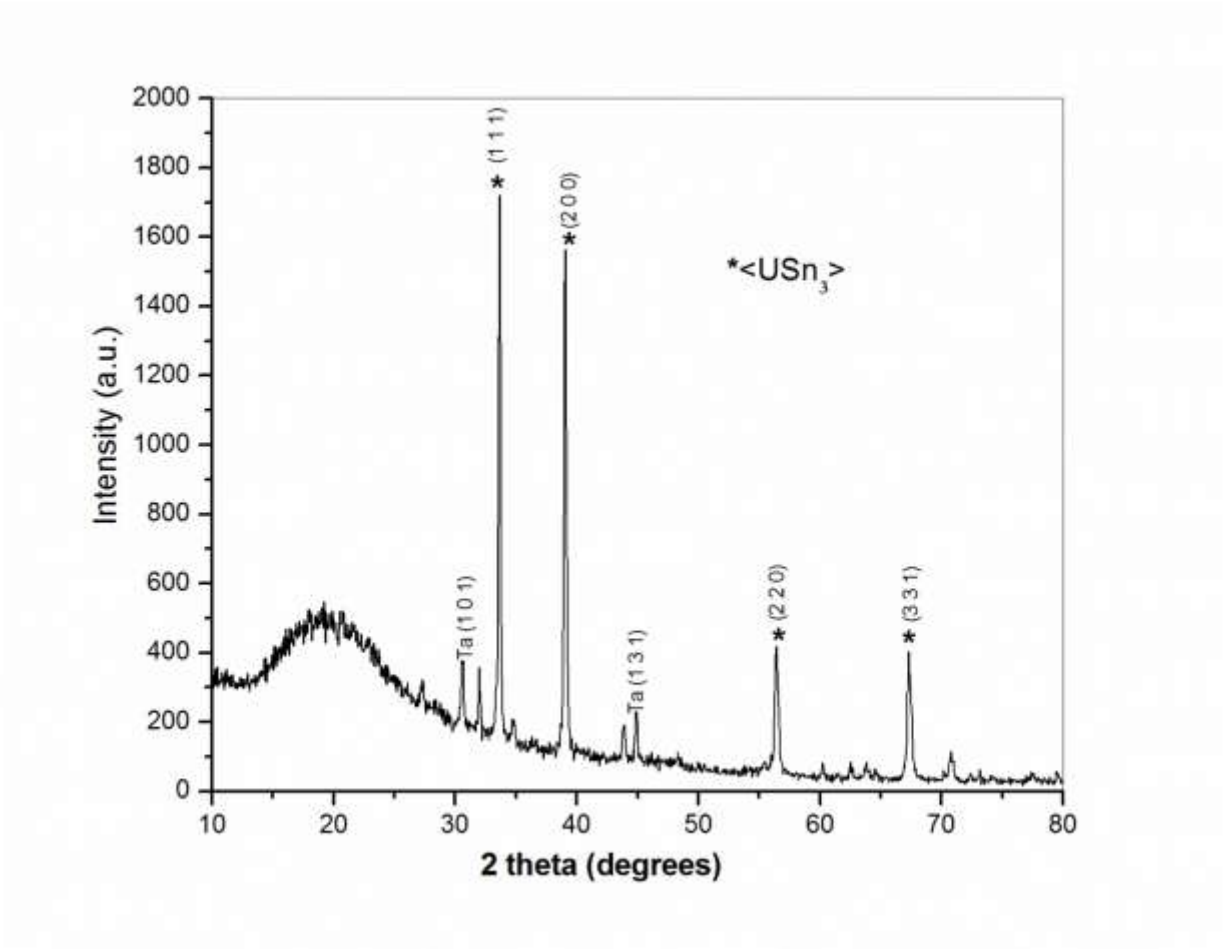

Fig. 5.6 XRD pattern of <USn_3>

The thermal effect of dissolution of <USn_3> ($Q^E_{USn_3}$) in liquid aluminium at 980 K are given in Table5.7. As it can be seen from Table 5.6 and 5.7, the thermal effect of dissolution of tin and <USn_3> are independent of the composition of the alloy in the crucible, within the experimental uncertainty. Hence the mean of Q^E values were taken as $Q^{E,\infty}$ as the thermal effect of dissolution at infinite dilution. The overall uncertainties in $Q^{E,\infty}$ values were computed by taking the uncertainties in the measurement as well as calibration, which are given in the respective tables. The thermal effect of dissolution of Uranium in liquid aluminum at infinite dilution ($Q^E_{USn_3}$) was earlier measured in our laboratory [7]. From the thermal effects of dissolution at infinite dissolution, of <U>, <Sn> and <USn_3> the enthalpy of formation of <USn_3> at 298.15 K was computed by using the following equation based on Hess law of heat summation:

$$\Delta_f H^0_{298.15}\langle U_{0.25}Sn_{0.75}\rangle = 0.25Q^{E,\infty}_U + 0.75Q^{E,\infty}_{Sn} - Q^{E,\infty}_{U_{0.25}\ Sn_{0.75}} \quad (5.25)$$

The enthalpy of formation of <USn_3> at 298.15 K was calculated to be -129.5 ± 11.8 kJ mol^{-1}.

The partial molar enthalpy of dissolution of tin in liquid aluminium at infinite dilution at 980 K was derived from the thermal effect of dissolution at infinite dilution given in Table5.5 and from the literature data [8] by using the following equation;

$$\overline{\Delta H^0_{Sn}} = Q^{E,\infty}_{Sn} - (H^0_T - H^0_{298.15}) \quad (5.26)$$

The partial molar enthalpy of tin in liquid aluminium at infinite dilution at 980 K was calculated to be -106.5 ± 7.6 kJ mol^{-1} and the value reported by Colinet et al. [5] is 100.4 which is in agreement with our value within experimental uncertianty.

Table 5.6 Experimental data for the thermal effects of dissolution of Tin in liquid Aluminum at 980 K

Calibration :

No.	Wt. of Al (mg)	Peak Area (Counts)
1.	32.26	227
2.	34.64	195
3.	36.97	250
4.	33.05	219
5.	35.90	230

Measurement :

$$<Sn>_{298.15} \longrightarrow [Sn]_{\{Al,980\}}$$

No.	Wt. of Sn (mg)	Peak Area (Counts)	X_{Sn} (at.%)	$Q_{Sn}^{E,\infty}$ (kJ mol^{-1})
1.	19.31	50	0.36	62.19
2.	14.2	56	0.63	81.64
3.	20.65	54	1.01	54.14
4.	20.37	51	1.40	41.67
5.	23.24	49	1.83	43.65

$Q_{Sn}^{E,\infty}$ = 56.66 ± 7.25 kJ mol^{-1}

Amount of aluminium in the calorimeter = 1.15 g
$(H_T^0 - H_{298.15}^0)$ of Al at 980 K = 30.31 kJ mol^{-1} [8].
Calibration constant = 0.1744 ± 0.0066 J Count^{-1}
Overall uncertainty in $Q_{Sn}^{E,\infty}$ = ± 7.58 kJ mol^{-1}

Table 5.7 Experimental data for the thermal effects of dissolution of <USn_3> in liquid Aluminum at 980 K

Calibration :

No.	Wt. of Al (mg)	Peak Area (Counts)
1.	33.89	243
2.	38.88	260
3.	30.90	225
4.	23.67	218
5.	32.78	237

Measurement :

$$\langle U_{0.25}Sn_{0.75}\rangle \rightarrow [0.25U + 0.75Sn]_{\{Al,980\ K\}}$$

No.	Wt. of sample (mg)	Peak Area (Counts)	X_U (at.%)	$Q^{E,\infty}_{U_{0.25}Sn_{0.75}}$ (kJ mol^{-1})
1.	28.48	58	0.42	45.76
2.	18.56	30	0.69	36.32
3.	20.33	54	0.99	59.68
4.	28.41	49	1.41	38.75

$Q^{E,\infty}_{U_{0.25}\ Sn_{0.75}}$ = 45.12 ± 5.25 kJ mol^{-1}

Amount of aluminium in the calorimeter = 1.22 g
$(H^0_T - H^0_{298.15})$ of aluminium at 980 K = 30.31 kJ mol^{-1}[8].
Calibration constant = 0.1512 ± 0.0077 J Count^{-1}
Overall uncertainty in $Q^{E,\infty}_{USn_3}$ = ± 5.72 kJ mol^{-1}.

Table-5.8:-Enthalpy of formation of <USn_3>

Compound	Method	Temp. (K)	Enthalpy of Formation gatom-1	Reference
	Al solution calorimetry	298	-141.2	Colinet at al. [5].
	Sn solution calorimetry	298	-139.8	Colinet et al. [5].
	Precipitation in tin	1145	-173.8	Colinet et al. [5].
<USn_3>	Vapor pressure	1150-11300	-96.24	Alcock et al. [3].
	Acid dissociation calorimetry	298	-90.36	Alcock et al. [3].
	emf	636-950	-167.2	Johnson et al. [2].
	emf	682-905	-172.8 ± 1.2	This study.
	Al solution calorimetery	298.15	-129.5 ± 11.8	This study.

The enthalpy of formation derived by our measurement is compared with those given in the literature is given in Table 5.8. It can be seen that values are good agreement with values of Colinet et al. [5] using both Al and Sn solution calorimetry.

References:-

1. P. Chiotti, V. V. Akhachinskij, I. Ansara, M. H. Rand, Uranium-Tin in The Chemical Thermodynamics of Actinide Elements and Compounds, Part 5, The Actinid Binary Alloys, International Atomic Energy Agency, STI/PUB/424/5, Vienna, 1981, p. 177.
2. I. Johnson, H. M. Federer, Thermodynamic Study of the Compounds of Uranium with Silicon, Germanium, Tin and Lead in the Proceedings of the International Symposium of Thermodynamics of Nuclear Materials, International Atomic Energy Agency,Vienna, 1962, p. 319.
3. C. B. Alcock, P. Grieveson, J. Inst. Met. 93 (1961) 304.
4. A. R. Miedema, R. Boom, F. R. De Boer, J.Less-Common Met. 41 (1975) 283.
5. C. Colinet, A. Bessound, A.Pasturel, J. Less-Common Met. 143 (1988) 265.
6. R. Babu, R. Kandan, Hrudananda Jena, K.V. Govindan Kutty, K. Nagarajan, J. Alloys Compd. 506 (2010) 565.
7. K. Nagarajan, R. Babu and C. K. Mathews, J. Nucl. Mater. 201 (1993) 142.
8. P. Hultgren, P. D. Desai, T. Hawkins, M. Glaser, K.K, Kelley and D.D. Wagmann, Selected values of the thermodynamic properties of the Elements (American society for Metals, Metals Park, OH, USA 1973) p.125.

Chapter 6: Summary and Scope for further work

6.1 Phase transformation temperatures in the U-Sn System

The U-Sn system consists of five intermetallics namely, <U_5Sn_4>, <USn>, < USn_2>, <U_3Sn_7> and <USn_3>. The first intermetallic melts congruently and last four melt peritectically. The peritectic transformation of these intermetallics is very close and earlier investigations on these intermetallic were not able to delineate the same. So the primary objective of this study was to resolve the uncertainties in the experimentally determined values of the peritectic formation temperatures of these intermetallics. The values were determined by using the spot equipment developed in house. The peritectic formation temperatures of the four intermetallic compounds viz., <USn>, <USn_2>, <U_3Sn_7> and <USn_3> were found to be 1642 ± 7 K, 1628 ± 1 K, 1622 ± 4 K, 1600 ± 4 K respectively. Special care was taken to avoid the interaction of the molten liquid with the container. This investigation helped delineate the separation between the cascades of peritectic isotherms. These values are more reliable and supersede the measurements reported earlier. From the calculation made using FactSage 6.2 and the experience gained during the experiments suggest that the yttria seems to be a better container material to hold this molten U-Sn alloy. Compatibility of uranium rich alloys (55-100 at %U) with yttria cups needs to be experimentally verified.

6.2 Galvanic cell emf method and calorimetric studies

Gibbs energy formation of <USn_3> has been reported in the literature, but there is a large difference in the values reported earlier. So the primary objective of this study was to re-examine the data reported for <USn_3> and to determine the Gibbs energies of formation of other intermetallic compounds for which no thermodynamic data are available. The Gibbs energies of

formation of <USn_3>, <U_3Sn_7>, <USn_2> and <USn> with respect to <α-U> and liquid {Sn}, in the temperature range 682-905 K, were determined as (-172.8 + 0.06 T), (-527.8 + 0.200 T), (-174.9 + 0.073 T) and (-176.9 + 0.064 T) kJ mol^{-1} respectively. There are no experimentally measured values available for the Gibbs energy of formation for <U_3Sn_7>, <USn_2> and <USn>. Based on Miedema's model the enthalpies of formation of <USn_3>, <U_3Sn_7>, <USn_2> and <USn> were computed to be -132, -393.6 -129.8 and -110.6 $kJmol^{-1}$ respectively. The enthalpy values for the above compounds calculated from the measured emf values at the mean temperature of measurement are.-172.8, -527.8,-174.9 and -176.9 kJ mol^{-1} respectively. Though the trends in the two sets of enthalpy data as a function of increasing Sn concentration are similar, the Miedema's values are less exothermic as this model is based on assumption of regular solution whereas U-Sn system shows more negative deviation from ideality. Further, the Miedema's model cannot predict the temperature dependence of enthalpy. Hence it is not appropriate to compare the enthalpy data measured at high temperatures with the values predicated by Miedema's model.

The enthalpy of formation of <USn_3> at 298.15 K calculated by using high temperature solution calorimeter was found to be-129.5 ± 11.8 kJ mol^{-1} and the partial molar enthalpy of tin in liquid aluminium at infinite dilution at 980 K was calculated to be -106.5± 7.6 kJ mol^{-1} and both the values were in good agreement with values reported in the literature.

6.3 Scope for further work

The intermetallic compounds of U-Sn system are highly pyrophoric and susceptible to oxidation. The phase transformation studies shows yttria to be a better container material to hold the molten alloy but further experiments are required with uranium rich alloys (< 56 %).

There are no experimental X-ray diffraction data (JCPDS files) and enthalpy increment data are for <U_3Sn_7>, <USn_2>, <USn> and <U_5Sn_4>. So further studies can be carried out in this area by preparing a line compound of the above intermtallics. The (U, Pu) Sn (Ru, Rh, Pd) compound that has been identified in the fuel matrix needs to be studied. Since Pu could be expected to be soluble in U-Sn intermetallic compound, the study of (U,Pu) Sn alloy are also of important to be studied.The solidus and liquidus temperatures in the binary system, Pu-Sn and those pertaining to the ternary system U-Pu-Sn can be measured by using the spot technique. The Gibbs energies of formation of the intermetallic compounds of the above systems can be measured by using the molten salt galvanic cell emf measurements and their enthalpies formation using high temperature calorimetry.